Federal University of Paraíba

Technology Centre

POSTGRADUATE PROGRAM IN CIVIL AND ENVIRONMENTAL ENGINEERING

– PhD THESIS–

Spatial-temporal improvement of long-term evapotranspiration estimates for all sky conditions in tropical biomes using satellite- and reanalysis-based datasets

By

Cinthia Maria de Abreu Claudino

PhD thesis defended at the Federal University of Paraíba for attaining the degree in Doctor of Civil and Environmental Engineering with emphasis on Water Resources

João Pessoa – Paraíba **October 2025**

Federal University of Paraíba

Technology Centre

POSTGRADUATE PROGRAM IN CIVIL AND ENVIRONMENTAL ENGINEERING

– PhD THESIS–

Spatial-temporal improvement of long-term evapotranspiration estimates for all sky conditions in tropical biomes using satellite- and reanalysis-based datasets

PhD Thesis submitted to the Postgraduate Program in Civil and Environmental Engineering at the Federal University of Paraíba, as part of the requisites for attaining the title of Doctor.

Cinthia Maria de Abreu Claudino

Advisor: Prof. Dr Victor Hugo Rabelo Coelho

Co-advisor: Prof. Dr Guillaume Francis Bertrand

João Pessoa – Paraíba **October 2025**

Catalogação na publicação
Seção de Catalogação e Classificação

C615s Claudino, Cinthia Maria de Abreu.
Spatial-temporal improvement of long-term evapotranspiration estimates for all sky conditions in tropical biomes using satellite- and reanalysis-based datasets / Cinthia Maria de Abreu Claudino. - João Pessoa, 2025.
121 f. : il.

Orientação: Victor Hugo Rabelo Coelho.
Coorientação: Guillaume Francis Bertrand.
Tese (Doutorado) - UFPB/CT.

1. Evapotranspiração. 2. Sensoriamento remoto. 3. Moderate Resolution Imaging Spectroradiometer (MODIS). I. Coelho, Victor Hugo Rabelo. II. Bertrand, Guillaume Francis. III. Título.

UFPB/BC CDU 551.573(043)

Elaborado por KAROLLYNE FERREIRA DANTAS - CRB-4/2319

PPGECAM

Programa de Pós-Graduação
Engenharia Civil e Ambiental

UFPB Universidade Federal da Paraíba

Mestrado e Doutorado

SPATIAL-TEMPORAL IMPROVEMENT OF LONG-TERM EVAPOTRANSPIRATION ESTIMATES FOR ALL SKY CONDITIONS IN TROPICAL BIOMES USING SATELLITE- AND REANALYSIS-BASED DATASETS.

CINTHIA MARIA DE ABREU CLAUDINO

Tese aprovada em 27 de outubro de 2025

Período Letivo: 2025.2

Documento assinado digitalmente
gov.br VICTOR HUGO RABELO COELHO
Data: 29/10/2025 09:55:00-0300
Verifique em https://validar.iti.gov.br

Prof(a). Dr(a). Victor Hugo Rabelo Coelho – UFPB
Orientador(a)

Documento assinado digitalmente
gov.br GUILLAUME FRANCIS BERTRAND
Data: 29/10/2025 11:01:35-0300
Verifique em https://validar.iti.gov.br

Prof(a). Dr(a). Guillaume Francis Bertrand – UFPB
Coorientador(a)

Documento assinado digitalmente
gov.br CRISTIANO DAS NEVES ALMEIDA
Data: 29/10/2025 17:48:03-0300
Verifique em https://validar.iti.gov.br

Prof(a). Dr(a). Cristiano das Neves Almeida – UFPB
Examinador(a) Interno(a)

Documento assinado digitalmente
gov.br RICHARDE MARQUES DA SILVA
Data: 29/10/2025 21:10:44-0300
Verifique em https://validar.iti.gov.br

Prof(a). Dr(a). Richarde Marques da Silva – UFPB
Examinador(a) Interno(a)

Documento assinado digitalmente
gov.br SUZANA MARIA GICO LIMA MONTENEGRO
Data: 30/10/2025 16:26:20-0300
Verifique em https://validar.iti.gov.br

Prof(a). Dr(a). Suzana Maria Gico Lima Montenegro - UFPE
Examinador(a) Externo(a)

Documento assinado digitalmente
gov.br RODOLFO LUIZ BEZERRA NOBREGA
Data: 29/10/2025 21:24:01-0300
Verifique em https://validar.iti.gov.br

Prof(a). Dr(a). Rodolfo Luiz Bezerra Nóbrega - University of Bristol
Examinador(a) Externo(a)

Documento assinado digitalmente
gov.br JAMIL ALEXANDRE AYACH ANACHE
Data: 01/11/2025 18:29:14-0300
Verifique em https://validar.iti.gov.br

Prof(a). Dr(a). Jamil Alexandre Ayach Anache - USP
Examinador(a) Externo(a)

João Pessoa/PB
2025

Dedico a minha mãe, Sandra Moura, por ser um exemplo de mulher forte e resiliente e por incentivar constantemente a minha educação.

AGRADECIMENTOS

Ao longo de 4 anos, ter pessoas ao meu lado que me ensinaram, escutaram e motivaram foi essencial para que essa etapa fosse concluída. Assim, agradeço primeiramente à minha família, em especial à minha Mãe, Sandra Moura e à minha Tia, Sônia Moura, que durante todos esses anos de estudo me incentivaram e não mediram esforços para que eu pudesse buscar mais conhecimentos, sendo exemplos presentes de mulheres independentes e resilientes em minha vida: vocês me ensinaram a parte humana de ser uma boa profissional. Ao meu namorado, Demis Melo, que viveu ao meu lado as conquistas e inseguranças do mundo acadêmico, obrigada por ter sido meu porto seguro e meu ponto de paz.

Agradeço aos professores que compartilharam seus conhecimentos para que esse trabalho pudesse ser realizado. Em especial, ao meu orientador, Victor Coelho, por ser um professor que, além de estimular meu potencial, foi um ponto de escuta e de confiança. Ao meu coorientador, Guillaume Bertrand, por me ensinar sobre a visão multidisciplinar e sobre o equilíbrio de vida. Ao professor Cristiano Almeida, que me ensinou muito sobre técnicas, mas também sobre manter-se em constante aprendizado e trabalhar em equipe. Ao professor Rodolpho Nóbrega, que abriu as portas para uma grande experiência na minha vida e me ensinou muito sobre a valorização da pesquisa e da carreira. Aos membros da banca, que contribuíram com tempo e conhecimentos valiosos para melhoria deste trabalho.

Aos meus amigos que fui construindo ao longo da trajetória de vida e me acompanharam ao longo dos anos e caminhos. Às minhas amigas de São João do Rio do Peixe, Izabelly, Elisa e Dalila, por compartilharem uma infância e uma adolescência comigo e por estarem presentes até hoje na minha vida. Aos amigos que levo desde a graduação, Thiago, Ingridy, Andresa, Daniel e Breno, que se tornaram família e apoio durante toda essa trajetória de formação. Aos meus amigos e colegas de pós-graduação, que me motivaram e me ajudaram com seus conhecimentos: Eduardo, Lindemberg, Cinthya, Vanine, Filipe, Jaqueline e Ana. Aos amigos que fiz em João Pessoa e se tornaram família, pelos abraços e pelos momentos especiais compartilhados: Filipe, Isabelle, Delma, Paulo e Enubia. Aos amigos que fiz em Bristol, que contribuíram com palavras e momentos especiais: Stéfani, Shirley, Rayane e Daniel. A Joelson e Rayanni, por me lembrarem da importância de cuidar da minha saúde. A todos, a minha gratidão por, mesmo na rotina bagunçada da minha vida, fazerem-se presentes de alguma forma.

Por fim, agradeço à Fundação de Apoio à Pesquisa do Estado da Paraíba (FAPESQ) pela bolsa de doutorado, e à Coordenação de Aperfeiçoamento de Pessoal de Nível Superior

(CAPES), pelo apoio financeiro por meio da bolsa CAPES-PDSE de doutorado sanduíche no exterior, assim como todas as instituições que contribuíram com a minha formação: Universidade Estadual da Paraíba (UEPB), Universidade Federal da Paraíba (UFPB) e University of Bristol.

A todos que passaram pelo meu caminho e, de alguma forma, contribuíram para a conclusão desta etapa, muito obrigada!

RESUMO

Este estudo desenvolveu um modelo de ET, denominado *Enhanced and Spatial-Temporal Improvement of MODIS EvapoTranspiration* (ESTIMET), para monitoramento local e regional de ET nos trópicos, com base no modelo de evapotranspiração (ET) MOD16 original. As principais características distintivas do ESTIMET são fornecer um produto quase em tempo real com resoluções espacial (de 500 para 250 m) e temporal (de 8 dias para diária) aumentadas, minimizando lacunas na cobertura de nuvens e ajustando características tropicais específicas de diversos tipos de vegetação e microclima. Comparamos os resultados do ESTIMET com os produtos ET MOD16A2GF, PML_V2 e GLEAM 4.1a, usando dados de covariância de vórtices turbulentos (EC) de 14 locais no Brasil, distribuídos entre cinco biomas, bem como a ET anual baseada no balanço hídrico em 25 bacias hidrográficas brasileiras. As estimativas do modelo ESTIMET ainda foram utilizadas para analisar a variabilidade e tendências da ET nos últimos 20 anos em dois biomas brasileiros contrastantes (Caatinga e Pantanal) e em regiões com mudanças de uso do solo causadas pela ocorrência de incêndios e desmatamentos. No geral, as estimativas do ESTIMET capturaram as variações sazonais diárias dos dados de EC, especialmente nos biomas Caatinga, Pantanal e Cerrado, com coeficientes de correlação de concordância (ρc) variando de 0,45 a 0,80 em oito locais desses três biomas. As comparações da ET cumulativa de 8 dias com a ET das EC mostram que o modelo ESTIMET apresenta um ρc médio de 0,63, maior que o do MOD16A2GF (ρc = 0,58), do GLEAM 4.1a (ρc = 0,47) e do PML_V2 (ρc = 0,45). Da mesma forma, no balanço hídrico da bacia hidrográfica, o ESTIMET apresenta uma melhor representação da ET anual do que outros produtos de ET nos três principais biomas sul-americanos — Amazônia, Mata Atlântica e Cerrado —, que cobrem mais de 85% do território brasileiro. Além disso, a análise das estimativas da ET nos últimos 20 anos permitiu destacar que em ambos os biomas existem ciclos de variação da ET, com alta correlação com a variação da precipitação e tendência geral de redução da ET nos diferentes usos em ambos os biomas, bem como nas áreas de ocorrência de incêndios e desmatamento, indicando que características como disponibilidade de água e mudanças na cobertura vegetal são fatores importantes para explicar a variabilidade da ET neses ecossistemas. Assim, o ESTIMET melhora as estimativas de ET baseadas em sensoriamento remoto em biomas tropicais, operando em uma escala espaço-temporal e latência mais refinadas (ou seja, mensal) em todas as condições do céu e sendo capaz de representar a variabilidade da ET de superfície naturais e com mudanças antropogênicas ao longo de décadas.

PALAVRAS-CHAVE: Sensoriamento remoto, MODIS, Evapotranspiração, Brasil.

ABSTRACT

This study developed an ET model, namely the Enhanced and Spatial-Temporal Improvement of MODIS EvapoTranspiration (ESTIMET), for local-to-regional ET monitoring and applications in the tropics, based on the original MOD16 evapotranspiration (ET) model. The main distinguishing features of ESTIMET are providing a near-real-time product with increased spatial (from 500 to 250 m) and temporal (from 8 days to daily) resolutions, minimising gaps in cloud cover, and adjusting for specific tropical characteristics of diverse vegetation and microclimate types. We compared the results of ESTIMET with those of MOD16A2GF, PML_V2, and GLEAM 4.1a ET products, using eddy covariance (EC) data from 14 sites in Brazil, as well as the water balance-based annual ET estimates in 25 Brazilian catchments. The results obtained from the ESTIMET model were also used to analyse the variability and trends of ET over the past 20 years in contrasting Brazilian biomes (Caatinga and Pantanal) and in regions with land-use changes caused by the occurrence of wildfires and deforestation. Overall, the ESTIMET estimates captured the daily seasonal variations of the EC data, especially in the Caatinga, Pantanal, and Cerrado biomes, with concordance correlation coefficients (ρc) ranging from 0.45 to 0.80 at eight sites located in these three biomes. The comparisons of the 8-day cumulative ET show that the ESTIMET model exhibits a mean ρc of 0.63, greater than that of MOD16A2GF (ρc = 0.58), GLEAM 4.1a (ρc = 0.47), and PML_V2 (ρc = 0.45). Similarly, for the catchment water balance, ESTIMET exhibits a better representation of annual ET than other ET products in the three major South American biomes, i.e. the Amazon, Atlantic Forest, and Cerrado, which cover over 85 % of the Brazilian territory. In addition, the analysis of ET estimates over the past 20 years highlighted that both biomes exhibit ET variation cycles strongly correlated with precipitation variability, with a general trend of decreasing in different land uses in both biomes and in areas affected by wildfires and deforestations, indicating that factors such as water availability and changes in vegetation cover are important drivers in explaining ET variability in these ecosystems. Thus, ESTIMET improves remote sensing-based ET estimates in tropical biomes, operating at a finer spatiotemporal scale and with lower latency (i.e. monthly) under all sky conditions, and it is capable of representing the variability of ET in natural surfaces and under anthropogenic changes over decades.

KEYWORDS: Remote sensing, MODIS, Evapotranspiration, Brazil.

SUMMARY

LIST OF FIGURES

LIST OF TABLES

LIST OF SYMBOLS

A - Available energy ($W.m^{-2}$)
a, b, c - Regression coefficients obtained by comparing remote sensing and field measurements
C_L - Mean potential stomatal conductance per leaf unit area ($m\ s^{-1}$)
Cp - Specific heat capacity of air at constant pressure ($J\ kg^{-1}°C^{-1}$)
β – Bowen ratio
E - Estimated value
$\bar{E}$ - Estimated value mean
ET - Actual evapotranspiration (mm)
ETp – Potential evapotranspiration
ETr – Actual evapotranspiration
ETo – Reference evapotranspiration
λET – Latent heat flux
EC – Eddy covariance
EVI - Enhanced Vegetation Index
EVI2 - 2-band EVI
$EVI2_{max}$ - Signal from dense green vegetation (LAI → ∞)
$EVI2_{min}$ - Signal from bare soil (LAI → 0)
e_s - Actual vapour pressure (kPa)
e_a - Saturation vapour pressure (kPa)
ε_a - Atmospheric emissivity (unitless)
ε_s - Surface emissivity (unitless)
f_{wet} - Water cover fraction (unitless)
G- Soil heat flux (MJ/ day m²)
H – Sensible heat flux
K_c - Crop coefficient (unitless)
K_s - Water stress coefficient (unitless)
L - Adjustment factor for SAVI (unitless, here L=0.1)
LAI – Leaf area index
m - Number of tied groups
$m(T_{min})$ - Limiting factor of potential stomatal conductance for minimum air temperature (unitless)
m(VPD) - Limiting factor of potential stomatal conductance for high vapour pressure deficit (unitless)
N - Sample size
n - Number of observations
NDVI – Normalised Difference Vegetation Index
O - Observed value
$\bar{O}$ - Mean of observed values
P - Observed catchment-scale total annual precipitation (mm)
PM – Penman–Monteith model
PT – Priestley–Taylor model
ρc - Correlation coefficient
Q - Observed annual streamflow at the catchment outlet (mm)
RS – Remote sensing
R_n - Net radiation (MJ/ day m²)
r - Pearson correlation coefficient
r_1- Spectral reflectance of band 1 (red)

r_2 - Spectral reflectance of band 2 (near-infrared
ra - Aerodynamic resistance (s m^{-1})
rs - Surface resistance (s m^{-1})
$R_{S\downarrow}$ - Downward shortwave incoming radiation ($W.m^{-2}$)
S - Annual changes in catchment water storage (mm)
SAVI - Soil Adjusted Vegetation Index (unitless)
σ - Stefan–Boltzmann constant ($5{,}67x10^{-8}$ W m^{-2} K^{-4})
sign(x) - Sign function of x
T_{air} - Air temperature (°C)
u_2 - wind speed at 2 m height (m/s)
X_i - Observation at time i
X_j- Observation at time j
x, y - Values of variables x and y
x, y - Mean values of variables x and y
Δ - Slope of the saturation vapour pressure–temperature curve (kPa/°C)
γ - Psychrometric constant (kPa/ °C)
ρ - Air density ($kg.m^{-3}$)

1 INTRODUCTION

Evapotranspiration (ET) plays a crucial role in the global water cycle, serving as the primary pathway for water loss to the atmosphere. Accurately quantifying ET is essential for many purposes, including drought prediction, efficient irrigation, plant productivity, water management, and the elucidation of climate change processes (Hu et al., 2015; Machado et al., 2014; Liu et al., 2020; Ahamed et al., 2022; Silva et al., 2024.). ET can be measured through a variety of direct methods or estimated using indirect approaches, which include measurements using the eddy covariance (EC) technique, surface renewal, lysimeters, estimates from soil-water monitoring, and meteorological methods (Li et al., 2009; Silva et al., 2015; Melo et al., 2021; Silva et al., 2024). However, these ground-based monitoring techniques are costly and time-consuming (Luo et al., 2015; Grosso et al., 2018;). Furthermore, landscape-level techniques are limited by their spatial coverage, due to the large spatial heterogeneity of forests (Tang et al., 2013; Andrade et al., 2021; Khan et al., 2021; Melo et al., 2021). This means that the information obtained from these field-based approaches cannot be easily extrapolated to produce regional values of ET, which are essential for driving hydrological models and monitoring systems that allow stakeholders to make more effective decisions (Chen et al., 2005; Immerzeel and Droogers, 2008; Luo et al., 2015; Grosso et al., 2018; Ollivier et al., 2021).

To provide spatially distributed information on ET at a regional scale, remotely sensed observations by satellite sensors have become a viable solution in the past few decades (Kalma et al., 2008; Wang and Dickinson, 2012; Zhang et al., 2016; Laipelt et al., 2021; Bezerra et al., 2023). Data from various remote sensing methods are currently available and used to produce regionally distributed ET at different spatiotemporal resolutions (Tang et al., 2013; Chen and Liu, 2020; Filgueiras et al., 2020; Khan et al., 2021). The most common remote sensing-based methods include: (1) empirical models that relate ET to vegetation indexes or land-surface temperature (Petropoulos et al., 2009); (2) residual methods based on the energy balance equation, such as the Two-Source Energy Budget (TSEB) (Norman et al., 1995; Kustas and Norman, 1999), Surface Energy Balance Model for Land (SEBAL) (Bastiaanssen et al., 1998a), and Mapping Evapotranspiration at high Resolution and with Internalised Calibration (METRIC) (Allen et al., 2007); and (3) methods based on the application of traditional calculations, such as the Penman-Monteith (Cleugh et al., 2007; Mu et al., 2007, 2011) and Priestley-Taylor equations (Fisher et al., 2008; Jin et al., 2011; Wong et al., 2021).

The energy balance models, such as SEBAL, typically compute the instantaneous latent heat flux (energy equivalent to instantaneous ET) as a residual term of the energy balance equation, by estimating the other energy fluxes (Bastiaanssen et al., 1998b). Hence, SEBAL is arguably one of the most common, validated and precise techniques for estimating distributed ET from local to regional scales and at high spatial resolutions (Andrade et al., 2024). This is valuable for hydrological modelling purposes in small and medium-sized river basins. For instance, Biggs et al. (2016) highlighted that the implementation of SEBAL yields lower errors over regions smaller than 10,000 km² compared to larger regions, due to the model's moderate sensitivity to surface roughness. Although widely used and validated, regionally, for a large number of different environments worldwide (e.g. Bastiaanssen et al., 1998a; Timmermans et al., 2007; Teixeira et al., 2009; Allen et al., 2011; Silva et al., 2015; Bala et al., 2016; Grosso et al., 2018; Ferreira et al., 2020; Mohan et al., 2020; Costa-Filho et al., 2021; Laipelt et al., 2021; Liu et al., 2021; Bezerra et al., 2023), the SEBAL model still has some limitations with regards to applications on seasonal timescales. This is because: (1) a range of preliminary procedures are required to compute the sensible heat flux, which include the selection of calibration pixels (hot and cold) and the availability of two-level wind speed data from meteorological stations (Bezerra et al., 2023); (2) the high-dependency of surface temperature and emissivity parameters, obtained from thermal infrared satellite data, limits its application to clear-sky days (Bhattarai et al., 2019); and (3) the errors generated when the instantaneous ET values for the satellite passage-time are extrapolated to daily, monthly, or annual scales (Van Niel et al., 2012, 2011).

To overcome the complex procedures and data dependencies of the models based on the energy balance, Cleugh et al. (2007) developed a more straightforward approach using Penman-Monteith logic to estimate ET with data obtained from the MODerate Resolution Spectroradiometer (MODIS) sensor onboard the Terra and Aqua satellites. Subsequently, Mu et al. (2007; 2011) improved the method to generate the first ET global product using MODIS and reanalysis-derived meteorological inputs (MOD16). The MOD16A2 dataset provides ET information globally, with a spatial resolution of 500 m and three different timescales (8 days, monthly, and annual) (Running et al., 2017). For example, the 8-day data represents the sum of ET for all eight consecutive days. In 2023, MOD16 was upgraded to version MOD16A2GF, where linear interpolations were used to fill data gaps caused by cloud contamination in the 8-day Leaf Area Index/Fraction of Photosynthetically Active Radiation (LAI/FPAR, MOD15A2H product) and surface albedo (MCD43 product) images. This interpolation procedure occurs at the end of each year (Running et al., 2021).

Several studies have tested the accuracy of the MOD16 ET product in complex areas under distinct climatic and vegetation aspects worldwide, mainly using information from EC flux towers (Vinukollu et al., 2011; Ramoelo et al., 2014; Chen et al., 2014; Hu et al., 2015; Tang et al., 2015; Biggs et al., 2016; Aguilar et al., 2018; Khan et al., 2018; Filgueiras et al., 2020; Zhu et al., 2022). More specifically, in Brazil, several studies showed that the accuracy of the MOD16 product varies according to certain environmental characteristics, such as climate, land cover, and a combination of both, depending on the biome classification (Ruhoff et al., 2013; Souza et al., 2016; Maeda et al., 2017; Moreira et al., 2018; Melo et al., 2021; Dias et al., 2021; Biudes et al., 2022). For instance, the assessment carried out by Ruhoff et al. (2013), at two sites located in the Brazilian Cerrado biome, showed that the MOD16 product overestimated the mean ET (8-days, monthly, and annual) but no long-term over or underestimation was found for a sugar cane cropland area. Maeda et al. (2017) also showed that the MOD16 model was unable to consistently represent the seasonal patterns of the ET at a river basin scale in the Amazon Forest.

The limitations faced by the MOD16 ET product, especially for regional and local applications, are the land cover and atmospheric characterisations, which are made through the MODIS Land Cover Type (MOD12Q1) and the Modern-Era Retrospective analysis for Research and Applications (MERRA-2) products; these inputs to the model obtain canopy conductance and meteorological data, respectively (Running et al., 2017; 2021). The meteorological input data have 0.5° x 0.6° or 1.0° x 1.25° spatial resolutions, which are too coarse for accurate evaluations, especially in regions characterised by marked climatic gradients (Alvares et al., 2013). Parallel to this, MCD12Q1 may misidentify some local or regional vegetation characteristics and introduce significant errors in ET estimates (Ruhoff et al., 2013; Laipelt et al., 2021). Moreover, the original MOD16 model was restricted to being used in clear sky conditions until recently, as the orbital remote sensors cannot measure cloud base parameters (Sur et al., 2015; Running et al., 2017). Consequently, despite using the best observations during eight consecutive days, many grid cells of the MOD16 ET product were still contaminated by clouds, especially in tropical regions, presenting gaps in the ET time series (Running et al., 2017). This problem was partially solved when the product was recently upgraded to version MOD16A2GF, in which the cloud-contaminated pixels are filled through linear interpolation, a correction occurring at the end of each year. Nevertheless, this renders the MOD16A2GF no longer a near-real-time product because it can only be generated at the end of a given year (Running et al., 2021).

Several studies have been undertaken in parallel, attempting to modify the MOD16 ET model to overcome the limitations mentioned earlier (e.g. Morillas et al., 2013; Yeom et al., 2015; Ke et al., 2016; Wu et al., 2016; Srivastava et al., 2017; Ke et al., 2017; Chang et al., 2018; El Masri et al., 2019; He et al., 2019; Zhang et al., 2019; Brust et al., 2021; Dias et al., 2021; Astuti et al., 2022; Liu et al., 2022; Lu et al., 2022; Guo et al., 2023; Kumar et al., 2023). These modifications generally involve the following processes: (1) improve the spatiotemporal resolutions; (2) make adaptations for obtaining information for all sky conditions; and (3) implement local parameterisations, such as land use and land cover (LULC) information. All of these improvements used distinct adjustment approaches, but none covered all aspects together for a more operational data extraction at local and regional scales.

In this context, to address these limitations for local and regional applications in tropical areas, this study developed and evaluated the Enhanced and Spatial-Temporal Improvement of MODIS EvapoTranspiration model (ESTIMET). This model offers lower latency (currently annual for the monthly MOD16A2GF) and improved temporal (from 8 days to daily) and spatial (from 500 m to 250 m) resolutions. Obtaining these distributed, continuous, and accurate estimates of ET enables more precise trend analysis and correlation of this component with biotic and climatic parameters in complex regions, which can be more effectively utilised in hydrological modelling, water resource management, and agricultural practices.

1.1 Hypotheses

This thesis is based on the hypotheses that modifications of the MOD16 model, including the use of refined input remote sensing and reanalysis datasets, can improve the long-term (2003-actual) spatiotemporal representativeness of distributed ET estimations in heterogeneous tropical regions mostly covered by clouds, which can be more effectively utilised for time sensitivity analyses or applications.

1.2 Main aims

To propose and evaluate the ESTIMET (Evolution and Spatial- Temporal Improvement of MODIS EvapoTranspiration) model, able to consistently provide a finer spatial (250 m) and temporal (daily) variability of long-term (2003-present) ET for tropical biomes with low latency (monthly) when compared to the global current datasets.

1.3 Specific aims

- Adjust a more regional/local model to estimate distributed evapotranspiration in tropical climates, overcoming limitations related to frequent cloud cover;
- Evaluate the performance of the ESTIMET model in representative sites of the main biomes found in tropical climates;
- Analyse long-term (2003–present) trends in evapotranspiration and their correlations with precipitation and land use/land cover changes in contrasting tropical biomes; and
- Assess the potential of ESTIMET for temporal sensitivity analyses in regions experiencing vegetation cover degradation.

1.4 Thesis structure

The thesis is divided into six chapters. Chapter one presents a contextualisation and justification that motivated the development of this study, including the hypotheses and aims. Chapter two presents a literature review, covering conceptual and foundational topics related to ET and orbital remote sensing, which are essential for a better understanding of the study. Chapter three presents the physical characteristics of the region chosen for applying and validating the ESTIMET model. Chapter four describes the materials and methods used to develop the ESTIMET model, along with the results of its evaluation and comparison with other ET satellite-based products. Chapter five presents the long-term trend analyses of the ET estimated by ESTIMET in the Brazilian biomes, as well as the model's potential for sensitivity analyses. Lastly, the final chapter presents the study's conclusions and recommendations.

2 LITERATURE REVIEW

2.1 Evapotranspiration

Evapotranspiration (ET) is a critical process in hydrology that involves the conversion of water from the liquid phase to atmospheric vapour (Melo et al., 2021). This loss of water to the atmosphere occurs through the process of evaporation, which involves the transfer of water from various sources, including the soil surface, water bodies, and plants (Allen et al., 2021). Vegetation releases water to the atmosphere by evaporation and transpiration. The transpiration releases water through stomata. As evaporation and transpiration occur simultaneously, they are not easily distinguishable, being estimated as ET (Bezerra et al., 2023). The ET process is influenced by different hydrometeorological factors, including available energy, precipitation, wind, temperature, and humidity (Oliveira, 2012; Gusmão, 2017).

ET represents between 50 and 80% of precipitation, being the second largest flux in the hydrological cycle and playing a crucial role in the global water, carbon, energy, and nutrient cycles, directly influencing climate at different spatial scales (Valle Júnior et al., 2020; Vargas Godoy et al., 2021). Quantifying ET is essential for several sectors, including agriculture, reservoir management, meteorological and hydrological modelling, and flood forecasting (Oliveira, 2012; Lima et al., 2013).

ET was defined in three types to approximate the quantification process for estimations: potential evapotranspiration (ETp), which is the loss of water to the atmosphere from a natural vegetated surface without water limitations for soil evaporation and plant transpiration; actual evapotranspiration (ETr, , which occurs on vegetated surfaces under real atmospheric and water conditions; and reference evapotranspiration (ETo), which considers a hypothetical surface similar to green grass, with a height of 0.12 m, a plant resistance of 70 s m^{-1}, and an albedo of 0.23 (Allen et al., 1998; Camargo and Camargo, 2000). In this study, for simplicity, we use ET referring to actual evapotranspiration.

Quantifying ET is a major challenge in hydrological research due to its complex interactions with atmospheric properties, vegetation, soil, and topography (Zheng et al., 2016; Bhattarai et al., 2019). Various approaches, ranging from direct measurement techniques to indirect energy balance models using remotely sensed data, have been developed to estimate ET, keeping pace with technological and scientific advances (Allen et al., 2011; Bezerra et al., 2023). The direct collection of ET is a complex and expensive task,

because requires special facilities and equipment with high associated costs. Overall, this approach is reserved for specific experimental conditions and is mainly used to calibrate indirect ET estimation methods (Pereira et al., 1997; Gusmão, 2017), including:

1) Class A tank, which consists of a tank full of water exposed to the environment (Fig. 1). Changes in the water level are recorded daily, and these data are adjusted by the amount of precipitation measured at the same weather station during the same measurement period. This is a traditional method to estimates ETp, which is widely used because of its simplicity and low cost (Abtew and Melesse, 2013).

Figure 1 – A typical class A tank.
Source: NOAA (2005)

2) Lysimeters, which consist of impermeable tanks containing a volume of soil with certain vegetation, making it possible to monitor the variation of the mass of water in this sampled volume (Fig. 2) (Cunha et al., 2011; Abtew and Melesse, 2013). This method enables a more detailed analysis of the water balance terms (e.g. precipitation, irrigation, and drainage) to obtain ET as a residual component in the soil block. (Pereira et al., 1997). The use of lysimeters is generally limited to short crops due to the size of the sampled area, which lacks representativeness of plant diversity (Rana et al., 2005).

Figure 2 – Lysimeter Installation.
Source: UFRGS (2004)

3) Basin water balance, where ET is calculated as the difference between precipitation and streamflow, assuming no significant changes in soil water storage over long periods of time (Bezerra, 2023). Although widely used for regional ET estimates, this approach mostly provides average values for the studied area, not fully reflecting the spatial variability of ET (Zhang et al., 2016).

4) Scintillometers, which are instruments with a transmitter and receiver unit separated by a horizontal distance (102 to 104 m). These instruments measure small variations in the refractive index of the air caused by changes in temperature, humidity, and pressure that induce variations in air density, i.e. providing an average value of the sensible heat flux (H) for a contribution area ranging from 50 to 12,000 m² (Fig. 3) (Allen et al., 2011). However, obtaining ET makes the estimates of other energy balance necessary, such as net radiation (Rn) and soil heat (G), at the same measurement scale as H (Allen et al., 2011; Cunha et al., 2011; Allen et al., 2021). On the other hand, a microwave scintillometer enables the direct obtaining of the H and latent (λET) heat fluxes (Lobos-Roco et al., 2022).

Figure 3 - Microwave Scintillometer.
Source: OTT HydroMet (2016)

5) Turbulent vortex correlation (eddy covariance – EC), which is a technique to directly measure the fluxes of sensible and latent heat, CO2, and methane between the Earth's surface and the atmosphere, directly obtaining the λET for different surface types (Fig. 4). This is technique obtain an average value of ET for an area of up to 10 km², which varies depending on the wind at the time of measurement (Chu et al., 2021). EC is considered the most accurate method for estimating energy fluxes. At the same time, the EC technique is complex to implement due to the need for rapid response instruments and the challenges of operation, calibration, and maintenance (Baldocchi et al., 2001; Ruhoff, 2011). Although EC flux tower data are often used to validate ET estimates, they can present energy balance closure problems where the sum of heat fluxes does not adequately match net radiation, resulting in errors of up to 10-30% (Foken, 2008; Allen et al., 2011; Mu et al., 2011; Ruhoff et al., 2013).

Figure 4 - Eddy covariance sensors.
Source: AMERIFLUX (2022)

Given the complexity and cost associated with direct methods to measure ET, indirect and empirical methods are also used to estimate ET. Several models and methods have been developed over the years to estimate ET, differing in their concepts and the number of variables considered (Araújo et al., 2007; Gusmão, 2017). The indirect and empirical methods include:

1) Bowen's ratio, which uses the atmospheric variables and the energy available on the studied surface to calculate the ratio between heat flows, allowing estimations of ET (Bezerra, 2023). The ratio is based on the relationship between H and λET heat fluxes, expressed by the formula $\beta = H/\lambda ET$ (Bowen, 1926). The Bowen's ratio is theoretically simple and widely recognised as one of the most used methods for determining H and λET fluxes on a given surface (Shuttleworth, 2012; Allen et al., 2021).

2) Classical equations, which consist of using various specific equations formulated based on mass transfer, energy balance, or water balance principles to estimate ET (BRUSAERT, 2005). The most widely used equations in hydrology for calculating ET include the Penman-Monteith (Penman, 1948; Monteith, 1965), Priestley-Taylor (Priestley-Taylor, 1972), and Thornthwaite (Thornthwaite, 1948).

2) Remote sensing (RS) approaches, based on empirical spectral indices (e.g. vegetation indices) or energy balance measurements at the surface, mainly obtained from orbital sensors (Bezerra, 2023). The estimation of ET from RS data has been applied to capture the spatial

and temporal variability of ET over large and heterogeneous areas (Tang and Li, 2014; Fisher et al., 2017; Trebs et al., 2021).

2.2 Remote sensing techniques

Remote sensing techniques are based on the acquisition and measurement of information regarding objects, areas, or properties of specific phenomena through recording devices that operate without requiring direct physical contact (Read et al., 2020). This methodology enables the acquisition of a synoptic and multitemporal view of extensive portions of the Earth's surface, based on the use of sensors onboard artificial satellites in orbit. Remote sensing has become a widely employed strategy in environmental analyses and monitoring (Souza et al., 2022). The field of remote sensing applications is vast, encompassing a range of applications, from agriculture (Li et al., 2023) and water resource management (Zegait et al., 2024) to land use and land cover mapping (Coelho et al., 2014) and climatology (Godoy and Markonis, 2023). This technology is essential for detecting and monitoring changes on the Earth's surface, resulting from both natural processes and anthropogenic activities (Binetti et al., 2023).

The transmission of information between Earth's surface objects and onboard satellite sensors occurs at the speed of light through electromagnetic radiation waves (Racetin and Krtalić, 2021). This radiation can be arranged according to its wavelength or frequency, which comprises the electromagnetic spectrum that ranges from gamma rays, x-rays, ultraviolet, visible light, infrared (near-, mid-, and far-infrared), microwaves, to radio waves. The most widely used regions of the electromagnetic spectrum for collecting environmental information of the Earth's surface include the microwaves ($\approx 10^8$ μm), the visible light (0.4 – 0.7 μm), and the infrared spectra (Fig. 5) (Schumann and Moller, 2015). Active sensors use the microwave bands, while passive sensors primarily use the visible and infrared spectrums.

When electromagnetic radiation from the Sun reaches the Earth's surface, its intensity is partially or totally reduced due to interactions with atmospheric constituents, including water vapour (H_2O), oxygen (O_2), ozone (O_3), and carbon dioxide (CO_2), among others. These gases play a fundamental role in the absorption of electromagnetic radiation, making it impossible to use some wavelengths obtained by passive sensors for collecting information about the Earth's surface from space (Golubkov et al., 2018). However, the visible and some infrared spectral regions present less interference from these gases, where

solar radiation transmission occurs more efficiently, consequently favouring the acquisition of the Earth's surface data from orbital sensors (Wang et al., 2021).

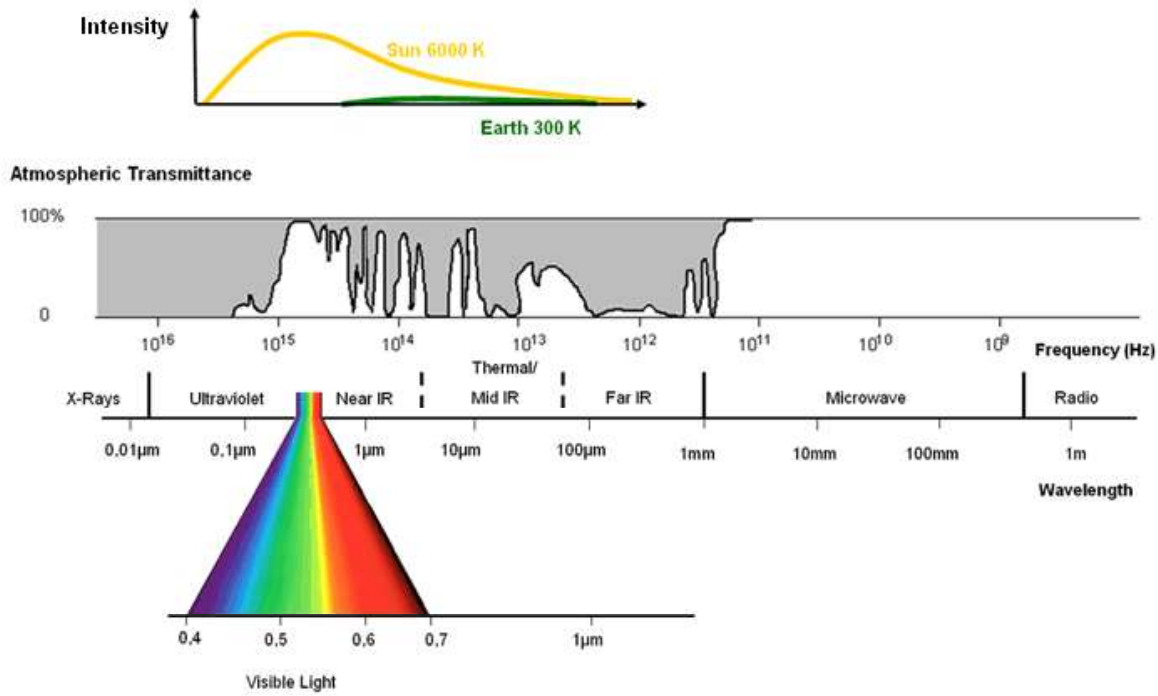

Figure 5 - The electromagnetic spectrum and atmospheric transmittance.
Source: Albertz (2007)

When the electromagnetic radiation interacts with the Earth's surface, it can be partially transmitted, reflected, or absorbed, with proportions varying according to the physical, chemical, and biological characteristics of the materials. Only the reflected shortwave radiation can be directly detectable by sensors and converted into processable electrical signals. The absorbed fraction is re-emitted in long waves by the surface as a result of thermal processes and/or dissipated in the form of heat, whose re-emission can also be detectable by passive sensors operating in the far-infrared (i.e. thermal infrared) spectrum (Farella et al., 2022). Changes in the reflectance and emittance signals, detected by passive sensors, point to physicochemical and biological modifications in natural and/or anthropogenic resources.

The radiation is captured and recorded by remote sensors according to four fundamental detection capabilities: spectral, spatial, radiometric, and temporal resolutions (Som-ard et al., 2021). The spectral resolution corresponds to the number and width of wavelength intervals (bands) that the sensor can discriminate, directly influencing its efficiency in distinguishing targets with similar spectral responses (Fig. 6). The spatial resolution defines the level of geometric detail of the image, being represented by the

smallest unit of the Earth's surface individualised by the sensor, i.e. higher spatial resolutions enable the identification of smaller features and subtle structures. The radiometric resolution refers to the sensitivity of the detection system in recording variations in the intensity of radiation reflected and/or emitted by targets, expressed by the number of binary digits (bits) available to quantify the energy recorded in each pixel. Lastly, the temporal resolution corresponds to the revisit frequency of the sensor to obtain data for the same region of the Earth's surface, i.e. a determining parameter for continuous and multitemporal monitoring of dynamic phenomena (Kakic and Kuenzer, 2022).

Despite being a powerful tool for environmental monitoring on large scales, orbital remote sensing presents limitations caused by cloud cover, scale factors, and low data acquisition frequency (Prudente et al., 2020).

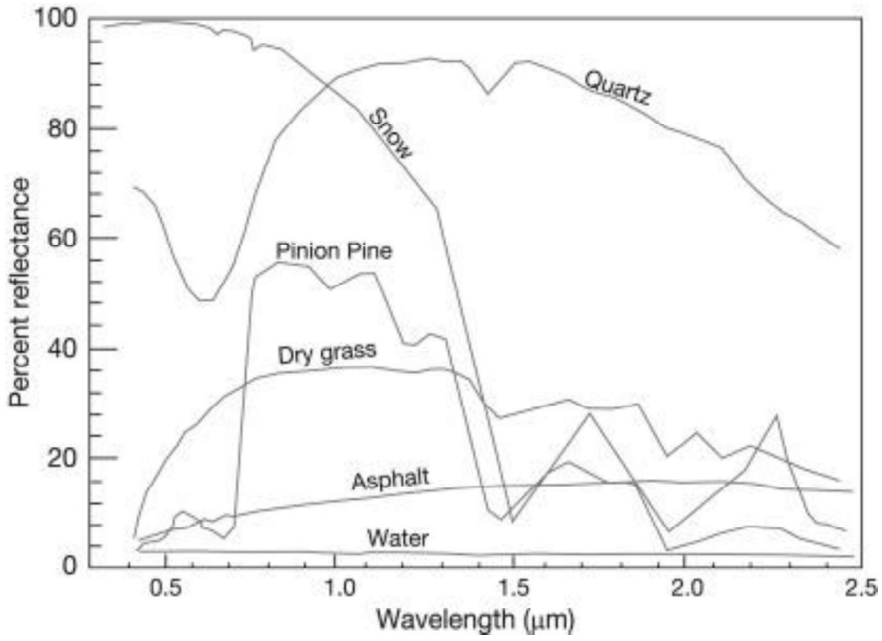

Figure 6 - Spectral responses for selected features.
Source: Horning (2019)

2.3 Evapotranspiration by remote sensing

The electromagnetic radiation reflected or emitted by Earth's surface and registered by remote sensors has been used to spatially estimate ET in large and heterogeneous areas, filling the gap left by direct measurements, which are punctual and only represent regions with homogeneous coverage (Andrade, 2023). Remote sensing data is essential for

understanding the factors that regulate ET, including radiative, atmospheric, and phenological aspects (Bezerra, 2023).

Several remote sensing products have been provided by applying these models to data obtained through remote sensing and field measurements, as listed in Table 1. The availability of these products is a significant advancement in hydrometeorological research, particularly in areas with limited data. However, it is crucial to assess the accuracy of these products on a local scale before conducting the study.

The integration of remote sensing data into ET modelling has significantly enhanced the understanding of hydrological processes at various temporal and spatial scales. However, some challenges persist, such as the dependence on cloud-based image availability and the management of large volumes of data (Gowda et al., 2008; Mu et al., 2011; Ruhoff et al., 2012; Chen and Liu, 2020; Andrade et al., 2021). Planetary-scale platforms for Earth science data and analysis, like Google Earth Engine (GEE), have made powerful cloud-based processing resources accessible to everyone, promoting innovation and the use of advanced techniques, including machine learning models to improve ET estimates (Lary et al., 2016; McCabe et al., 2017; Käfer et al., 2020; Andrade et al., 2021).

Over the past years, several models using satellite-based remote sensing data have been developed and successfully applied to estimate spatially distributed ET rates. However, none of these models is fully comprehensive, as they need to be adapted to different climatic conditions and local characteristics (Li et al., 2009; Allen et al., 2011; Chen and Liu, 2020; Seibert and Berstrom, 2022). These ET models can be categorised into two main remote sensing approaches. The first approach considers land surface temperature from far-infrared, while the second is based on vegetation indices using shortwave sensors (visible and near-infrared) (Andrade, 2023).

Models that use satellite-retrieved surface temperature are based on the surface energy balance (SEB) fluxes, which are known as SEB models. These models rely on selecting boundary conditions in pixels where ET is zero or potential, where a fraction of evapotranspiration for each pixel is calculated based on its land surface temperature value in relation to the extremes. The main models in this category are: Surface Energy Balance Index (SEBI) (Menenti and Choudhury, 1993), Two-Source Energy Budget (TSEB) (Norman et al., 1995; Kustas and Norman, 1999), Surface Energy Balance Model for Land (SEBAL) (Bastiaanssen et al., 1998), Mapping Evapotranspiration at high Resolution and with Internalised Calibration (METRIC) (Allen et al., 2007); Atmosphere-Land Exchange Inverse (ALEXI) (Anderson et al., 1996), Simplified Surface Energy Balance Index (S-

SEBI) (Roerink et al., 2000), Surface Energy Balance System (SEBS) (Su, 2002), Atmosphere-Land Exchange Inverse flux disaggregation approach (DisALEXI) (Norman et al., 2003). Although widely used, these models have limitations in large-scale applications and operationalisation due to subjectivity in the selection of boundary conditions, which makes extrapolations to larger areas uncertain (Senay et al., 2013; Liou and Kar, 2014). Ruhoff et al. (2012) highlight that the SEBAL model is a promising tool for determining energy fluxes in cloudless conditions. However, estimating energy fluxes on cloudy days remains a challenging yet crucial task for obtaining accurate seasonal, monthly, and annual ET projections.

SEBAL is one of the most common SEB models. Bezerra et al. (2023) developed the Seasonal Tropical Ecosystem Energy Partitioning (STEEP) model, which is an adaptation of SEBAL for applications in seasonally dry tropical forests. The application of STEEP to the Caatinga region in Brazil achieved comparable or superior performances to the original SEBAL and some global ET products (MOD16 and PMLv2), representing a significant improvement where ET is typically overestimated in this region by SEBAL. However, the model has limitations in spatial representation, as it was applied and evaluated only in the Caatinga region, which limits its generalizability to other tropical biomes. Furthermore, its implementation depends on the availability of high-quality satellite imagery, a factor that may limit the model's operational applicability in tropical regions with high cloud cover.

Andrade et al. (2024) developed the geeSEBAL-MODIS for monitoring climate change and anthropogenic impacts of ET in different biomes in Latin America. geeSEBAL-MODIS resulted in a 13% error reduction at the local scale and a 30% error reduction at the basin scale. However, the study also has limitations in terms of temporal continuity. geeSEBAL-MODIS still relies on cloud-free satellite images, which results in the exclusion of rainy or transitional days, or even months, generating temporal gaps and greater uncertainties in tropical regions with high cloud frequency.

On the other hand, models based on vegetation indices (e.g. leaf area index LAI; normalised difference vegetation index, NDVI; Soil-Adjusted Vegetation Index, SAVI), surface albedo, and land use and land cover classification are used to obtain the resistance terms in the Penman-Monteith (PM) (Monteith, 1965) or Priestley-Taylor (PT) (Priestley and Taylor, 1972) equations.

PM models provide a comprehensive solution for SEB and mass transport, while PT models simplify the PM approach by replacing the mass transport component with an empirical value that depends on the local climate (Monteith, 1965; Priestley and Taylor,

1972). With the advancement of computational technology and the availability of space-based remote sensors, the PT approach has become increasingly feasible. The main model based on the PT methodology is the Priestley-Taylor Jet Propulsion Laboratory (PT-JPL) (Fisher et al., 2008), developed from the integration of concepts and improvements present in previous models, such as Global Land Evaporation Amsterdam Model (GLEAM) (Miralles et al., 2011), MOD16 (Mu et al., 2011), Penman-Monteith-Leuning (PML) (Leuning et al., 2008), and Breathing Earth System Simulator (BESS) (Ryu et al., 2011). However, although models based on the PT approach are widely used because they are simpler and faster, they still have some limitations. The PT-JPL model relies on empirical parameters and adjustments made for specific regions, meaning it cannot always accurately represent ET variations, especially in areas with highly varied vegetation or extreme climatic conditions (Fisher et al., 2008). Thus, due to the existing gaps identified in previous models, this research focuses on developing a model based on the Penman-Monteith logic.

Table 1 - Summary of global orbital remote sensing-based products that estimate ET.

Name	Description	Principle	Spatial resolution	Spatial Coverage	Temporal Resolution	Temporal Coverage	Reference
PML v2. 0.1.7	Penman-monteith-leuning evapotranspiration v2	Penman-monteith	500 m	Global	Daily	1981- present	Zhang et al. (2016); Gan et al (2018); Zhang et al. (2019).
MOD16A2 GF.061	Terra Moderate Resolution Imaging Spectroradiometer (MODIS) Version 6.1	Penman-monteith	500 m	Global	8 days	1981- present	Running et al. (2021)
GLEAM **v3**	Global Land Evaporation Amsterdam Model	Priestley-Taylor	0.25°	Global	Daily	1980–2022	Miralles et al. (2011); Martens et al. (2017)
ALEXI	Atmosphere-Land Exchange Inverse	Two-source energy balance	0.05°	Global	Daily	2002–2019	Anderson et al. (1997)
FLDAS-Global	Famine Early Warning Systems Network (FEWS NET)	Datasets derived from satellite measurements and atmospheric analyses	0.1°	Global	Mensal	1982 - present	McNally et al. (2017)
GLDAS2.1	Global Land Data Assimilation System	forced with a combination of model and observation data	0.25°	Global	with 3-h	2000 - present	Rodell et al. (2004)
ERA5-Land	ECMWF Reanalysis 5	Reanalysis combines model data with observations from across the world into a globally complete and consistent dataset using the laws of physics	0.1º	Global	hourly	1950 - present	Muñoz (2019)

SSEBop v. 4	Simplified Surface Energy Balance	Simplified surface energy balance	1 km	Global	Monthly	2003- present	Senay et al. (2013); Senay et al. (2020)
BESS	Breathing Earth System Simulator	Biophysical process-based model	5 km	Global	8 days	2000-2016	Ryu et al. (2011); Jiang and Ryu (2016)
Terra Climate	Monthly Climate and Climatic Water Balance for Global Terrestrial Surfaces	One-dimensional water balance, modified Thornthwaite-Mather equation	2.5 arcmin	Global	Monthly	1958-2023	Abatzoglou et al. (2018)

2.4 Evapotranspiration models based on Penman-Monteith logic

The FAO (Food and Agriculture Organisation) Penman-Monteith method uses both the energy balance and mass transport to calculate ET of a reference crop surface (ETr) (Allen et al., 1998; ASCE-EWRI, 2005), combining crop (kc) and soil (ks) water stress coefficients to determine daily ET using Equations 1 and 2.

$$ET = K_s \, x \, K_c \, x \, ET_r \tag{1}$$

$$ET_r = \frac{0.408 \, \Delta(R_{n24h} - G_{24h}) + \frac{1600}{T_{air24h} + 273.15} x \, \gamma \, x \, u_{2\,24h}(e_{s\,24h} - e_{a\,24h})}{\Delta + \gamma(1 + 0.38 \, u_{2\,24h})} \tag{2}$$

where R_{n24h} is the daily net radiation (MJ/ day m²), G_{24h} is the daily soil heat flux (MJ/ day m²), T_{air24h} is the daily mean air temperature (°C); γ is the psychrometric constant (kPa/ °C), $u_{2\,24h}$ is the daily mean wind speed (m/s) at 2 m height; $e_{s\,24h}$ and $e_{a\,24h}$ are the saturation and the actual vapour pressure for the daily time step (kPa), and Δ is the slope of the saturation vapour pressure-temperature curve (kPa/°C).

As previously mentioned in item 2.3, the Penman-Monteith logic was used to develop three well-known and widely used satellite-based products to estimate ET: PML, which calculates surface conductance using LAI (Leuning et al., 2008); BESS, which calculates ET for both soil and plant canopy, as well as estimates gross primary productivity (Ryu et al., 2011); and MOD16, which uses vegetation indices and surface characteristics, along with meteorological information (Mu et al., 2011).

PML is a diagnostic model used to estimate ET and gross primary productivity through a simplified biophysical approach. The model couples carbon and water flows through the canopy conductance used in the PM equation. PML is practical as it requires only a few data, including LAI from MODIS sensors and meteorological information, making it applicable on a large spatial scale and over the long term (Gan et al., 2018). The product PML V2 provides global daily ET estimates with 500-m spatial resolution from 1981 to the present.

BESS is a simplified process-based model that integrates atmospheric and canopy radiative transfers, canopy photosynthesis, transpiration, and energy balance. At a global scale, this system continuously monitors and maps carbon and water fluxes using atmospheric and land data from MODIS and other satellite sources, with spatial and temporal

resolutions of 1-5 km and 8 days, respectively (Table 1) (Ryu et al., 2011). BESS is a simplified model that couples a one-dimensional atmosphere radiative transfer module, a two-leaf canopy radiative transfer module, and an integrated carbon assimilation-stomatal and conductance-energy balance module (Jiang and Ryu, 2016). The model uses MODIS information to calculate radiation, temperature, and humidity data, which triggers land surface modules. Ryu et al. (2011) showed that GPP and ET estimates from BESS presented good performance when compared to observed flows in various land cover types and climate zones (arctic and tropical).

MOD 16 uses reflectance data from MODIS and climate information from MERRA (Modern-Era Retrospective analysis for Research and Applications) to calculate ET as the sum of soil evaporation (Es), canopy transpiration (Tc), and wet canopy evaporation (Ec) (Fisher et al., 2008). Mu et al. (2007) proposed the model, which was improved by Mu et al. (2011) to include soil heat flux (G) and restrictions on stomatal conductance. Further subtle updates were carried out by Running et al. (2019, 2021). The latest version of the MOD16 product is currently available with a spatial resolution of 500 m, providing 8-day cumulative values of ET. MOD16 is a single, advanced and accurate approach to estimating ET without requiring specific data for parameterisation (Melo et al., 2021). However, Ruhoff et al. (2013) found underestimations of ET related to misclassifications of land-use and land-cover input data. Despite this, the MOD16 remains a crucial tool for hydrological studies on both global and regional scales.

2.5 Application, evaluation and improvement studies of the MOD16 evapotranspiration model

Several studies have tested the accuracy of the MOD16 ET product in complex areas under distinct climatic and vegetation aspects worldwide, mainly comparing ET estimates obtained from EC flux towers (e.g. Vinukollu et al., 2011; Chen et al., 2014; Ramoelo et al., 2014; Hu et al., 2015; Tang et al., 2015; Biggs et al., 2016; Aguilar et al., 2018; Khan et al., 2018; Filgueiras et al., 2020; Zhu et al., 2022). These studies provided contrasted evaluations. While Vinukollu et al. (2011), Chen et al. (2014), Hu et al. (2015), Aguilar et al. (2018), Chen et al. (2020), Li et al. (2021) showed satisfactory agreements with local ground-truth data, other studies observed some inaccuracies in different ecosystems (e.g. Ramoelo et al., 2014; Tang et al., 2015; Autovino et al., 2016; Du and Song, 2018; Khan et al., 2018; Zhu et al., 2022). More specifically in Brazil, Ruhoff et al. (2013), Souza et al.

(2016), Maeda et al. (2017), Moreira et al. (2018), Melo et al. (2021), Dias et al. (2021), Biudes et al. (2022) showed that the accuracy of the MOD16 product varies according to some characteristics, such as climate, biome, and land cover. For instance, the assessment carried out by Ruhoff et al. (2013) in two sites located in the Brazilian Cerrado biome showed that the MOD16 product overestimated the mean ET (8-day, monthly, and annual), while no long-term over- or underestimation was found for a sugar cane cropland area. Maeda et al. (2017) also demonstrated that the MOD16 model was unable to consistently represent ET seasonal patterns at the river basin scale in the Amazon Forest.

Recently, studies proposed some trajectories of improvements of the MOD16 ET model for overcoming the limitations and operating at a regional scale and consistently with its local characteristics (e.g. Morillas et al., 2013; Sur et al., 2015; Yeom et al., 2015; Ke et al., 2016; Wu et al., 2016; Srivastava et al., 2017; Ke et al., 2017; Chang et al., 2018; El Masri et al., 2019; He et al., 2019; Zhang et al., 2019; Brust et al., 2021; Dias et al., 2021; Astuti et al., 2022; Liu et al., 2022; Lu et al., 2022; Guo et al., 2023; Kumar et al., 2023). These modifications mainly include the following processes: (1) changes in the spatiotemporal resolutions; (2) adaptations to obtain information for all sky conditions; and (3) implementation of local parameterisations, such as land use and land cover information (Table 2). All these improvements employed distinct adjustment approaches, but none of them addressed all aspects simultaneously for a more effective extraction of data at local and regional scales. Such modifications covering all aspects together may enable a more detailed and continuous long-term analysis of ET in Brazil, considering that the patterns and factors of this component remain poorly understood, especially in tropical regions (Fleischmann et al., 2023).

Table 2 - Summary of studies with enhancements of the MOD16 evapotranspiration model to fit more local and regional characteristics.

Study	Region	Enhancements
Jang et al. (2013)	Northeast Asia	Use of surface meteorological data from the Korea Land Data Assimilation System (KLDAS) and MODIS to facilitate continuous regional ET estimates.
Di et al. (2015)	United States	A combination of two layers of soil relative humidity parameters with a surface resistance model.
Yeom et al. (2015)	South Korea	Application of a multilayer feed-forward neural network approach with Levenberg–Marquardt back propagation (LM-BP), using input from various satellite-based products of ET, NDVI, NDWI, land surface temperature, air temperature, and insolation.
Srivastava et al. (2017)	Kangsabati River Basin, India	Use indirect ET estimation methods, such as MODIS and the water budget approach, incorporated into the semi-distributed variable infiltration capacity (VIC-3L).
Baik et al. (2018)	Australia	Applies two mixing approaches, Maximise R and simple Taylor skill's score, to generate a fused ET product using combinations of the GLDAS, GLEAM, MOD16, and MERRA datasets.
Chang et al. (2018)	China	Integration of wind speed and vegetation height to estimate aerodynamic resistance, using the Fisher et al. method. (2008) to constrain temperature and humidity for stomatal conductance and reduce soil evaporation uncertainties.
He et al. (2019)	United States (CONUS)	Calibration for agricultural land, model parameters according to crop types and incorporation of finer-scale satellite vegetation data.
Zhang et al. (2019)	Global	Application of the sensitivity analysis method, combined with the Markov chain method of differential evolution, for each key parameter in a variety of biomes, to obtain an optimised model.
Dias et al. (2021)	Brazil	Use of 8 regression algorithms (multiple linear regression, random forest, cubist, partial least squares, principal components regression, adaptive forward-backwards greedy, generalised boosted regression, and generalised linear model by likelihood-based boosting) and machine learning.
Brust et al. (2021)	United States	Use of SMAP soil moisture to constrain ET and local observations to calibrate ET.
Astuti et al. (2022)	Brantas river basin, Indonesia	Application of an artificial neural network and machine learning to characterise the spatiotemporal patterns of ET in the basin.
Liu et al. (2022)	Central China	Integrates NDWI as a soil moisture adjustment, enhancing the estimation of soil surface resistance and stomatal conductance.
Lu et al. (2022)	Three different scenic areas in China	Spatial downscaling based on the correlation between surface ET differences and corresponding land cover types and spectral mixture analysis theory.
Xue et al. (2022)	South Korea, Japan, China, the Philippines, India, Spain, Italy, and the USA	Sensitivity analysis of the MOD16 model and parameter optimisation strategies (Radiation and temperature, and LAI and Rn).

Guo et al. (2023)	China	Restrictions of moisture based on the ratio of antecedent accumulated precipitation to soil evaporation balance.
Kumar et al. (2023)	Kangsabati River Basin (India)	Use of a Genetic Algorithm (GA), inspired by natural selection, to determine whether a string will participate in the reproduction process, and thus improve the fit to local conditions.

3 STUDY AREA CHARACTERISTICS

The ESTIMET model was applied to the entire Brazilian territory and evaluated in different parts of the country. Brazil covers approximately 8.5 million km² between coordinates 5°16′N-33°45′S and 34°47′W-73°59′W (Fig. 7). According to Alvares et al. (2013), Brazil has twelve different Koppen climate types, divided into three main zones: Tropical (Zone A), Semi-arid (Zone B), and Humid Subtropical (Zone C). Moreover, six terrestrial biomes are featured in the territory, namely: Amazon Forest (rainforest, 49% of land area), Cerrado (wooded savannah, 24% of land area), Atlantic Forest (13% of land area), Caatinga (tropical dry forest, 10% of the land area), Pantanal (tropical wetland, 2% of the land area), and Pampa (grassland, 2% of the land area) (Roesch et al., 2009) (Fig. 1a). The mean annual rainfall in Brazil ranges from 380 (Caatinga) to 4000 mm (Amazon Forest), while the mean annual air temperature ranges from below 10 °C to greater than 26 °C (Gadelha et al., 2019).

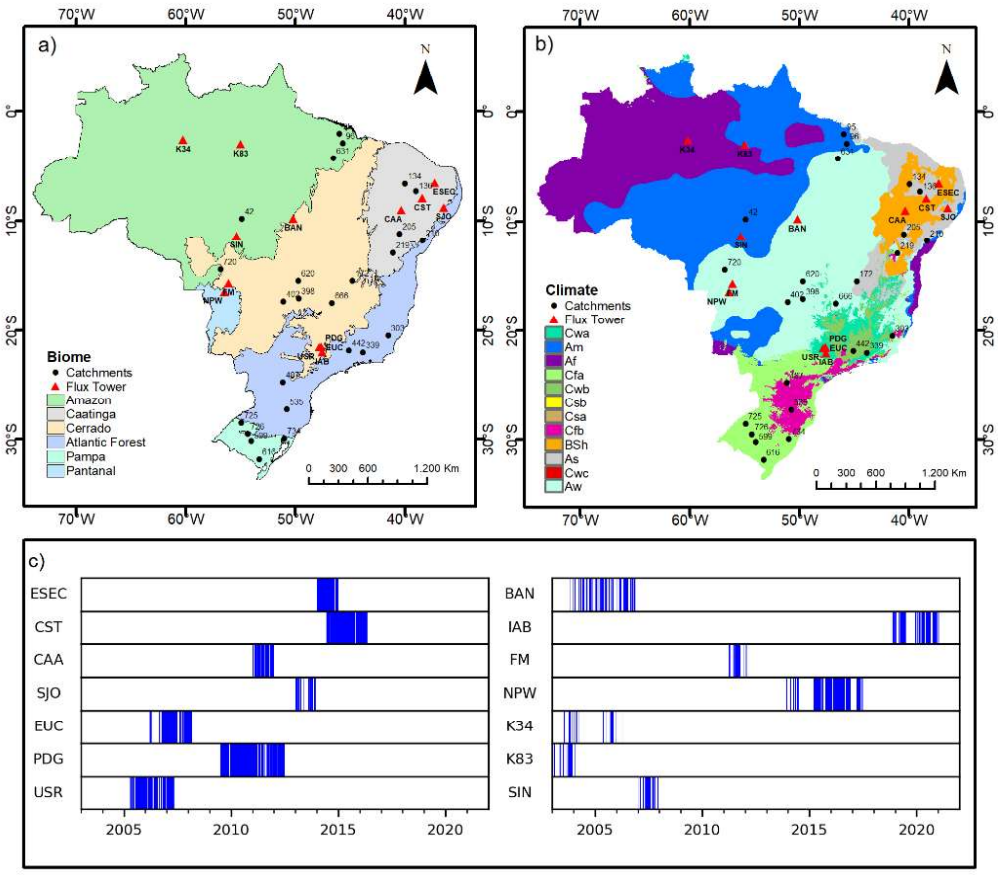

Figure 7 - (a) Brazilian biomes and (b) Köppen climate classification for Brazil, according to Alvares et al. (2013), showing the spatial distribution of the 14 eddy covariance flux towers (red triangles) and the 25 catchments (black dots) used for this study. (c) Data availability in the flux towers.

This variety of biomes not only contributes to the ecological richness but also plays a crucial role in maintaining carbon stocks in its forests and soils, as well as in global freshwater reserves (Berenguer et al., 2014; Bernoux et al., 2002). In recent decades, Brazilian biomes have undergone significant spatiotemporal changes in terms of land use, with emphasis on the replacement of natural vegetation by livestock and agricultural activities (Souza et al., 2020). Considering the role of Brazil as a major producer of agricultural commodities and one of the largest contributors to global greenhouse gas emissions due to these activities (Sousa-Neto et al., 2017; Cait, 2024) these changes have significant implications for biodiversity, water resources, carbon emissions, and climate change (Butchart et al., 2010; Davidson et al., 2012; Verburg, 2015).

The impact of the land-use and land-cover changes can be observed by analysing contrasting biomes in terms of water availability. On the one hand, Pantanal is a large wetland, while Caatinga is a biome located in a semiarid region with water scarcity. In recent decades, these biomes have experienced pressure on the hydrological cycle due to land-use and land-cover conversion, with impacts on water availability. While Caatinga presented the highest rate of surface water reduction, with an annual average of -5.1% in the 2010s, the Pantanal biome has shown the greatest variation, with an increase in surface water of an average of 5% per year after 2005 (Souza et al., 2020).

Despite being predominantly covered by primary forests, the Caatinga biome is highly threatened by land conversion for agriculture, with deforestations that degrades the environment and worsen the risk of desertification (Araújo et al., 2023; Costa et al., 2024; Rocha et al., 2024). Similarly, the Pantanal is under increasing pressure due to the expansion of livestock and sugarcane cultivation, as well as the frequent occurrence of wildfires. (Guerra et al., 2020; Hernandes et al., 2022; Galvanin and Caldas; 2025).

Livestock farming and the expansion of sugarcane drive deforestation, pasture conversion, hydrological alteration, soil carbon loss, increased fire susceptibility, and landscape fragmentation in the Pantanal, with cascading impacts on habitat, species composition, and ecosystem services. Governance and policy gaps hinder effective conservation.

Caatinga is a semi-arid climate biome with a unique biodiversity located in northeastern Brazil (Rocha et al., 2024). The region is mainly characterised by the hot and dry climate BSh (Fig. 2), with low precipitation typically concentrated in a period of 3 to 6 months (300 to 800 mm/year) and dry periods that can last more than 11 months per year, facing challenges with water scarcity caused by intermittent rivers and irregular rainfall

(Miranda et al., 2018; Bezerra et al., 2023). In addition, high temperatures (26° to 30°C) and high potential ET rates (1,500 to 2,000 mm/year) are commonly observed in Caatinga (Moro et al., 2016; Miranda et al., 2018; Paloschi et al., 2020). The region presents diverse physiognomies, ranging from forests to sparse shrublands, composed mainly of xerophytic, woody, and thorny species, as well as deciduous physiognomies adapted to heat and drought (Silva et al.,2017; Sampaio, 1995; Bezerra et al., 2023).

Pantanal is considered one of the most significant wetlands in the world, with high landscape and ecological diversity (Alho and Sabino, 2011; Bergier, 2013). The region presents well-defined dry and rainy seasons, characteristic of the Aw climate, with flood cycles that are crucial to its ecology (Fig. 2). In the Pantanal, the hydrological cycle is characterised by a high rainfall index, contributing to river flow and evapotranspiration, which account for half of the total flow (Hamilton, 2002; Valeriano et al., 2012). The vegetation in this biome is characterised by the presence of forests, savannas, and wetlands. Livestock, tourism, fishing, and mining are significant economic activities in Pantanal (Seidl, 2001; Alho and Sabino, 2011). In this study, the analyses were carried out based on the biome division proposed by IBGE (2004).

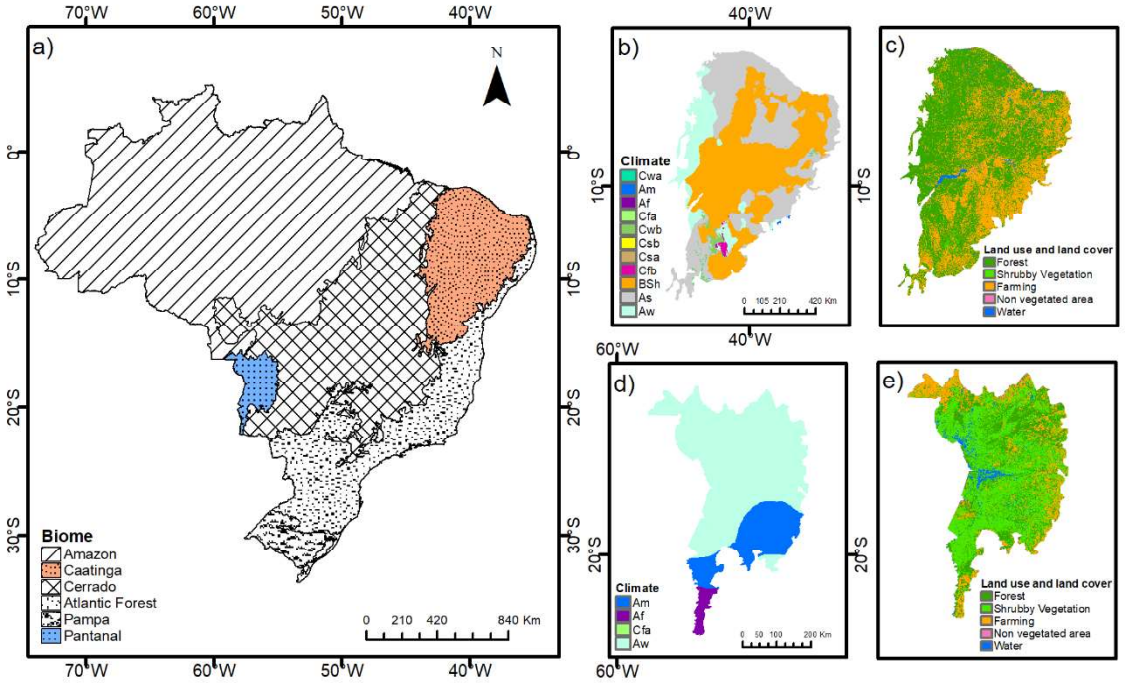

Figure 8 - (a) Brazilian biomes and Köppen climate classification for (b) Caatinga (d) Pantanal according to Alvares et al. (2013), land use and land cover for (c) Caatinga and (e) Pantanal according to MapBiomas (2025).

4 DEVELOPMENT AND EVALUATION OF THE ESTIMET MODEL

4.1 Contextualisation

In this chapter, we focus on the development and validation of the ESTIMET (Enhanced and Spatial-Temporal Improvement of MODIS EvapoTranspiration) model, which uses reflectance data from the MODIS sensors (MOD and MYD), land use and land cover data from the MapBiomas initiative, and climate reanalysis (ECMWF Climate Reanalysis-ERA5-Land and Global Land Data Assimilation System - Noah - GLDAS 2.1) data as input to the adapted MOD16 model based on the Penman-Monteith equation. Thus, the general and transferable strategy of this new model takes into account: (a) fitting a more regional/local model by using LULC adjusted to the vegetation characteristics in Brazil; (b) overcoming data loss due to frequent cloud cover, whilst reducing the latency period to provide a near-real-time product; (c) modifying the stomatal conductance and net incoming radiation parameterisation schemes to generate a new product at a daily time scale (currently being accumulated for 8 days with the MOD16A2GF) for all sky conditions; (d) enhancing the spatial resolution of the MOD16A2GF ET product (from 500 to 250 m); and (e) changing the meteorological forcing dataset to high-quality data for accurate flow estimates, differentiating microclimates. The entire model was developed and processed on the cloud-based platform Google Earth Engine (GEE).

4.2 Materials and methods

4.2.1 Development of the ESTIMET model

MOD16 ET, and its adaptation under the ESTIMET model, is based on the Penman-Monteith equation (Monteith, 1965; Mu et al., 2011). Both models estimate the latent heat flux density (λE; W m^{-2}), allowing for the calculation of the total daily ET (mm) from the conversion factor, corresponding to the sum of evaporation from the wet canopy surface (λEwet), the transpiration from vegetation with a dry surface (λEtrans), and the soil evaporation (λEsoil) (Mu et al., 2011; Running et al., 2017) (Eq. 3):

$$\lambda E = \lambda E_{wet} + \lambda E_{trans} + \lambda E_{soil} = \frac{sA+\rho C_p(e_s-e_a)/r_a}{\Delta+\gamma(1+\frac{r_s}{r_a})} \quad (3)$$

where Δ is the slope of the curve relating saturated water vapour pressure to temperature (kPa $^{o}C^{-1}$), A is the available energy ($W.m^{-2}$), ρ is the air density ($kg.m^{-3}$), Cp is the specific heat capacity of air at a constant pressure (J kg-1 $°C^{-1}$), ea is the actual water vapour pressure (kPa), es is the saturated water vapour pressure (kPa), rs is the surface resistance ($s\ m^{-1}$), ra is the aerodynamic resistance ($s\ m^{-1}$), and γ is the psychrometric constant (kPa $°C^{-1}$).

Similar to Mu et al. (2011), ESTIMET also considers daytime and nighttime ET. We modified specific procedures to adopt a more local/regional model that can be applied daily and provide accurate ET estimates under all sky conditions (Fig. 9), as detailed in the following subsections. These modifications are crucial for capturing ET's spatial and temporal variability in Brazilian regions, where climate dynamics and vegetation cover exhibit significant variations. We included calculations of the net radiation, vegetation cover fraction, surface albedo, and vegetation indices. Furthermore, higher-resolution spatiotemporal meteorological data were incorporated as input for obtaining the ET product, as well as information on LULC, which is more closely aligned with the vegetation characteristics in Brazilian forests. The model's modifications were made to adapt it to these new, higher-resolution, or improved input datasets.

4.2.1.1 Changes in canopy conductance and plant transpiration

Canopy conductance and plant transpiration are important components of ET and play a crucial role in the Penman-Monteith method (Shuttleworth and Wallace, 2007; Chang et al., 2018). MOD16A2GF ET uses the leaf area index (LAI) to scale stomatal conductance (C_s, leaf level) up to canopy conductance (C_c, surface level) (Landsberg and Gower, 1997). Stomatal conductance is mainly expressed as a function of minimum air temperature (T_{min}) and vapour pressure deficit (VPD), as follows (Oren et al., 1999; Xu and Baldocchi, 2003) (Eq. 4 and Eq. 5):

$$C_S = C_L * m(T_{min}) * m(VPD) \quad (4)$$

$$C_C = C_S * LAI * (1 - f_{wet}) = \frac{1}{r_s} \quad (5)$$

where C_L and f_{wet} correspond to the mean potential stomatal conductance per leaf unit area ($m\ s^{-1}$) and the water cover fraction (unitless) obtained from Fisher et al. (2008), respectively, while $m(T_{min})$ and m(VPD) are limiting factors of potential stomatal conductance for

minimum air temperatures and VPD high enough to reduce canopy conductance, respectively. This step was estimated from a ratio established by Running et al. (2017), using parameterised values for each land cover type (Table 3).

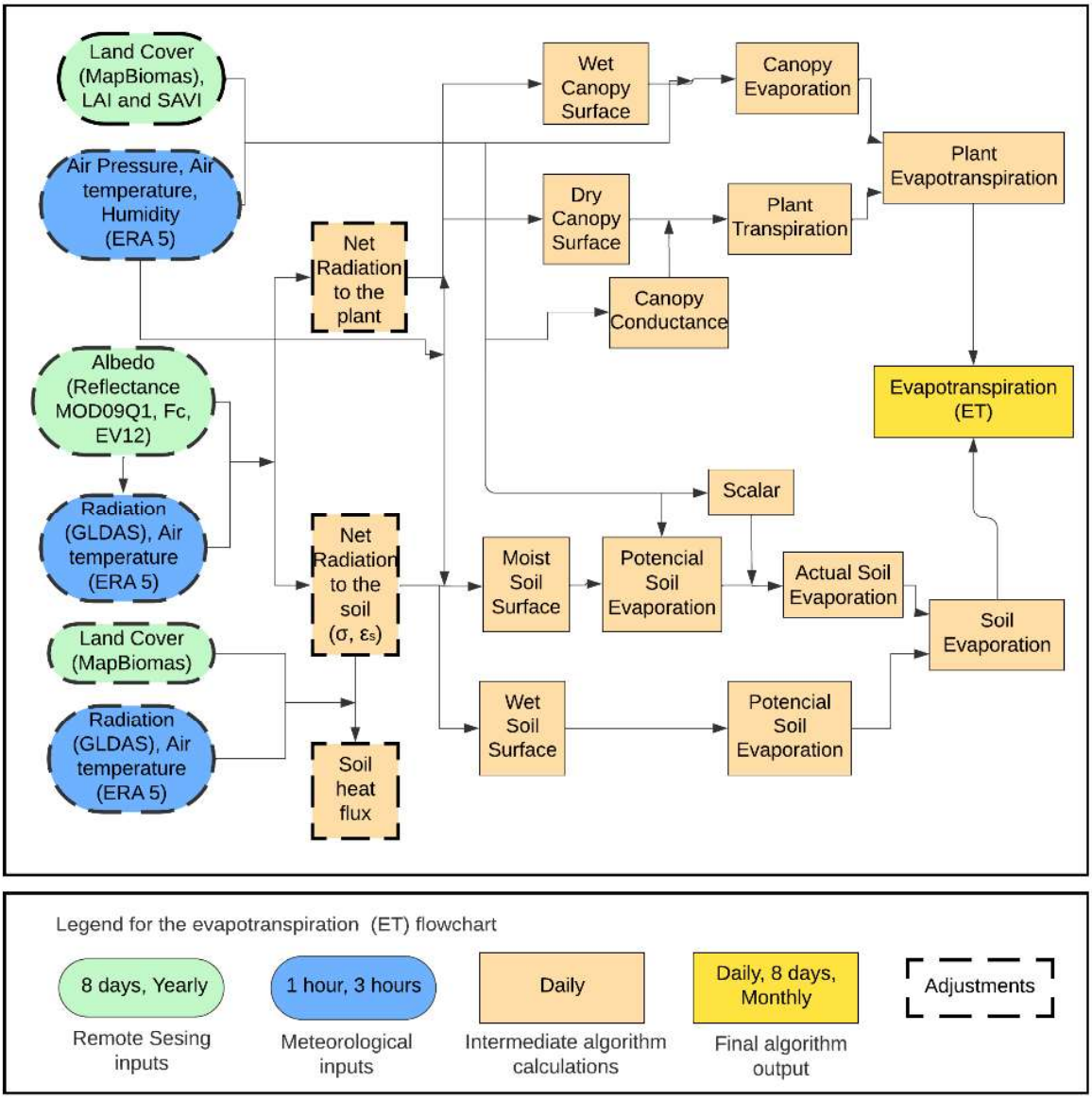

Figure 9 - Flowchart of the ESTIMET model, indicating the adjustments made in this study, in relation to the MOD16A2GF product (adapted from Mu et al., 2011).

Table 3 - Land cover types provided by the MapBiomas project for Brazil and reclassified in this study through the merging of classes, with their respective biophysical parameters, according to Running et al. (2017).

MapBiomas classes (ID)	**Reclassification**	**$Tmin_{close}$ (°C)**	**$Tmin_{open}$ (°C)**	**VPD_{open} (Pa)**	**VPD_{close} (Pa)**	**gl_{sh} (m/s)**	**$gl_{e\ wv}$ (m/s)**	**g_{cu} (m/s)**	**C_L (m/s)**	**rbl_{min} (s/m)**	**rbl_{max} (s/m)**
Forest (1); Forest Formation (3); and Forest Plantation (9)	Evergreen Broadleaf Forest (EBF)	-8	9.09	1000	4000	0.01	0.01	0.00001	0.00240	60	95
Farming (14); Pasture (15); Temporary Crop (19); Sugar Cane (20); and Mosaic Agriculture and Pasture (21)	Croplands (Crop)	-8	12.02	650	4500	0.02	0.02	0.00001	0.00550	60	95
Mangrove (5)	Mixed forests (MF)	-7	9.50	650	2900	0.01	0.01	0.00001	0.00240	60	95
Savanna Formation (4); Non-Forest Natural Formation (10); Wetlands (11); Grassland (12); and other Non-Forest Formations (13)	Savannah	-8	11.39	650	3600	0.04	0.04	0.00001	0.00550	60	95
Urban Area (24)	Non-vegetated Area	0	0	0	0	0	0	0	0	0	0
Water (26); River; Lake and Ocean (33); and Aquaculture (31)	Water	0	0	0	0	0	0	0	0	0	0
Salt Flat (32); Non-vegetated Area (22); Beach, Dune, and Sand Spot (23); Rocky Outcrop (29); Mining (30); and other Non-Vegetated Areas (25)	Other Non-vegetated Area	0	0	0	0	0	0	0	0	0	0

The MOD16A2GF model utilises two remote-sensing products as inputs for calculating canopy conductance and plant transpiration. First, C_L, VPD (open indicates no inhibition to transpiration and close indicates nearly complete inhibition with full stomatal closure), and T_{min} (open and close) parameters were set differently, according to the biome type from the MODIS Land Cover Type (MCD12Q1) product, which globally provides data characterising 12 land cover types at 500-m spatial resolution. Because the values of these parameters can significantly affect the calculation of plant transpiration, model accuracy is essentially driven by the quality of that classification (Ruhoff et al., 2013). Hence, the global representation of the MCD12Q1 product, associated with the limited number of classes covering the globe, inevitably mischaracterises or ambiguously renders some local/regional variations of LULC (Jung et al., 2006).

Regional LULC classification allows us to account for the more specific characteristics and landscape complexity of some regions (Jung et al., 2006). A multi-institutional initiative launched in 2015, the MapBiomas Project (http://mapbiomas.org), provides annual national-level LULC maps for the entire Brazilian territory with a 30 m spatial resolution. This project has data from 1985 to the present, based on a pixel-per-pixel automatic classification of Landsat images. Therefore, to fit more regional/local information, adjusted to the characteristics of the Brazilian vegetation, we merged the 33 LULC types available from the MapBiomas project into seven classes of similar characteristics, to match the biophysical parameters proposed by Running et al. (2017) (Table 2) and preserve the heterogeneity of Brazilian land use and coverage.

Additionally, MOD16A2GF ET utilises LAI information from MOD15A2H, an 8-day composite product with a spatial resolution of 500 m. This implies that LAI does not vary during a given 8-day period and helps to provide information with less cloud contamination. However, in some tropical regions, such as Brazil, the frequency of cloud cover is high, which often leads to incorrect ET estimates (Running et al., 2017). To deal with the cloud cover issue and increase the spatial resolution to 250 m, the ESTIMET model uses the soil-adjusted vegetation index (SAVI) proposed by Huete (1988) to compute LAI from both 8-day MOD09Q1 (Terra Satellite) and MYD09Q1 (Aqua Satellite) reflectance products, with a 250 m spatial resolution (Eq. 6 and Eq. 7):

$$\mathrm{LAI} = -\frac{\ln\left(\frac{0{,}69-\mathrm{SAVI}}{0{,}59}\right)}{0{,}91} \tag{6}$$

$$SAVI = \frac{(1+L)(r_2 - r_1)}{(L + r_2 + r_1)} \quad (7)$$

where r_1 and r_2 are the spectral reflectance of the bands 1 (red) and 2 (near-infrared) of the MOD09Q1 and MYD09Q1 products, and L is an adjustment factor. In this study, the adjustment factor is set to 0.1, the same value used by Silva et al. (2015) in a study conducted in Brazil. To exclude the impact of as much cloud cover as possible, the SAVI data calculated from both MOD09Q1 and MYD09Q1 were composed monthly, based on the selection of pixels with higher values obtained from the eight images made available each month (i.e. four from MOD09Q1 and four from MYD09Q1), assuming that clouds possibly contaminated the lower or negative values of this biophysical parameter. This overlapped monthly SAVI was considered a fixed biophysical input parameter for each month, used to estimate daily ET.

4.2.1.2 Changes in vegetation cover fraction

To distinguish the net radiation between the canopy and the soil surface, the cover fraction (F_C) information is required, varying from 0 to 1. The latest version of the MOD16 product utilises 8-day information from the MOD15A2H (FPAR, Fraction of Absorbed Photosynthetically Active Radiation) product, with a spatial resolution of 500 m, as a substitute for F_C (Mu et al., 2011; Running et al., 2017). As an alternative, Cleugh et al. (2007) used the Normalised Difference Vegetation Index (NDVI) to calculate F_C. Still, this vegetation index is very sensitive to background canopy variations and atmospheric influences (Huete et al., 2002). Conversely, Mu et al. (2007) calculated F_C in the MOD16A2GF, replacing NDVI with the Enhanced Vegetation Index (EVI), to adjust for the background canopy and reduce atmospheric influence (i.e. using three reflectance bands, including blue). To reduce the pixel size and deliver a final ET product with a spatial resolution of 250 m, we calculated the F_C using the 2-band EVI (EVI2), as suggested by Jiang et al. (2008). Unlike EVI, EVI2 only uses red and infrared bands but presents satisfactory results, especially when atmospheric effects are insignificant or corrected (Rocha and Shaver, 2009; Bolton and Friedl, 2013), making it possible to use the MOD09Q1 and MYD09Q1 products (Eq. 8 and Eq. 9):

$$F_C = \frac{EVI2 - EVI2_{min}}{EVI2_{max} - EVI2_{min}} \quad (8)$$

$$EVI2 = 2{,}5 \times \frac{r_2 - r_1}{r_2 + 2{,}4r_1 + 1{,}0} \quad (9)$$

where $EVI2_{min}$ is the signal from bare soil (LAI → 0) and $EVI2_{max}$ is the signal from dense green vegetation (LAI →∞) during the study period; these are generally set as invariant constants varying between 0.05 and 0.95, respectively. Similar to the SAVI procedures, EVI2 was also considered a fixed input parameter throughout the month, using the highest values obtained from the eight available MOD09Q1 reflectance products and assuming that the lower values reflect clouds.

4.2.1.3 Changes in net incoming radiation to the land surface

In the MOD16A2GF ET model, the net incoming radiation to the land surface (R_{net}) is calculated following Mu et al. (2011), using the same equation stemming from Mu et al. (2007) and Cleugh et al. (2007) (Eq. 10).

$$R_{net} = (1 - \alpha)\, R_{S\downarrow} + \sigma\, (\varepsilon_a - \varepsilon_s)\, (273.15 + T)^4 \quad (10)$$

where α corresponds to the surface albedo, $R_{S\downarrow}$ is the downward shortwave of incoming radiation, σ is the Stefan-Boltzmann constant ($5{,}67 \times 10^{-8}$ W m^{-2} K^{-4}), ε_s is surface emissivity, ε_a is atmospheric emissivity, and T represents the air temperature in °C.

The original model obtains α from the 8-day composite MCD43A2/A3 product with 500 m of spatial resolution. This evaluation may suffer from cloud contamination, resulting in a dramatically increased α (Running et al., 2017). To minimise this risk, we made use of the two 250 m reflectance bands of the MOD09Q1 product to calculate α, as proposed by Teixeira et al. (2013) (Eq. 11):

$$\alpha = a + br_1 + cr_2 \quad (11)$$

where a, b, and c are regression coefficients obtained by comparing remote sensing and field measurements. The values of a, b and c found by Teixeira et al. (2013), for the Caatinga biome, were 0.08, 0.41, and 0.14, respectively. Since these values are not available in the literature for the other Brazilian biomes, three flux towers (EUC, FM, and K34; see topic 4.2.2.1 for their descriptions), which are distributed throughout the country and located in the other Brazilian biomes, were used to obtain their respective regression coefficients

(Table 4). The same regression coefficients used for the Amazon and Pantanal biomes were considered for the Atlantic Forest and Pampa biomes, respectively, due to the absence of free available flux tower data for these two biomes and the most similarities between them. Similar to SAVI and EVI2, the monthly composition of α was also considered in this step, to reduce the influence of clouds in the ET estimates, using the lowest values obtained from the eight MOD09Q1 reflectance products available within 30 days and assuming that the highest values were possibly contaminated by clouds. Such monthly compositions applied to the vegetation indexes and surface albedo result in a maximum latency of one month after the event for ESTIMET, which remains significantly lower than the one-year latency of the MOD16A2GF product.

Table 4 - Regression coefficients obtained for each biome using the data from the flux towers and used for estimating surface albedo (α).

Biome	**Flux tower**	**a**	**b**	**c**
Amazon	K34	0.118	-0.016	0.016
Atlantic Forest	-	0.118	-0.016	0.016
Caatinga	-	0.08	0.41	0.14
Cerrado	PDG	0.124	-0.009	0.043
Pantanal	FM	0.168	-0.032	0.117
Pampa	-	0.168	-0.032	0.117

In addition, contrasting with the original MOD16 ET model, which considers surface emissivity (ε_s) as a constant parameter of 0.97, this study used the following empirical equation by Allen et al. (2007), integrating the effects of LAI and NDVI and calculated from the two reflectance bands of the MOD09Q1 product (Eq. 12):

$$\varepsilon_s = 0.95 + 0.01\ \mathrm{LAI} \quad (12)$$

with $\varepsilon_s = 0.98$ when LAI > 3 and $\varepsilon_s = 0.99$ when NDVI < 0 (Eq. 13).

$$\mathrm{NDVI} = \frac{r_2 - r_1}{r_2 + r_1} \quad (13)$$

4.2.1.4 Changes in the meteorological forcing data

The global meteorological re-analysis data MERRA-2, provided by NASA's Global Modelling and Assimilation Office (GMAO), with a spatial resolution of 0.5° x 0.6° or 1.0°

x 1.25°, were used as input to the original MOD16 model (Mu et al., 2007, 2011; Running et al., 2017). MERRA-2 incorporates both ground-based and satellite-based observations, providing information with a 6-hour resolution. However, some studies have emphasised that some uncertainties of the MOD16 product may be mainly due to the coarse spatial resolution of the MERRA-2 climate database (Ruhoff et al., 2013; Ramoelo et al., 2014; Zhang et al., 2016; Chang et al., 2018). For instance, Chang et al. (2018) found a considerably lower performance of MOD16 driven by GMAO data, compared to the same model driven by observation data, which suggests that the re-analysis data led to substantial errors in the ET estimation. Indeed, high-quality meteorological data are required for accurate flow retrievals, which differentiate microclimates, although spatial resolution requirements may be less stringent than for other land surface variables (Fischer et al., 2017). Unlike the original model, we used the ERA5-Land meteorological dataset (ECMWF Climate Reanalysis) to obtain hourly information of T and dew point T at 2 m levels ('temperature_2m' and 'dewpoint_temperature_2m'), and surface atmospheric pressure ('surface_pressure') with 0.1º x 0.1º spatial resolutions (Muñoz, 2019). In parallel, downward shortwave solar radiation was retrieved from GLDAS 2.1 (Global Land Data Assimilation System – Noah), making this variable available with 3-h and 0.25° resolutions (Rodell et al., 2004). The ERA5-Land and GLDAS 2.1 meteorological dataset was evaluated in Brazil (Araújo et al., 2022; Matsunaga et al., 2023) and other regions (Liu et al., 2024; Vicente-Serrano et al., 2021; Wang et al., 2024; Zou et al., 2022), mostly presenting improved results compared with MERRA-2 (Zuo et al., 2023; Kara et al., 2024; Liu et al., 2025). We also found that T and solar radiation values from ERA-5 Land and GLDAS 2.1 are closest to the observed data recorded in some flux towers in Brazil, when compared with MERRA-2 (Fig. 10). Additionally, meteorological data from ERA5-Land and GLDAS 2.1 were also used as input by other models and products to estimate ET, such as geeSEBAL-MODIS (Andrade et al., 2024), STEEP (Seasonal Tropical Ecosystem Energy Partitioning) (Bezerra et al., 2023), and PML_V2 (Penman-Monteith-Leuning Evapotranspiration, Version 2) (Zhang et al., 2019).

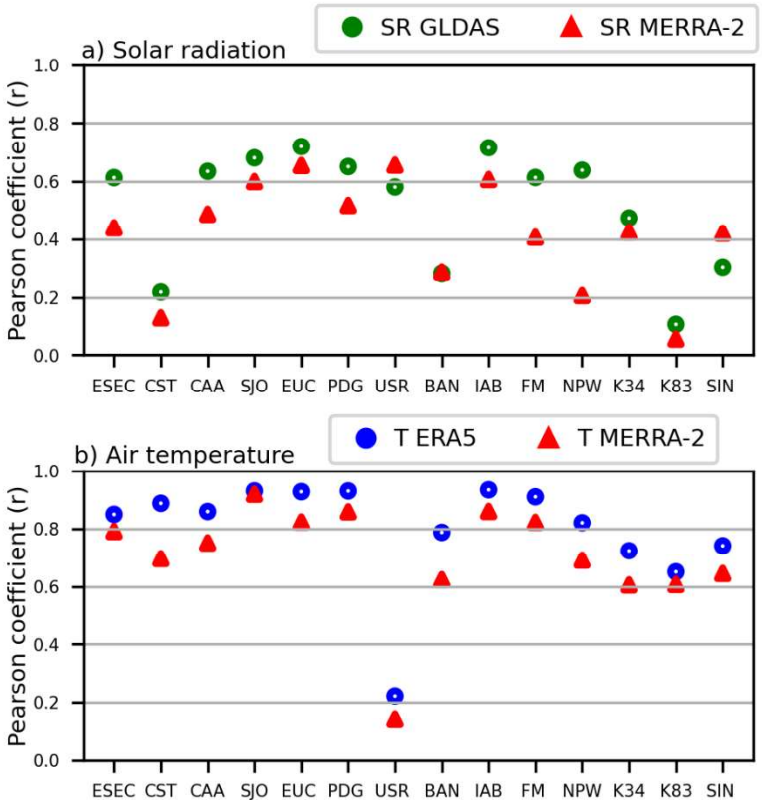

Figure 10 - (a) Pearson's coefficient correlation (r) of the solar radiation (W/m²) estimated by MERRA-2 (red triangles) and GLDAS (green dots) versus the solar radiation (W/m²) obtained at the flux towers. (b) Pearson's correlation coefficient (r) of the air temperature (ºC) estimated by MERRA-2 (red triangles) and ERA5 (blue dots) versus the air temperature (ºC) obtained at the flux towers.

4.2.2 Model evaluation

4.2.2.1 Local scale

We compared daily and 8-day accumulated ET estimates from orbital remote sensing with the eddy covariance (EC) data from flux towers at 14 sites throughout Brazil (Fig. 7). The towers belong to the AmeriFlux network, EMBRAPA (Brazilian Agricultural Research Cooperation), and three universities (the University of São Paulo – USP, the Federal University of Mato Grosso – UFMT, and the Federal University of Mato Grosso do Sul – UFMS). These flux towers represent all of the main climate zones and almost all the terrestrial biomes found in Brazil. The land covers of the EC sites include both the natural vegetation of the Brazilian Biomes and anthropised environments, such as irrigated croplands, pasture, and eucalyptus plantations.

The EC method is accepted as being the most reliable technique for the direct and continuous measurement of sensible (H) and latent (LE) heat fluxes (Sun et al., 2013). The EC data used in this study, and considered to be observed ET (ET_{Obs}), were obtained for different years, ranging from 2003 to 2021, according to their availability (Fig. 7b). The altitude of the studied sites ranged from 90 to 710 m above sea level (Table 5).

For comparison, half-hour EC measurements were used to compute daily and 8-day flux data. In parallel, to achieve the spatial representativeness of the measured data for each site, daily values of ET (estimated by ESTIMET) were spatially averaged over a 750 x 750 m^2 window, centred at each flux tower to ensure the spatial representativeness of the estimations for each site (Ruhoff et al., 2012). ET product data from MOD16A2GF Version 6.1, covering the image cells of the proposed model at the flux tower sites, and were also used for comparison. Additionally, ESTIMET was compared with two other consolidated global satellite-based ET products at a local scale: (i) version 4.1a of the Global Land Evaporation Amsterdam Model (GLEAM 4.1a) product, which is based on a set of models and also uses re-analysis data to provide daily ET with grid cells of 0.1º x 0.1º (~10 km); and (ii) version 02 of the Penman-Monteith-Leuning Evapotranspiration (PML_V2) product, which provides ET at 500 m (spatial) and 8-day (temporal) resolutions. As MOD16A2GF and PML_V2 are 8-day composite products at a 500 m pixel resolution, we accumulated the daily values initially obtained from ESTIMET, GLEAM 4.1a, and the EC systems, to produce the 8-day values. Days with imbalances ≤ 0.75 or ≥ 1.25 in the surface energy balance ratio were disregarded for the ET_{Obs} computation to ensure the quality of the data used for the comparison. For the same reasons, we excluded the days with precipitation > 0.5 mm from the daily-based comparisons. For the accumulated 8-day comparisons, only the ET_{Obs} data featuring less than 50% of rainy days in each 8-day window were considered for the comparison with ESTIMET and the other three products. In order to identify the rainy days and analyse the response of remotely sensed ET (i.e. the ET variation in dry and wet seasons), we used rainfall data from automatic rain gauges associated with the flux towers.

Table 5 - Main characteristics of the eddy covariance (EC) sites used in this study.

Location	Code	Latitude, Longitude (WGS84)	Biome	Climate	Land cover	Altitude (m)	Ecological description	Reference
Serra Negra do Norte, Rio Grande do Norte	ESEC	-6.578, -37.251	Caatinga	Bsh	Savanna	205	Conservation unit of the Caatinga biome, characterised by dry xerophilous forest and deciduous plant species, presenting predominance of widely dispersed small trees and shrubs with less than 7 m in height and herb patches, which develop and grow only during the wet season.	(Campos et al., 2019)
Serra Talhada, Pernambuco	CST	-7.968, -38.384	Caatinga	Bsh	Savanna	468	Vegetation characterised by bushes and trees typical of the Caatinga biome, where cattle graze during part of the year. This site is considered preserved and representative of the dry forests of this region.	(Souza et al., 2016; Silva et al., 2017)
Petrolina, Pernambuco	CAA	-9.047, -40.321	Caatinga	Bsh	Savanna	391	A region characterised by dry and spiny deciduous shrub/forest vegetation, without anthropogenic activities.	(Souza et al., 2016)
São João, Pernambuco	SJO	-8.81, -36.41	Atlantic Forest	As	Agriculture	702	Cultivated area with signal grass (Brachiaria decumbens Stapf) intercropped with maize (Zea mays L.) to recover the pasture.)	(Machado et al., 2016; Souza et al., 2016)
Ribeirão Preto, São Paulo	EUC	-21.583, -47.6	Cerrado	Cwa	Agriculture	710	Presence of a Eucalyptus plantation (Eucalyptus urophylla x Eucalyptus grandis clonal hybrid), whose trees were two years old in 2006, and the average canopy-top height was 12 m.	(Cabral et al., 2011)
Luíz Antônio, São Paulo	PDG	-21.621, -47.63	Cerrado	Cwa	Forest	710	Natural vegetation of Cerrado, surrounded by eucalyptus and sugarcane plantations.	(Cabral et al., 2015)
Luís Antônio, São Paulo	USR	-21.637, -47.79	Cerrado	Cwa	Agriculture	541	Sugarcane plantation, surrounded by pasture, citrus fruit orchards, and the native savanna forest (Cerrado).	Cabral et al., 2012)

Araguaia, Tocantins	BAN	-9.824, -50.159	Cerrado	Aw	Forest	168	A floodplain area covered by Cerrado (Brazilian savanna), whose ecosystem is composed of semideciduous forests, a high woodland savanna with 18 m canopy height and sparse shrubs, and a dense Cerrado with 5 m height trees and grass understory.	(Borma et al., 2009)
Itirapina, São Paulo	IAB	-22.10, -47.52	Cerrado	Cwa	Forest	780	An area of undisturbed woodland, a 300-hectare area with vegetation physiognomy cerrado woodland, has a characteristic arborous cover of 50–70% and trees with heights of 5–8m, and an absolute density of trees 13 976 individuals per hectare.	(Oliveira et al., 2015)
Fazenda Miranda, Mato Grosso	FM	-15.716, -56.067	Pantanal	Aw	Agriculture	154	A mixed forest-grassland that was partially cleared of trees over 35 years ago. The predominant vegetation consists of grasses and tree species, particularly C. americana and Diospyros hispida A. DC.	(Rodrigues et al., 2014)
Pantanal, Mato Grosso	NPW	-16.498, -56.412	Pantanal	Aw	Savanna	120	A preserved area of the Pantanal biome, which is a seasonally flooded forest dominated by Combretum lanceolatum (Combretaceae) with a small presence of macrophytes fixed and rooted to the soil with floating leaves that emerge during the flood cycle. The forest cover height exceeds 2 metres.	(Dalmagro et al., 2018; Vourlitis et al., 2019)
Manaus, Amazonas	K34	-2.609, -60.209	Amazon	Af	Forest	90	An area of largely contiguous forest on flat terrain, with a closed canopy and a mean height of approximately 40–45 m, with some trees reaching up to 55 m. Forest classified as ‘primary’ with abundant large logs, numerous epiphytes, an uneven age distribution, and emergent trees.	(Hutyra et al., 2007)

Santarém, Pará	K83	-3.02, -54.97	Amazon	Am	Forest	181	The Tapajós National Forest, a tropical rainforest near the confluence of the Tapajós and Amazon rivers. The site was selectively logged in September 2001, becoming a logged forest.	(Paca et al., 2019; Miller et al., 2004)
Sinop, Mato Grosso	SIN	-11.412, -55.325	Amazon	Am	Forest	349	A vast expanse of humid forest, with dense forest cover and large trees that form a closed canopy and reach heights that often exceed 30 metres.	(Vourlitis et al., 2008)

4.2.2.2 Catchment scale

The annual performance of ESTIMET was also evaluated at a catchment scale. A multi-criteria approach was applied to select these catchments. First, we filtered non-nested catchments in each biome with a total area of 1–5 km² and without substantial surface water reservoirs. After meeting this first criterion, we selected five catchments from each biome that contained a larger area of natural land cover and exhibited high Kling-Gupta Efficiency (> 0.5) during the calibration and validation of the simulated streamflow performed by Andrade et al. (2024). As no streamflow data were available for the Pantanal, this biome was excluded from this evaluation, resulting in a total of 25 catchments. The total annual ET at the catchment scale (ET_{Catch}) was calculated as a residual of the water balance between 2003–2009 (Eq. 14):

$$ET_{Catch} = P - Q - S\Delta T \quad (14)$$

where P is the observed catchment-scale total annual precipitation (mm), Q represents the observed annual streamflow at the catchment's outlet (mm), and S represents annual changes in the catchment's water storage (mm).

P and Q data were obtained from the Catchment Attributes for Brazil (CABra) dataset (Almagro et al., 2021), while S was derived from the Gravity Recovery and Climate Experiment (GRACE) (Tapley et al., 2004) by calculating the average of the three equivalent water thickness products from GFZ (Geo Forschungs Zentrum Potsdam), CSR (University of Texas Centre for Space Research), and JPL (NASA's Jet Propulsion Laboratory). The calculation of the annual water balance was based on the hydrological year. We identified the start of the rainy season by decomposing the monthly precipitation time series from each catchment using the seasonal component of an additive data series decomposition method (Kendall and Stuart, 1983), which is available through the 'decompose' function in R (R Core Team, 2017). This method separates the series into three parts, namely the 'trend', 'seasonality', and 'noise'. The seasonality was transformed into a binary vector, assigning a value of 1 to rainy months and 0 to dry months. The transition from the dry season to the rainy season was identified by detecting a change from 0 to 1, marking the beginning of the rainy season. The month corresponding to this change was recorded as the starting point of the rainy period.

4.2.2.3 Evaluation metrics

We used three statistical metrics to evaluate the ESTIMET model's ($ET_{ESTIMET}$) performance regarding the ground-based and water balance measurements. We also compared its performance with that of global satellite-based ET products, including the MOD16A2GF data (ET_{MODIS}).

To measure both the precision and accuracy between the ET estimates and observations, we computed the concordance correlation coefficient (ρc), which evaluates how well bivariate data fall on the 1:1 slope (Eq. 15).

$$\rho c = \frac{2\sum_{i=1}^{N}(O_i-\bar{O})(E_i-\bar{E})}{\sum_{i=1}^{N}(O_i-\bar{O})^2+\sum_{i=1}^{N}(E_i-\bar{E})^2+(N-1)(\bar{O}-\bar{E})^2} \quad (15)$$

where N is the sample size, O is the observed value, E is the estimated value, $\bar{O}$ is the observed mean, and $\bar{E}$ is the estimated mean. The metric presents values ranging from -1 to 1, with desirable values close to 1, indicating perfect agreement.

To evaluate the model's errors against the ET_{Obs} and ET_{Catch} data, we used: (1) the Percent Bias (PBIAS), which measures the trend as a percentage of estimated values in relation to observed values (Eq. 16); and (2) the root mean square error (RMSE), which gives the sample standard deviation of the differences between ETs (Eq. 17).

$$PBIAS = [\frac{\sum_{i=1}^{N}(M_i-O_i)}{\sum_{i=1}^{N}O_i}]x\ 100 \quad (16)$$

$$RMSE = \sqrt{\frac{\sum_{i=1}^{N}(M_i-O_i)^2}{N}} \quad (17)$$

The metrics of this second group range from 0 to +∞] (RMSE) and from -∞ to +∞ (PBIAS), with more desirable numbers close to 0 indicating smaller errors in the estimated values, in relation to the ET obtained from flux towers.

4.3 Results of the model's evaluation

4.3.1 Daily based evaluation of ESTIMET at the local scale

Fig. 3 shows the daily variations of $ET_{ESTIMET}$, ET_{Obs}, and precipitation. Overall, the daily $ET_{ESTIMET}$ similarly tracks seasonal fluctuations in ET_{Obs}, with most curves showing an upward trend during the wet season and a downward trend during the dry season. In the Caatinga biome, very similar variations of $ET_{ESTIMET}$ were observed (Fig. 11a-c), especially at the ESEC ($ET_{ESTIMET}$ = 1.15 mm/day and ET_{Obs} = 1.10 mm/day, on average) and CST ($ET_{ESTIMET}$ = 1.17 mm/day and ET_{Obs} = 0.98 mm/day, on average) sites. In contrast, some differences occurred at CAA ($ET_{ESTIMET}$ = 2.17 mm/day and ET_{Obs} = 1.91 mm/day, on average), mainly in March 2011 (the rainy season), which was characterised by greater gaps in ET_{Obs}. Similar concurrent variations of ET were also observed at the SJO site, although average $ET_{ESTIMET}$ (2.39 mm/day, on average) was ~90% greater than ET_{Obs} (1.25 mm/day, on average) during the rainy period (April-September) (Fig. 11d).

In the Cerrado biome (Fig. 11e-i), the $ET_{ESTIMET}$ and ET_{Obs} remarkably overlapped over the three years of continuous monitoring at the PDG site ($ET_{ESTIMET}$ = 2.64 mm/day and ET_{Obs} = 3.30 mm/day, on average). Conversely, notably lower and slightly greater values of $ET_{ESTIMET}$ were identified at the BAN ($ET_{ESTIMET}$ = 1.05 mm/day and ET_{Obs} = 3.85 mm/day, on average) and USR ($ET_{ESTIMET}$ 3.75 mm/day and ET_{Obs} = 2.89 mm/day, on average) sites in the Cerrado biome during the dry (May-September) and rainy (October-March) seasons, respectively. In the Pantanal biome, daily $ET_{ESTIMET}$ at the NPW (4.94 mm/day, on average) site followed the seasonal fluctuations of ET_{Obs} (4.03 mm/day, on average), with some overestimations from October to April during the rainy season ($ET_{ESTIMET}$ = 6.90 mm/day and ET_{Obs} = 4.70 mm/day, on average). At the FM site, the $ET_{ESTIMET}$ (1.73 mm/day, on average) was also close to ET_{Obs} (1.70 mm/day, on average) but exhibited small underestimates in the dry period (May-September) ($ET_{ESTIMET}$ = 0.70 mm/day and ET_{Obs} = 1.22 mm/day, on average). For the Amazon biome, although ~62, ~74, and 93% of the time series of the three flux towers (SIN, K83 and K34, respectively) were missing, a good overlap was observed between the $ET_{ESTIMET}$ and ET_{Obs}, especially at K34 ($ET_{ESTIMET}$ = 3.23 mm/day and ET_{Obs} = 3.76 mm/day, on average) and K83 ($ET_{ESTIMET}$ = 3.80 mm/day and ET_{Obs} = 3.99 mm/day, on average) (Fig. 11l-n). Nevertheless, during the driest period at SIN (from June to September), differences of ~40% between the ET values estimated by the two sources were observed ($ET_{ESTIMET}$ = 1.69 mm/day and ET_{Obs} = 2.82 mm/day, on average).

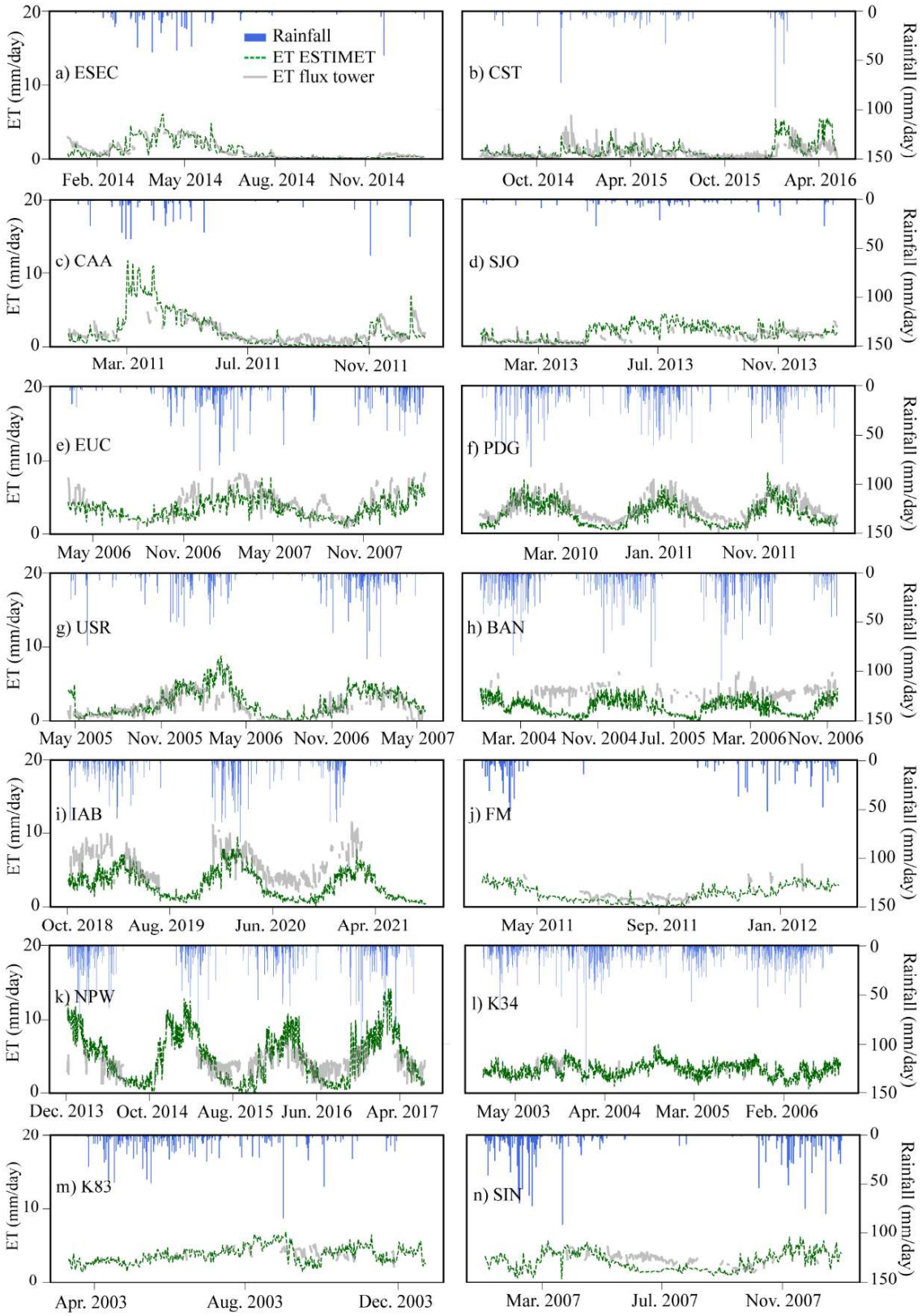

Figure 11 - Daily evapotranspiration (mm) obtained by the Eddy Covariance method (ET_{Obs}) and modelled by the ESTIMET model ($ET_{ESTIMET}$), plotted with the daily precipitation data (mm) obtained by the flux towers located in the Caatinga (ESEC, CST, CAA, and SJO), Cerrado (EUC, PDF, USR, BAN, and IAB), Pantanal (FM and NPW), and Amazon (K34, K83, and SIN) biomes.

Fig. 12 shows the scatter plots with the metrics to compare the daily similarity between ETESTIMET and ETObs statistically. Overall, the ET variability was well estimated by ESTIMET, with ρc values ranging from 0.45 (EUC; Cerrado) to 0.80 (ESEC; Caatinga) at eight control sites. For some sites presenting ρc values lower than 0.45, the clouds of points were nevertheless concentrated close to the lines of equality, as observed at K34 (ρc = 0.23) and SIN (ρc = 0.28), in the Amazon. At eight control sites, ESTIMET appears to underestimate ET (ESEC, EUC, PDG, BAN, IAB, FM, K34, and SIN), while at the other six sites, ET appeared to be overestimated, compared to EC evaluations (CST, CAA, SJO, K83, USR, and NPW), as shown by the trend lines above and below the lines of equality, respectively.

ESTIMET exhibited better overall performance at the Caatinga sites (Fig. 12a-d), with ρc values ranging from 0.46 to 0.80 (ρc = 0.62, on average). Satisfactory ρc values of $ET_{ESTIMET}$ were also obtained for the Pantanal (Fig. 4j-k) (ρc = 0.45, on average) and Cerrado (Fig. 12e-i) (ρc = 0.41, on average) biomes. On the other hand, the lowest agreements between daily $ET_{ESTIMET}$ and ET_{Obs} were noted for the sites in the Amazon biome (Fig. 12l-n), with a mean value of ρc equal to 0.22 (0.28 for SIN, 0.23 for K34, and 0.15 for K83).

Compared to the ET_{Obs} data, $ET_{ESTIMET}$ only showed positive PBIAS at CST, SJO, and USR, and negative PBIAS at ESEC, CAA, EUC, PDG, BAN, IAB, FM, NPW, K34, K83, and SIN. This suggests a more general trend of underestimating daily ET (Fig. 13 and Table 6). The $ET_{ESTIMET}$ at K83 (PBIAS = -4.00%; Amazon) and CST (PBIAS = 7.78%; Caatinga) exhibited the lowest negative and positive biases, respectively. Conversely, the highest positive and negative biases of $ET_{ESTIMET}$ were identified for the USR (PBIAS = 26.95%) and BAN (PBIAS = -56.45%) sites in the Cerrado biome. The daily values of RMSE varied between 0.66 mm/day (ESEC; Caatinga) and 3.08 mm/day (IAB; Cerrado), with the highest average values for Cerrado (average RMSE = 2.06 mm/day) and the lowest for Caatinga (average RMSE = 0.96 mm/day).

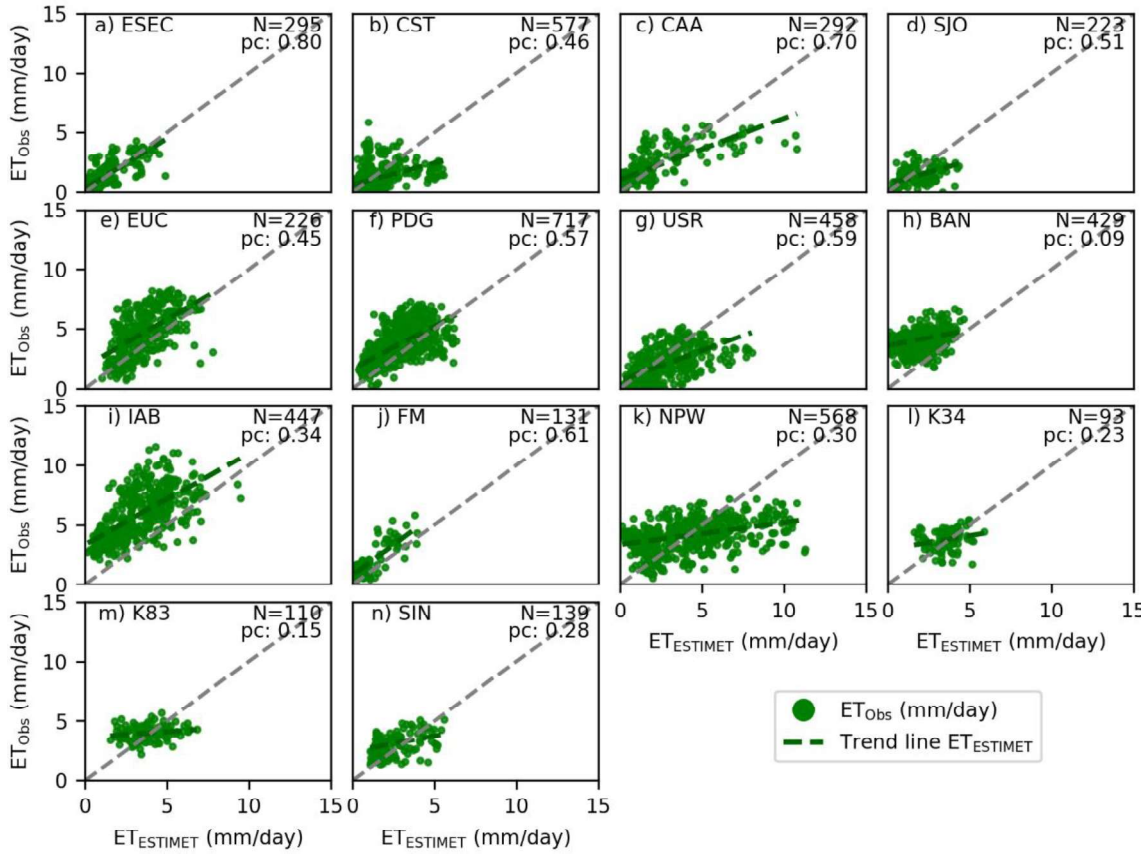

Figure 12 - Scatter plots of daily evapotranspiration modelled by the ESTIMET ($ET_{ESTIMET}$) model versus the daily estimations obtained by the Eddy Covariance (ET_{Obs}) method in the 14 flux towers located in the Caatinga (ESEC, CST, CAA, and SJO), Cerrado (EUC, PDF, USR, BAN, and IAB), Pantanal (FM and NPW), and Amazon (K34, K83, and SIN) biomes. The metric ρc (concordance correlation coefficient) is shown to statistically compare the similarity between the daily variations of ET_{Obs} and $ET_{ESTIMET}$. N represents the sample size.

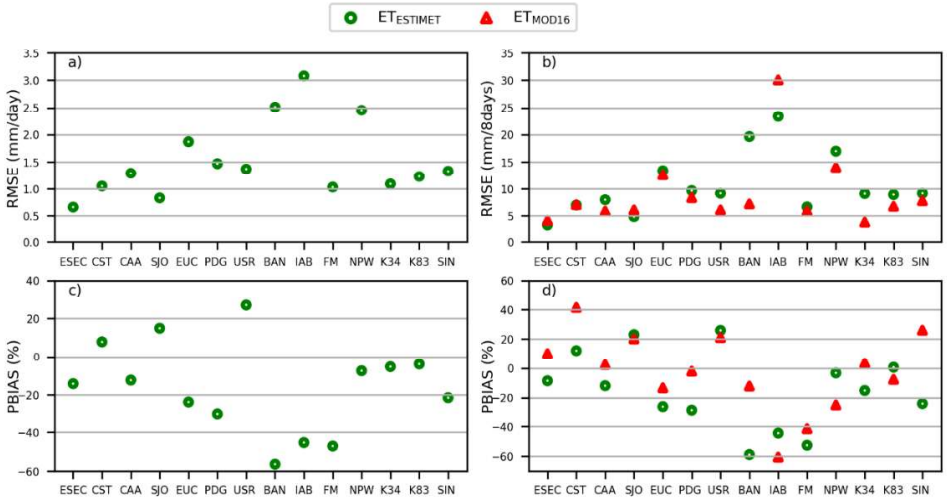

Figure 13 - (a-b) RMSE and (c-d) PBIAS statistics for ESTIMET ($ET_{ESTIMET}$) and MOD16A2GF (ET_{MODIS}) evapotranspiration data when compared to the Eddy Covariance (ET_{Obs}) observations in the flux tower sites, on a (a-c) daily and (b-d) 8-day accumulated basis.

Table 6 - Pearson's correlation coefficient (r) obtained for the daily and 8-day accumulated evapotranspiration modelled by the (a) ESTIMET (ETESTIMET), (b) MOD16A2GF (ETMODIS), (c) PML_V2 (ETPML), and (d) GLEAM 4.1a (ETGLEAM) models, versus the daily and 8-day accumulated estimations by the Eddy Covariance (ETObs) approach in the 14 flux towers.

Flux towers	**r (mm/day)**	**r (mm/8-days)**			
	$ET_{ESTIMET}$ X ET_{Obs}	$ET_{ESTIMET}$ X ET_{Obs}	ET_{MODIS} X ET_{Obs}	ET_{PML} X ET_{Obs}	ET_{GLEAM} X ET_{Obs}
ESEC	0.81	0.94	0.89	0.69	0.64
CST	0.48	0.59	0.73	0.60	0.60
CAA	0.76	0.83	0.86	0.59	0.83
SJO	0.55	0.72	0.61	0.39	0.67
EUC	0.58	0.72	0.53	0.15	0.75
PDG	0.57	0.85	0.64	0.50	0.85
USR	0.64	0.75	0.85	0.85	0.77
BAN	0.37	0.25	0.29	0.16	0.19
IAB	0.66	0.74	0.81	0.65	0.91
FM	0.82	0.81	0.72	0.63	0.11
NPW	0.41	0.51	0.36	0.62	0.76
K34	0.23	0.02	0.40	0.23	0.37
K83	0.18	0.03	0.12	0.46	0.40
SIN	0.35	0.41	0.73	-0.58	-0.23

4.3.2 8-day based evaluation of ESTIMET at the local scale

To assess the performance of the model in comparison to global satellite-based ET products (MOD16A2GF, PML_V2, and GLEAM 4.1a), we further evaluated the quality of daily ETESTIMET accumulated over 8 days against ground-based measurements (ET_{Obs}). Overall, similar behaviour was identified between the $ET_{ESTIMET}$ and ET_{MODIS} values, especially in the Caatinga, Cerrado, and Pantanal biomes (Fig. 14). When compared to MOD16A2GF, ESTIMET showed an improved linear relationship with the EC-based ET values for six flux towers (Fig. 15) (i.e. ESEC and SJO in Caatinga; EUC, PDG, and IAB in Cerrado; and NPW in Pantanal), with higher values of ρc (0.93 vs 0.88, 0.61 vs 0.50, 0.51 vs 0.34, 0.68 vs 0.63, 0.37 vs 0.18, and 0.33 vs 0.24, respectively) (Fig. 7). Conversely, ESTIMET presented lower values of ρc (0.54 vs 0.61, 0.77 vs 0.85, 0.69 vs 0.81, 0.05 vs 0.21, 0.05 vs 0.21, 0,42 vs 0.45, 0.01 vs 0.38, 0.02 vs 0.09, and 0.30 vs 0.50) when compared to the estimations of MOD16A2GF at eight control sites (i.e. CST and CAA in Caatinga, USR and BAN in Cerrado, FM in Pantanal, and K34, K83, and SIN in the Amazon, respectively). Although presenting lower linear relationships with the ET_{Obs} in these sites,

$ET_{ESTIMET}$ also reached high or similar values of ρc at CST, CAA, USR, and FM. At the same time, at K34, K83, and SIN, the number of samples was low (i.e. 9, 15, and 19, respectively) for this 8-day ET aggregation, which hampered a more in-depth analysis.

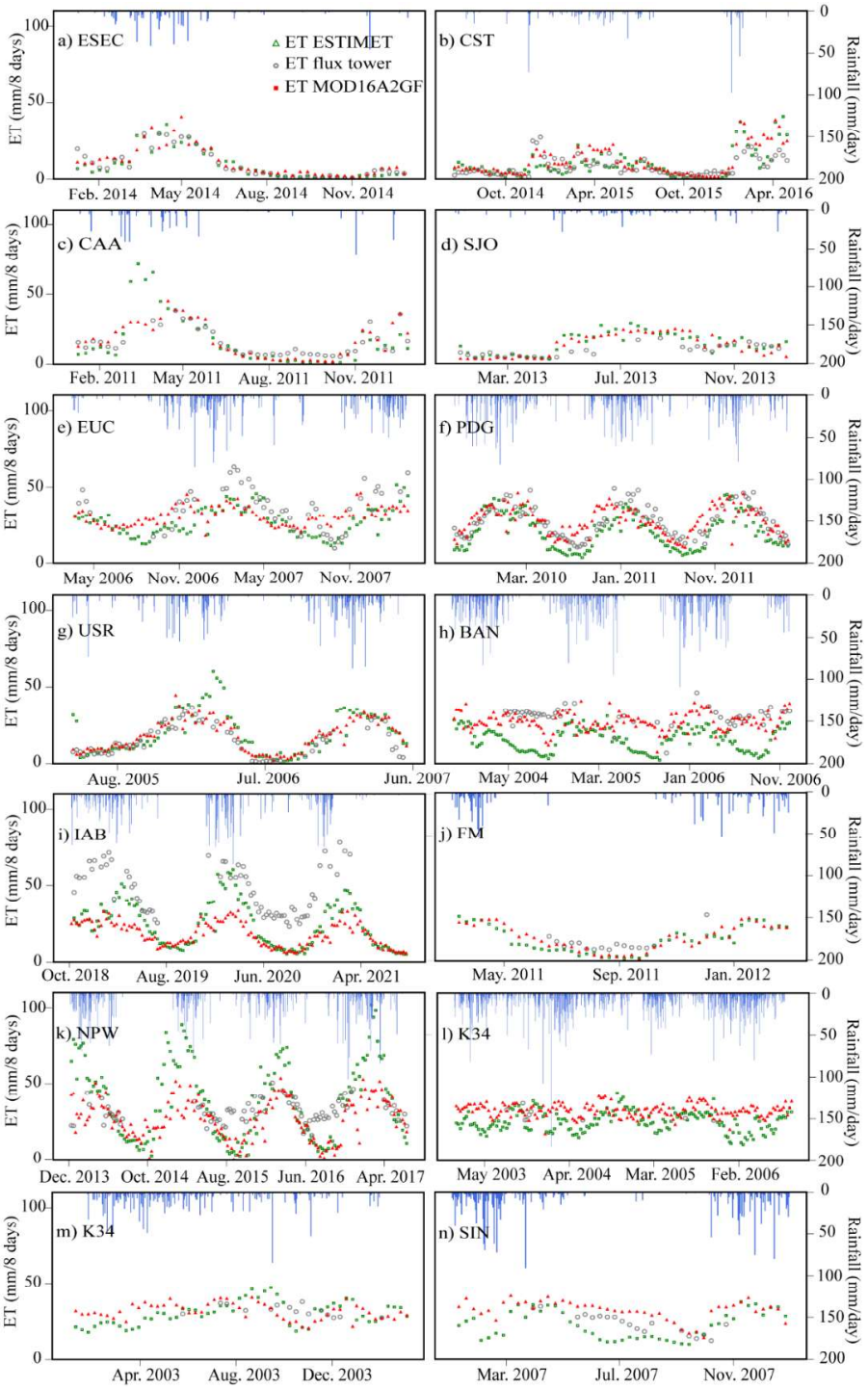

Figure 14 - Accumulated 8-day ET (mm) modelled by the ESTIMET ($ET_{ESTIMET}$) and MOD16A2GF (ET_{MODIS}) models, compared to those obtained by the Eddy Covariance method (ET_{Obs}), at the flux towers located in the (a-d) Caatinga, (e-i) Cerrado, (j-k) Pantanal, and (l-n) Amazon biomes. The measured daily precipitation data (mm) at each site is also shown.

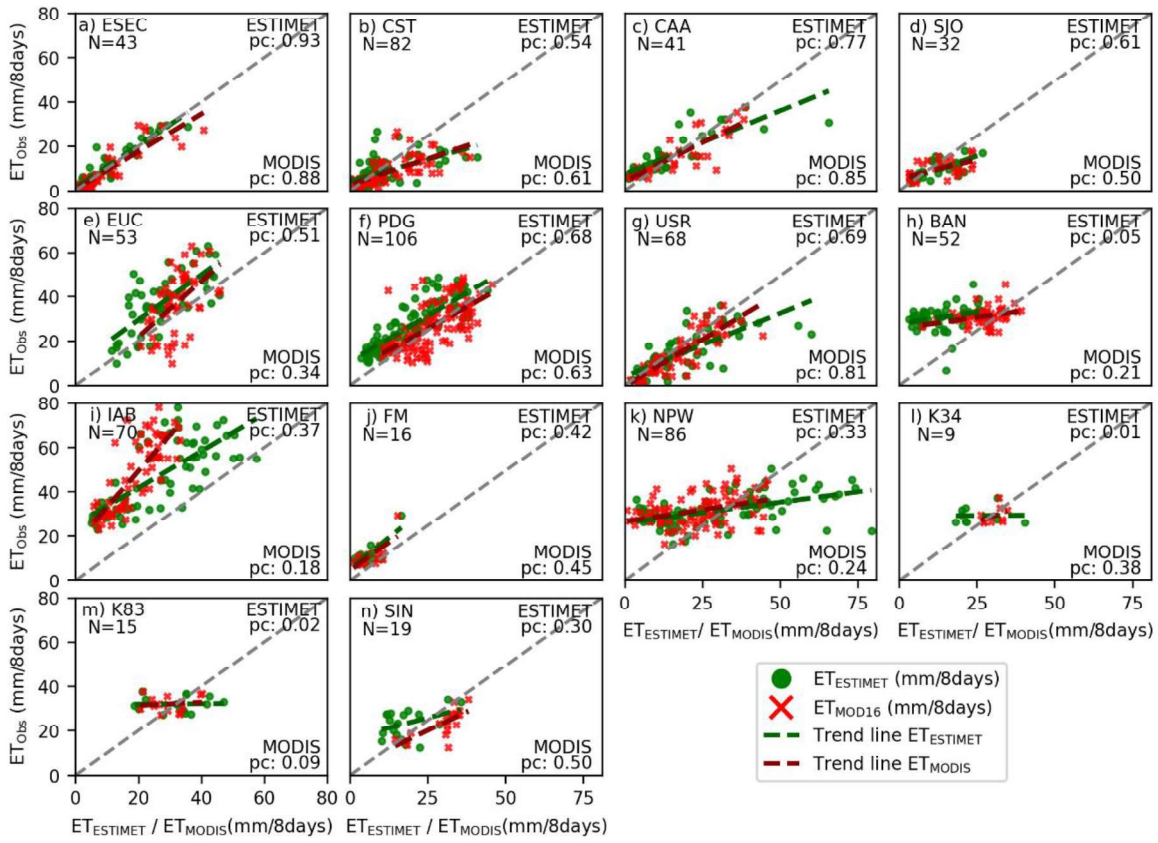

Figure 15 - Scatterplots of 8-day accumulated evapotranspiration, modelled by the ESTIMET ($ET_{ESTIMET}$) and MOD16A2GF (ET_{MODIS}) models, versus the 8-day accumulated estimations by the Eddy Covariance (ET_{Obs}) method at the 14 flux towers located in the (a-d) Caatinga, (e-i) Cerrado, (j-k) Pantanal, and (l-n) Amazon biomes. The metric ρc (concordance correlation coefficient) is shown to statistically compare the similarity between the 8-day variations of ET_{Obs}, $ET_{ESTIMET}$, and ET_{MODIS}. N represents the sample size.

The smallest bias between the accumulated 8-day $ET_{ESTIMET}$ and ET_{Obs} was found at the NPW (PBIAS = -3.28%; Pantanal) and K83 (PBIAS = 0.56%; Amazon) sites, while the largest was at BAN (PBIAS = -58.92%; Cerrado) (Fig. 16). MOD16A2GF presented its smallest accumulated 8-day biases at CAA (PBIAS = 2.43%; Caatinga) and its highest at IAB (PBIAS = -60.60%; Cerrado). Overall, $ET_{ESTIMET}$ presented a mean PBIAS $\leq \pm 13\%$ for six sites (ESEC, CST, IAB, NPW, K83, and SIN), while this performance was reached for ET_{MODIS} at seven sites (CAA, SJO, EUC, PDG, USR, BAN, FM and K34) (Fig. 16d).

The lowest RMSE were observed at sites located in the Caatinga and Pantanal biomes (i.e. ESEC, with RMSE = 3.32 mm/8-days; SJO, with RMSE = 4.84 mm/8-days; and FM, with RMSE = 6.64 mm/8-days; respectively) (Fig. 16c). When comparing the mean 8-day accumulated RMSE data from $ET_{ESTIMET}$ with that from ET_{MODIS}, both were similar for eleven sites (ESEC, CST, CAA, SJO, EUC, PDG, USR, FM, NPW, K83, and SIN), with

differences lower than 3 mm/8-days and $ET_{ESTIMET}$ presenting the largest overall errors. The largest mean RMSE for the $ET_{ESTIMET}$ estimations were found at the BAN (Cerrado) and NPW (Pantanal) sites (RMSE = 19.64 and 16.98 mm/8-days, respectively). The evaluation of ESTIMET and MOD16A2GF for all 14 experimental sites indicates that both models presented a reasonable performance for ET estimates (Fig. 8ab). However, using ESTIMET statistically resulted in a slightly better performance in terms of similarity (ρc = 0.63) when compared to MOD16A2GF (ρc = 0.58). A higher value of ρc was also observed for ESTIMET in comparison to PML_V2 (ρc = 0.45) and GLEAM 4.1a (ρc = 0.47) when all experimental sites were considered (Fig. 16c-d).

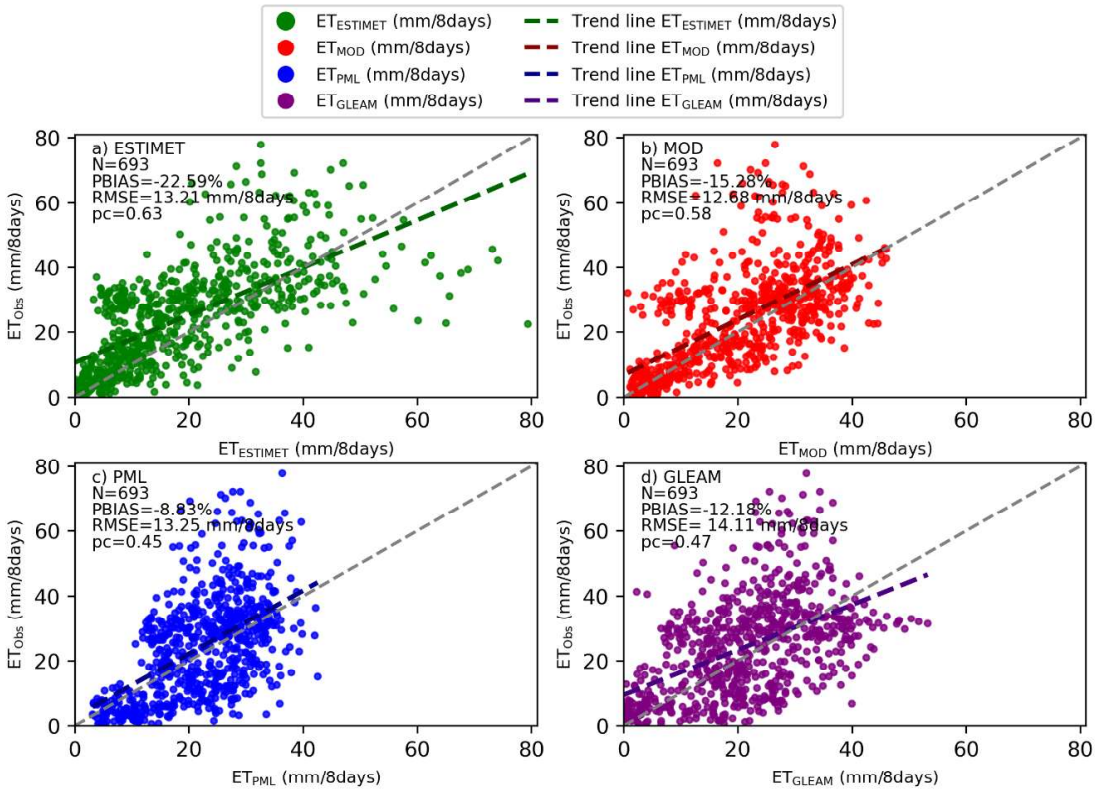

Figure 16 - Scatterplots of 8-day accumulated evapotranspiration modelled by the (a) ESTIMET ($ET_{ESTIMET}$), (b) MOD16A2GF (ET_{MODIS}), (c) PML_V2 (ET_{PML}), and (d) GLEAM 4.1a (ET_{GLEAM}) models, versus the 8-day accumulated estimations using the Eddy Covariance (ET_{Obs}) method for all 14 experimental sites. The metrics ρc (concordance correlation coefficient), root mean square error (RMSE), and Percent Bias (PBIAS) are shown to statistically compare the similarity between the 8-day variations of ET_{Obs} and the satellite-based datasets. N represents the sample size.

Overall, ESTIMET presented a better linear relationship than PML_V2 and GLEAM 4.1a at ten and nine sites, respectively, highlighting the best performance of ESTIMET, particularly at the Caatinga and Cerrado sites. This was particularly the case when compared

with the PML_V2 product (Figs. 17 and Fig. 19). Regarding the RMSE, $ET_{ESTIMET}$ and ET_{MODIS} presented lower values (13.21 and 12.68 mm/8-days, respectively) compared to the ET estimations by PML_V2 (13.25 mm/8-days) and GLEAM 4.1a (14.11 mm/8-days), considering all of the experimental sites (Fig. 16). The lower values of RMSE for ESTIMET were observed in 8 and 9 out of 14 sites, compared to PML_V2 and GLEAM 4.1a, respectively (Fig. 17 and Fig. 18). All products presented negative values of PBIAS, with values closer to zero being observed for PML_V2 (-8.83%) and GLEAM 4.1a (-12.18%) when compared to $ET_{ESTIMET}$ (-22.59%) and ET_{MODIS} (-15.28%) (Fig. 16). This was probably influenced by the mutual annulment between positive and negative differences. When considering all metrics in the Taylor diagram (Fig. 20), ESTIMET exhibits the best correlation, the second smallest RMSE, and the standard error closest to the observations.

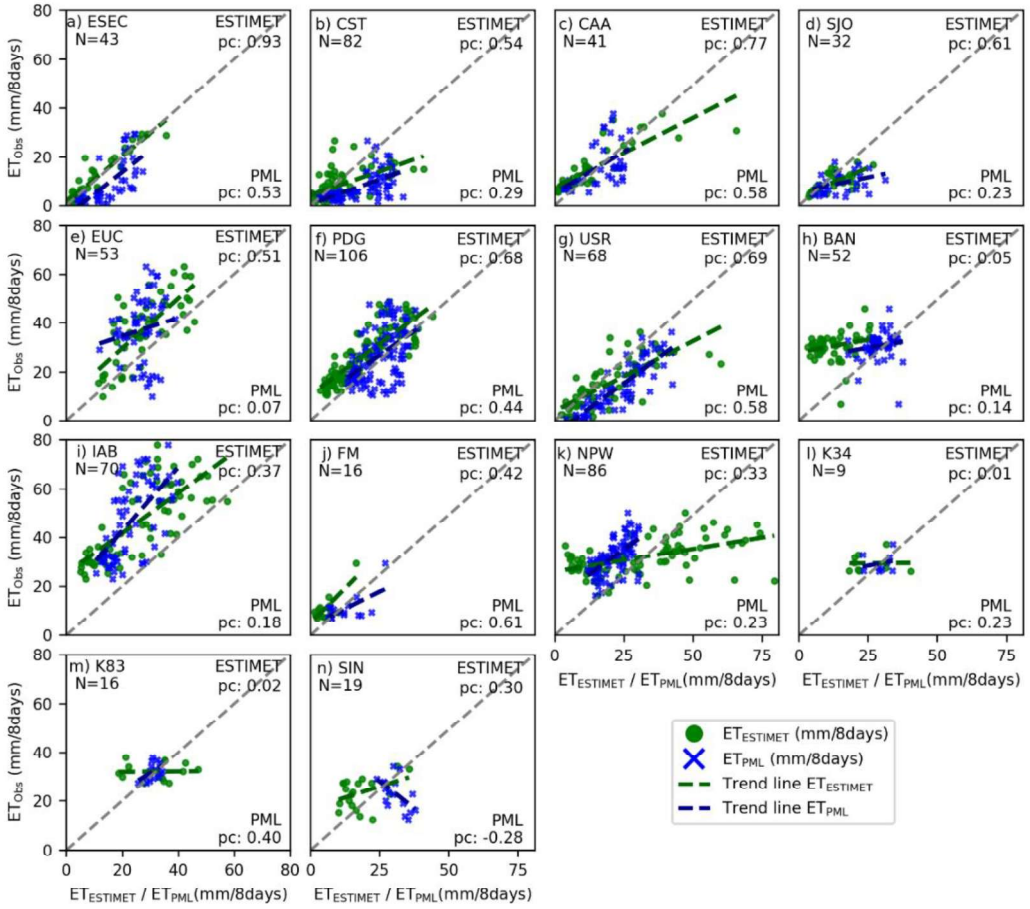

Figure 17 - Scatterplots of 8-day accumulated evapotranspiration modelled by the ESTIMET ($ET_{ESTIMET}$) and PML_V2 (ET_{PML}) models, versus the 8-day accumulated estimations by the Eddy Covariance (ET_{Obs}) method in the 14 flux towers located in the (a-d) Caatinga, (e-i) Cerrado, (j-k) Pantanal, and (l-n) Amazon biomes. The metrics r (Pearson's correlation coefficient) and concordance correlation coefficient (ρc) are shown to statistically compare the similarity between the 8-day variations of ET_{Obs}, $ET_{ESTIMET}$, and ET_{MODIS}. N represents the sample size.

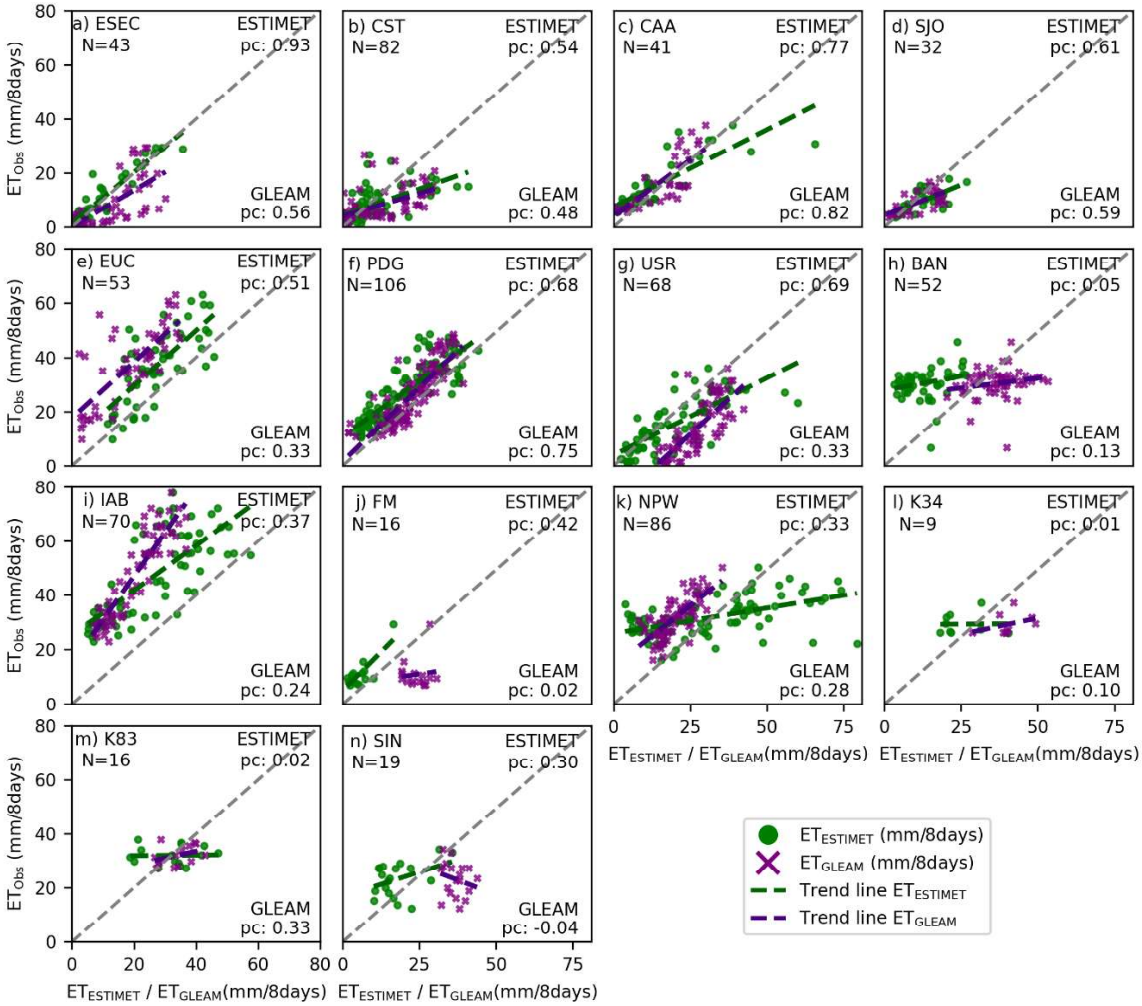

Figure 18 - Scatterplots of 8-day accumulated evapotranspiration modelled by the ESTIMET ($ET_{ESTIMET}$) and GLEAM 4.1a (ET_{GLEAM}) models, versus the 8-day accumulated estimations by the Eddy Covariance (ET_{Obs}) method in the 14 flux towers located in the (a-d) Caatinga, (e-i) Cerrado, (j-k) Pantanal, and (l-n) Amazon biomes. The metrics r (Pearson's correlation coefficient) and concordance correlation coefficient (ρc) are shown to statistically compare the similarity between the 8-day variations of ET_{Obs}, $ET_{ESTIMET}$, and ET_{MODIS}. N represents the sample size.

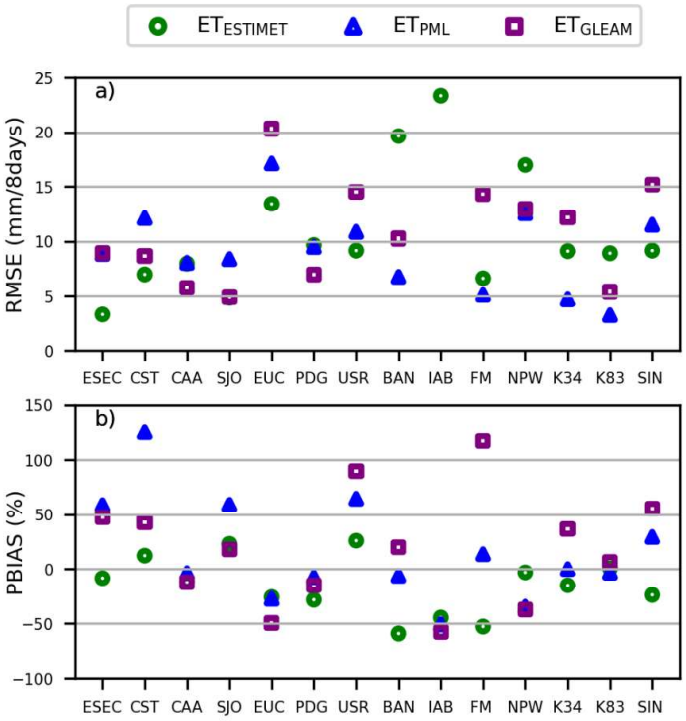

Figure 19 - (a) RMSE and (b) PBIAS statistics for ESTIMET ($ET_{ESTIMET}$), PML_V2 (ET_{PML}), and GLEAM 4.1a (ET_{GLEAM}) evapotranspiration data when compared to the Eddy Covariance (ET_{Obs}) observations in the flux tower sites.

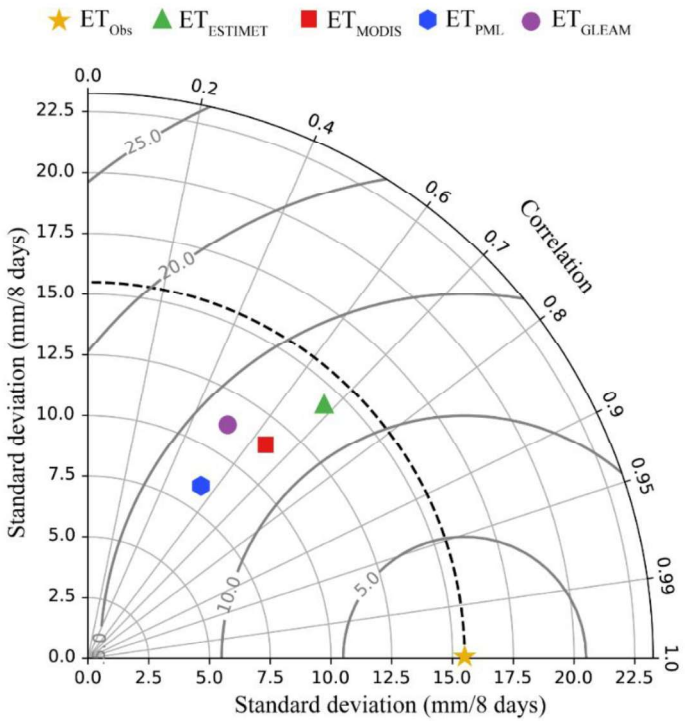

Figure 20 - Taylor diagram of 8-day accumulated evapotranspiration modelled by the ESTIMET ($ET_{ESTIMET}$), MOD16A2GF (ET_{MODIS}), PML_V2 (ET_{PML}), and GLEAM 4.1a (ET_{GLEAM}) models against the 8-day accumulated estimations using the Eddy Covariance (ET_{Obs}) method for all 14 experimental sites.

4.3.3 Annually based evaluation of ESTIMET at a catchment scale

Fig. 21 shows the scatterplots of annual accumulated ET modelled by ESTIMET and the three global satellite-based ET products, compared to the ET_{Catch} calculated by the water balance in 5 Brazilian biomes. The evaluations show that $ET_{ESTIMET}$ presented higher values of ρc in the Amazon (0.49), Atlantic Forest (0.37), and Cerrado (0.52) biomes when compared to the other three products, which ranged from -0.08 (GLEAM 4.1a) to 0.36 (MOD16A2GF) in the Amazon, from 0.02 (PML_V2) to 0.14 (GLEAM 4.1a) in Atlantic Forest, and from 0.01 (PML_V2) and 0.35 (MOD16A2GF) in Cerrado. Overall, ESTIMET also exhibited low values of RMSE and PBIAS in the Amazon (RMSE = 170.77 mm/year and PBIAS -1.49%), Atlantic Forest (RMSE = 152.99 mm/year and PBIAS 7.13%), and Cerrado (RMSE = 164.57 mm/year and PBIAS -10.75%) biomes. This can be likened to the other satellite-based products. For instance, the ET estimated by GLEAM 4.1a in the Amazon presented an elevated RMSE (301.60 mm/year).

A low similarity was observed between all products and the water balance calculations in the Caatinga biome, with a particular emphasis on ESTIMET, which presented ρc values close to 0 (-0.01) and high RMSE (422.27 mm/year) and PBIAS (52.74%). These pronounced discrepancies between the ET_{Catch} and those estimated by the products in the Caatinga biome were noted in three catchments (Fig. 22), with an overall tendency for the satellite-based products to overestimate the ET calculated by the water balance over the years, especially those modelled by ESTIMET. Similar statistic metrics (i.e. ρc ≈ 0.10, RMSE ≈ 220 mm/year, and PBIAS ≈ 15%) were observed for the three Penman–Monteith-based models (i.e. ESTIMET, MOD16A2GF, and PML_V2) in the Pampa biome, where GLEAM 4.1a stood out (ρc = 0.23, RMSE = 141.18 mm/year, and PBIAS = 3.05%).

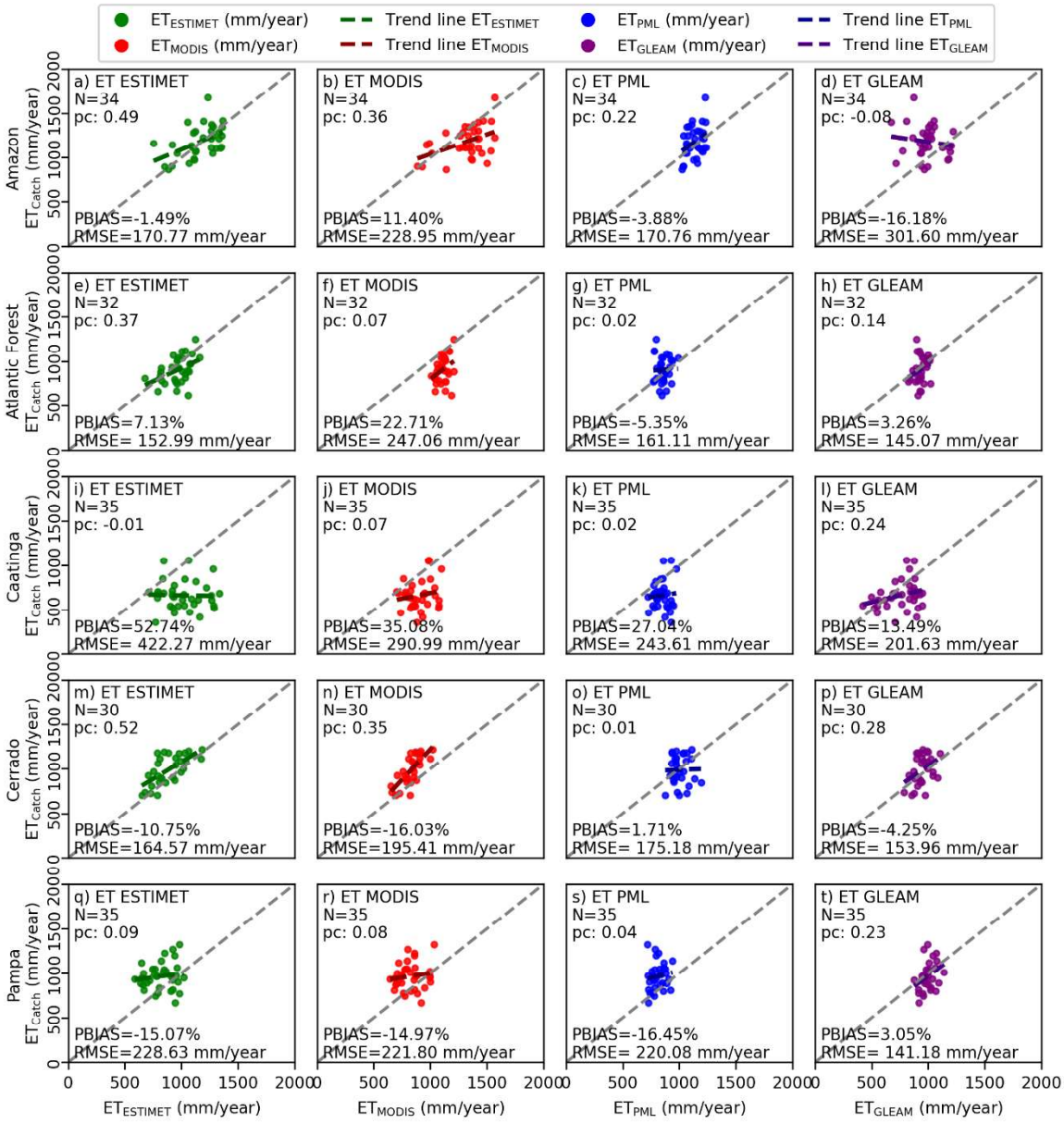

Figure 21 - Scatterplots of annual accumulated evapotranspiration modelled by the ESTIMET ($ET_{ESTIMET}$), MOD16A2GF (ET_{MODIS}), PML_V2 (ET_{PML}), and GLEAM 4.1a (ET_{GLEAM}) models, versus the annual accumulated evapotranspiration calculated by the water balance in the catchments (ET_{Catch}) of the (a-d) Amazon, (e-h) Atlantic Forest, (i-l) Caatinga, (m-p) Cerrado, and (q-t) Pampa biomes. The metrics concordance correlation coefficient (ρc), root mean square error (RMSE), and Percent Bias (PBIAS) are shown to statistically compare the similarity between the calculated and modelled annual evapotranspiration. N represents the sample size.

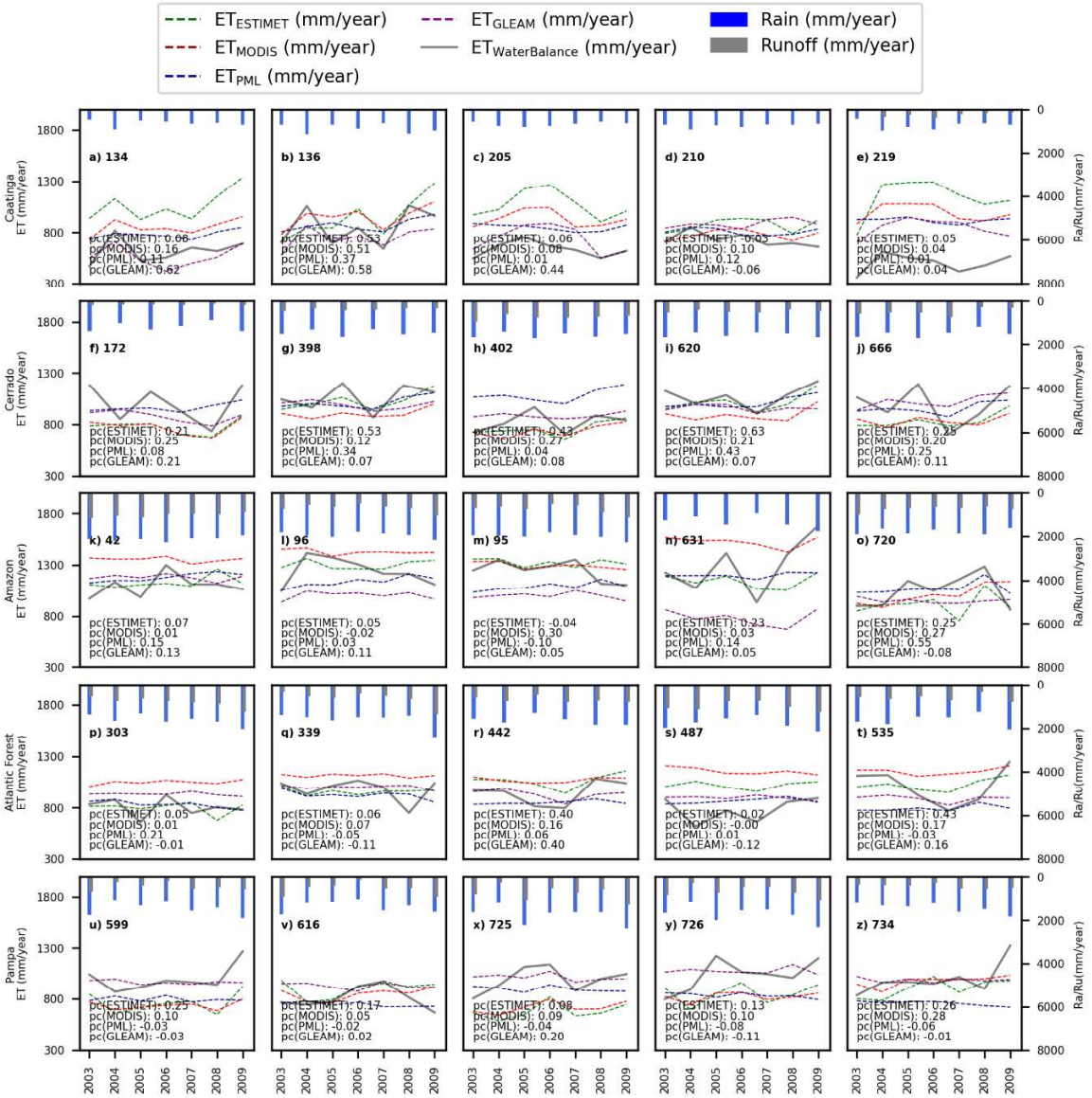

Figure 22 - Annual time series of actual evapotranspiration estimated by ESTIMET (ETESTIMET), MOD16A2GF (ETMODIS), PML_V2 (ETPML), and GLEAM 4.1a (ETPML) compared to the evapotranspiration calculated by the water balance approach in 25 catchments located in the (a-e) Caatinga, (f-j) Cerrado, (k-o) Amazon, (p-t) Atlantic Forest, and (u-z) Pampa biomes.

4.4 Discussion

4.4.1 Accuracy of ESTIMET in estimating ground ET in tropical biomes

The selection of ET products for scientific research necessitates consideration of their varying performances at a spatial scale, as well as the impact of land cover and climate conditions (Zhu et al., 2022). Our study indicates that the general trend is for $ET_{ESTIMET}$ and ET_{MODIS} to be underestimated at a local scale, with most ET values presenting the lowest

PBIAS (Fig. 13cd) and located above the 1:1 line in the scatterplots (Fig. 15, 17, and 18). This finding is consistent with those from other studies conducted in South America (e.g. Salazar-Martinez et al., 2022; Andrade et al., 2024). Similar to the study by Melo et al. (2021), which evaluated four remote sensing-based ET models forced by ground-based meteorological data in South America, EC-based analyses also found that the best overall performance of the Penman–Monteith-based models was noted at sites located in semi-arid regions, such as the Caatinga biome. For such a biome, the correlations of the daily ET estimations obtained in our study using ESTIMET (ρc ranging from 0.46 to 0.80) were similar to, or better than, those reported by Bezerra et al. (2023). This study employed two remote sensing-based surface energy balance models (i.e. SEBAL and STEEP) at three identical flux towers (i.e. ESEC, CAA, and CST), with values of ρc ranging from 0.18 to 0.67 for SEBAL and from 0.41 to 0.80 for STEEP. The good performance of ESTIMET in Caatinga was achieved after the monthly composition of the reflectance-based parameters was carried out to mitigate the impact of clouds, which could affect the variability of land surface information used as input for the model, especially in highly dynamic hydroclimatic vegetation systems such as the Caatinga and Cerrado biomes. For instance, the disagreements between $ET_{ESTIMET}$ and ET_{Obs} in these two biomes were not associated with the beginning or end of the rainy seasons.

Regarding the quality of estimations at some of the flux towers, in which the concordance/correlation between ET_{MODIS} and ET_{Obs} was already reasonable (Fig. 15) because of the greater seasonality of ET drivers, significant improvements in the correlations were observed between $ET_{ESTIMET}$ and ET_{Obs} (i.e. ESEC, pasture in Caatinga; EUC, monoculture in Cerrado; and PDG, Forest in Cerrado). Nevertheless, some flux towers, already reasonably characterised through MODIS, featured a slight degradation of this concordance/correlation by ESTIMET (i.e. USR, pluriculture in Cerrado; and CST and CAA, deciduous forest in Caatinga). Lower quality RMSE and PBIAS are also found for USR, suggesting that a patchwork-like zone might be more difficult to characterise for ESTIMET. This is counterintuitive as ESTIMET has a finer spatial resolution. However, these discrepancies seem to be related to some outliers in specific periods, with much higher values of $ET_{ESTIMET}$ in February and March 2006 (Fig. 14g), while EC provided remarkably low ET values. Except for this specific period, ESTIMET achieves better ρc and RMSE for daily (0.59-0.64 and 1.37-1.15 mm/day) and 8-day analyses (0.69-0.75 and 9.15-7.06 mm/8-days). Similarly, despite a lower concordance/correlation for CST, the errors (PBIAS = 12.11% and RMSE = 6.99 mm/8-days) were lower when compared to MOD16A2GF

(PBIAS = 41.45% and RMSE = 7.05 mm/8-days) and, especially, GLEAM 4.1a (PBIAS = 42.60.% and RMSE = 8.68 mm/8-days) and PML_V2 (PBIAS = 125.33% and RMSE = 12.10 mm/8-days). These trends suggest that the variability and complexity of land use may significantly impact the comparison between remote-sensing strategies and ground-based estimations (Ruhoff et al., 2013).

This difficulty appears to be even greater in specific flux towers, where both MODIS and ESTIMET present discrepancies with the in-situ measurements, such as SJO (Caatinga, near the limit with the Atlantic Forest) and K34 (Amazon), in which RMSE increases when using ESTIMET. These findings corroborate previous studies, which reported that the performance of the MOD16 ET product was better in semi-arid regions than in semi-humid or humid regions. The performance of MOD16 ET was also better during dry seasons than in wet seasons (Mu et al., 2011; Degano et al., 2021). Apparently, ESTIMET followed the same trend. This larger difference, already pointed out by Salazar-Martinez et al. (2022) and Andrade et al. (2024) for tropical forested areas, is clearly the case for sites located in or near to the Amazon basin featuring low seasonality, which was also observed for the GLEAM 4.1a and PML_V2 products in our analyses and previous studies (Zhang et al., 2023; Yang, 2025). The weaker correlations of the satellite-based products in the tropics compared to greater latitudes are thought to be the result of differences in seasonality rather than differences in performance (Salazar-Martinez et al., 2022; Miralles et al., 2011; Yilmaz et al., 2014). In or near the Amazon, the seasonal ET variability remains moderate, whereas sites at greater latitudes typically exhibit a greater range of variability, which favours larger correlations with ET_{Obs}. This is consistent with the latitude effect on energy parameters (e.g. T and Rn) identified by Patriota et al. (2024), which presents lower variations due to moderate changes in the seasonal solar angle. In addition, precipitation seasonality is generally lower in the Amazon than elsewhere in the tropics (Feng et al., 2013; Lemos et al., 2023), which contributes to buffering vegetation (NDVI or EVI2) and surface parameter changes (albedo) (Andrade et al., 2024). Such vegetation parameters, especially NDVI, often saturate evergreen broad-leaved forests holding tropical climates (e.g. the Amazon and Atlantic Forest), causing a non-linear response of such parameters in vegetation index-based models (Laipelt et al., 2021; Oliveira et al., 2022). However, the calibrated equations of such models are based on adjustments using linear regressions. Our results indicate that ESTIMET, although not always improving the 8-day error estimations of ET (i.e. PBIAS and RMSE) compared to MODIS, usually catches the seasonality (correlations) of ET for some of these specific sites (e.g. SJO in Caatinga but in a transition zone near the limit with

the Atlantic Forest) (Fig. 15). The ability of ESTIMET to capture the fluctuations of ET is especially noted when analysing the daily-based comparisons (Fig. 12).

For NPW (Pantanal Biome) and BAN (Cerrado Biome), ESTIMET provided lower-quality results with larger RMSE and, sometimes, weaker correlations compared to the three global satellite-based ET products, although they presented low PBIAS in NPW (likely compensated by the positive and negative values). For this site, ET is overestimated (Fig. 15), which is consistent with the observations in Andrade et al. (2024), who used a hybrid SEBAL-MODIS-based model to analyse data between November and March of each year. Likewise, in USR, such discrepancies in NPW seem to be related to some outliers during the rainy seasons, presenting ET values higher than 60 mm/8-days (see Fig. 14). This phenomenon is still not fully understood, and the reasons for the remote sensing data deviating from the measured values should still be clarified in this context. Allen et al. (2021) suggested that an artificial increase in atmospheric demand may occur, potentially overcompensating for the reduction in available surface moisture observed during the dry season, and thereby generating higher values of ET. In parallel, waterlogging is known to occur during wet seasons at NPW (Pantanal Biome) and BAN (Cerrado Biome) (Table 5). This would be a consistent explanation for the difference between ET_{Obs} and $ET_{ESTIMET}$ trends in some accumulated 8-day data, both of which could be highly altered for these sites.

Even though the energy balance closure issue has been addressed by excluding data with higher energy imbalances at each flux tower, the assessment outcomes can still be influenced by the difference in scale between the footprint of the eddy covariance observations and the pixels of the ET products. The flux footprint typically spans less than 1 km² (Chu et al., 2021), depending on each site flux tower deployment, and the pixel sizes of ET products range from 0.062 (ESTIMET) to 100 km² (GLEAM 4.1a). While the remote sensing products should fit well within the flux footprint of each tower, there might still be a disparity in the scales of the ET contributions, potentially combined with changing meteorological conditions that can lead to a discrepancy in vegetation representativeness between the pixels and the flux tower observations (Hobeichi et al., 2018; Jiménez et al., 2018). Such a mismatch can also arise from inaccuracies in the models' vegetation and land cover input data, such as incorrect classifications. Since many models compute ET using parameters which are specific to land cover (Anderson et al., 2007; Miralles et al., 2011; Mu et al., 2011), a mismatch between the actual vegetation at the observation site and that detected in the model's pixels could potentially impact the assessment results (Hu et al., 2015; Melo et al., 2021). This probably occurred at the SJO site, which is located in a

transitional zone between the Caatinga and Atlantic Forest biomes, presenting a mixture of cover vegetation (pasture and natural vegetation) (Machado et al., 2016), which was probably not well represented by the MOD16A2GF, PML_V2, and GLEAM 4.1a datasets.

Another potential limitation in the ground-truth data, for comparison with 8-day accumulated satellite-based data (e.g. MOD16A2GF and PML_V2), is related to the low availability of EC data in tropical regions (Salazar-Martínez et al., 2022) like Brazil. When excluding all rainy days from the analyses within this window, it consequently reduces the data availability for validation even further. However, the gap-filling method used for the 8-day EC data in this study (i.e. the average of ET on non-rainy days of the same week) also introduces uncertainties into the accumulated analyses, which could compromise the performance of the satellite-based datasets.

Regarding the catchment scale, ESTIMET presents better correlation/concordance associated with the lower RMSE, when compared to the ET calculated by the water balance in the three major biomes (i.e. Atlantic Forest, Amazon, and Cerrado), which cover more than 85% of the Brazilian territory. Our regional analysis also revealed an overall tendency for the MOD16A2GF product to overestimate the ETCatch in the Amazon biome, a finding also observed in previous studies (Maeda et al., 2017; Andrade et al., 2024). For this larger Brazilian biome, most mean estimations of MOD16A2GF were between 1,250 and 1,500 mm/year in the analysed catchments, while ESTIMET mostly presented annual mean values lower than 1,250 mm/year. Such annual ranges of ET values in the Amazonian catchments (as estimated by ESTIMET) were closer to those obtained from the other two satellite-based products (i.e. PML_V2 and GLEAM 4.1a) and by other studies using different approaches (e.g. Ruhoff et al., 2022; Andrade et al., 2023). The map showing the mean annual ET between 2003 and 2022 (estimated by ESTIMET and MOD16A2GF) illustrates that the main (absolute and relative) differences between the two datasets are in the Amazonian biome. ESTIMET presents lower overall values of ET and better captures the spatial variability of ET in the Amazon region, possibly due to the higher spatial resolution and more detailed LULC and meteorological data, which are able to better differentiate vegetation types and microclimates (Fig. 23).

The general inclination of MOD16GFA2 to overestimate the ET_{Catch} was also identified in our analysis in the Atlantic Forest, featuring evergreen broad-leaved vegetation, which was not observed in ESTIMET, GLEAM 4.1a, or PML_V2. Such overestimation of MOD16A2GF was not identified in previous studies (e.g. Ruhoff et al., 2022). Fig. 23 shows that the twenty-year mean ET estimated by ESTIMET in the Atlantic Forest mostly ranges

from 1,000 to 1,500 mm/year, whereas for MOD16A2GF, this value is generally equal to or greater than 1,500 mm/year. Unlike the local analyses, where ESTIMET exhibited good performance at daily and 8-day accumulated ET, when likened to the flux towers in Caatinga, the comparisons at the catchment scale of ET estimated by the satellite-based products in this biome overestimated the water balance calculations. These lower values of ET_{Catch} in Caatinga can be attributed to the predominance of catchments with non-perennial rivers in this biome, which are primarily dependent on surface runoff (Almagro et al., 2021). Another reason for this underestimation of ET_{Catch} may be related to the underrepresentation of ground-based rainfall, which can reduce ET calculations via water balance (Andrade et al., 2022). Overall, Fig. 23 also shows that ESTIMET better captures ET variability, not only in the Amazon but also in all other biomes.

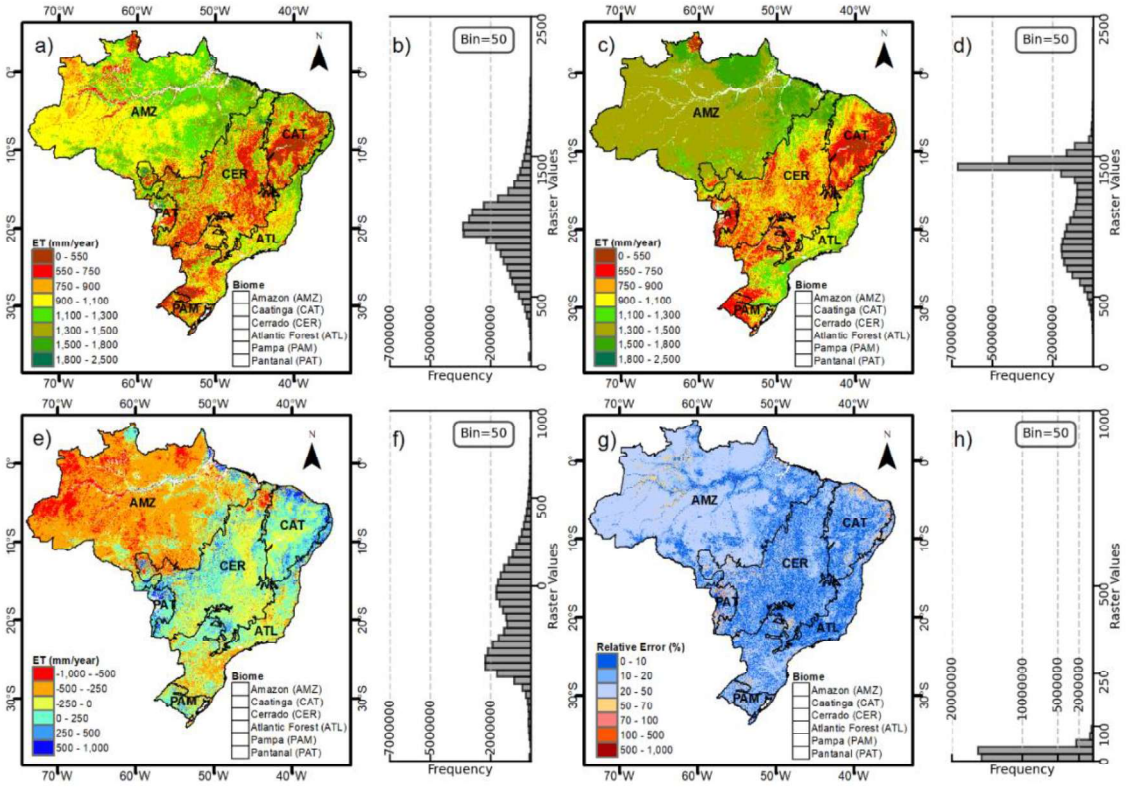

Figure 23 - Spatial distribution of the mean annual evapotranspiration between 2003 and 2022 estimated by (a) ESTIMET and (c) MOD16A2GF, with panels showing their respective (b and d) latitudinal profiles. (e) Spatial distribution of the absolute and (g) relative differences between the estimations of ESTIMET and MOD16A2GF, with panels showing their respective (f and h) latitudinal profiles. The symbols AMZ, CAT, PA, CER, ATL, and PAM refer to the Amazon, Caatinga, Pantanal, Cerrado, Atlantic Forest, and Pampa biomes, respectively.

Such local and regional observations suggest that ESTIMET may be a valuable tool for estimating daily ET. However, some specific conditions may lead to a lack of confidence,

such as wet conditions that favour waterlogging, which hinders robust comparison with ground-based EC towers. Beyond this, the effect of the relative complexity of land use at a fine scale could appear overwhelming. For future research, another option could be to utilise reflectance data to estimate the biophysical parameters with even higher spatial resolution than the 250 m MODIS data. This could involve using sources such as the 10-m Sentinel-2 NDVI or the 3-m Planet NDVI. An example of this approach is seen in the study by Aragon et al. (2018), who utilised 3-m Planet NDVI to create ultra-high-resolution ET estimates using the Priestley-Taylor Jet Propulsion Laboratory (PT-JPL) model. In areas with a tendency towards land use homogeneity, ESTIMET yielded better results than MOD16A2GF (e.g., PDG and EUC), while more complex areas presented similar difficulties in capturing seasonality, as also observed in GLEAM 4.1a and PML_V2.

4.4.2 ESTIMET as new support for remote long-term ET evaluation at a finer spatiotemporal resolution

Despite some specific limitations mentioned above, ESTIMET makes it possible to evaluate continuous daily ET for any day since 2003 in tropical latitudes, even when the area was overcast by clouds, with better latency (monthly) and spatial resolution (250 m) than other global ET datasets (i.e. having the best 8-day and 500-m resolutions, as well as annual latency). In the challenging context of a large cloud presence between the tropics (Liu et al., 2020; Ahamed et al., 2021), the information from ESTIMET has the potential to be an important tool for providing reliable and continuous regional ET series. For example, these refined data can be used as input for water resource management strategies and agricultural activities. Furthermore, the daily availability of ET data expands the potential for hydrological analyses and simulations, allowing precise water balance modelling for catchments (Guerschman et al., 2022). Indeed, ESTIMET allows access to one of the most important terms of the hydrological balance, at the same temporal resolution usually obtained for precipitation and, therefore, provides the possibility for estimating the water deficit or water surplus at a daily scale from remote sensing; this being of great interest for water resource, agricultural and risk management. This type of data also enables a more detailed and continuous long-term analysis of ET in tropical latitudes, considering that the patterns and (environmental and anthropogenic) factors of this component remain poorly understood, especially in such regions (Fleischmann et al., 2023).

The two insets exhibiting the spatial variability of ET around the EUC site (Cerrado), obtained by MOD16A2GF (Fig. 24a) and ESTIMET (Fig. 24b) in an 8-day window between 18 May 2007 and 25 May 2007 during the beginning of the dry season, show how finer the spatial resolution of ESTIMET (250 m) is when compared to MOD16A2GF (500 m). Such improved spatial resolution enables a more accurate representation of land contrasts in ET estimation. For instance, ESTIMET captured four distinct values of ET, ranging from 17.29 to 18.78 mm/8-days in a 0.25 km² inset containing eucalyptus-dominated vegetation with different growth stages, as shown by the contrasting reflectance responses and textures (Fig. 24b). In contrast, this was represented by only one averaged value of ET (i.e. 22.6 mm/8-days) by the MOD16A2GF product. The daily information in ESTIMET also enables a better representation of the ET sensitivity to meteorological variations, as shown in Fig. 24e. For instance, while the ET_{MODIS} remains unchanged within the same 8-day window, represented by an average of 2.86 mm/day of the accumulated ET, the values modelled by the ESTIMET varied between 1.66 and 3.01 mm/day, presenting sensitivities to daily rain events observed at the EUC site.

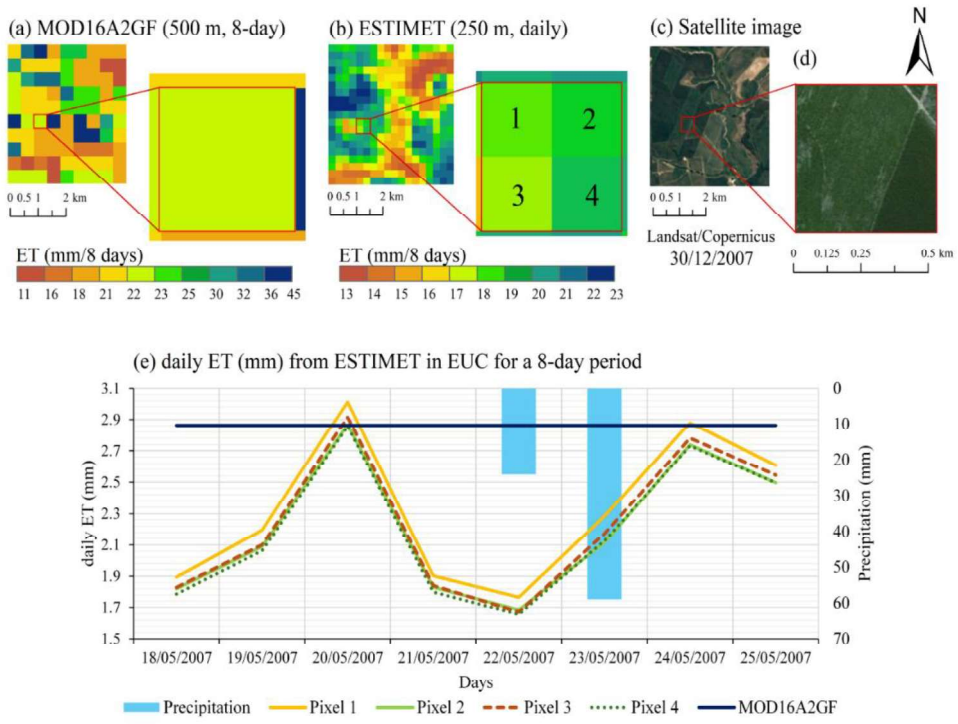

Figure 24 - Spatial variability of 8-day accumulated evapotranspiration modelled by the (a) MOD16A2GF (ET_{MODIS}) and (b) ESTIMET ($ET_{ESTIMET}$) models between 18th May 2007 and 25th May 2007 in the surroundings of the EUC site (Cerrado), with 500 and 250 m spatial resolutions, respectively. (c) Temporal variability of daily evapotranspiration modelled by the two models and precipitation within this temporal window. True coloured satellite images (Landsat/Copernicus) of 30th December 2007 from Google Earth, corresponding to the (d) largest and (e) smallest evapotranspiration map insets.

5 POTENTIALITIES OF ESTIMET FOR TREND AND TIME-SENSITIVITY ANALYSIS OF ET

5.1 Contextualisation

Several studies have been carried out to understand the trends and influences of other biophysical and climatic parameters on ET at global (e.g. Zhang et al., 2016; Hobeichi et al., 2021) and local (e.g. Adeyeri et al., 2021; Lang et al., 2024; Sabino et al., 2024) scales. ET variability has already been analysed for Brazil and the entire South American continent using the SEBAL model, where a general trend of increasing ET was identified, with variations according to climates and biomes (Fleischmann et al., 2023; Laipelt et al., 2021; Andrade et al., 2024). However, these studies have limitations in terms of temporal continuity (i.e. due to the limited number of images used in the analysis caused by the exclusion of many days with high cloud cover or rainy months) and scale (i.e. at the river basin level, with the exclusion of some biomes from the analyses). As ET is the terrestrial hydrological flux most sensitive to vegetation changes (DeBano et al., 1998; Collar et al., 2023), its understanding associated with each type of land cover and land use modification helps the sustainable management of natural resources (Saddique et al., 2020; Cabral Júnior et al., 2022; Antunes et al., 2024).

Due to the limitations of the regional and global products currently available for obtaining distributed, continuous, and high-resolution ET information from satellite data, the patterns and factors of this component remain poorly understood, especially in tropical regions such as Brazil (Fleischmann et al., 2023). However, Claudino et al. (2025) have recently proposed an improved model, specifically adapted for tropical areas, which mitigates the impact of cloud cover. This model, called ESTIMET, is based on an improvement of the MOD16 product and enables the daily estimation of ET at a 250 m resolution, without temporal gaps, thereby permitting detailed spatiotemporal analysis of ET variability.

Therefore, in order to evaluate the applicability of this refined product and illustrate its interest in environmental studies, this chapter explores the potentialities of ESTIMET to continuously estimates distributed daily ET, focusing on i) the analysis of long-term (2003-present) ET trends and their correlations with climatic (precipitation) and anthropogenic (land use and land cover) factors in two contrasting Brazilian biomes (Caatinga and Pantanal) to understand on a large scale the impacts of vegetation cover evolution/alteration

and precipitation changes on this main output of the water balance; and the investigation of ET variability in scenarios of land use and land cover changes caused by wildfires and deforestation processes in these two contrasting biomes.

5.2 Materials and methods

5.2.1 Trend analysis

The long-term spatiotemporal trends of ET for the two biomes were statistically analysed by the nonparametric Mann-Kendall test (Mann, 1945; Kendall, 1948) with a significance level of 95%, calculated according to Eq. 17.

$$S = \sum_{i=1}^{n-1} \sum_{j=i+1}^{n} \operatorname{sign}(X_j - X_i), \operatorname{sign}(X_j - X_i) = \{+1\ (X_j - X_i) > 0\ 0\ (X_j - X_i) = 0\ -1\ (X_j - X_i) < 0 \quad (17)$$

where n is the number of observations, X_i represents the observation at time i, X_j represents the observation at time j, and sign(x) is the sign function of x.

Eqs. 18 and 19 were used to calculate the variance of S (Var(S)) and the standard normal distribution (Z), respectively.

$$\mathrm{Var}(S) = \frac{n(n+1)(2n+5) - \sum_{i=1}^{m} ti(ti-1)(2ti+5)}{18} \quad (18)$$

$$Z = \{\frac{S-1}{\sqrt{\mathrm{Var}(S)}}, S > 0\ 0, \qquad S = 0\ \frac{S+1}{\sqrt{\mathrm{Var}(S)}}, S < 0 \quad (19)$$

where n is the number of data, m is the number of tied groups, which indicates sample data with the same value in extension i.

Positive Z values indicate increasing trends, while negative Z values indicate decreasing trends. In addition, the corresponding p-value was calculated to determine the statistical significance of the trends, and the Theil-Sen slope (Sen, 1968) was used to estimate the slope of the observed trends.

5.2.2 Correlation between ET patterns and precipitation

The variability of ET can be amplified or constrained by several climatic factors (e.g. precipitation, relative humidity, surface temperature, and biomass), with the precipitation playing a key role (Moreira et al., 2019; Fleischmann et al., 2020). In this study, the precipitation patterns were selected to analyse the variability of ET estimated by ESTIMET in the face of changes in climatic patterns in the two contrasting biomes: Pantanal and Caatinga.

The monthly and annual precipitation data (2003-2022) used to assess its correlation with ET in the Caatinga and Pantanal biomes were obtained from the satellite-based IMERG BraMaL product (Freitas et al., 2024). IMERG BraMaL provides monthly precipitation data with a spatial resolution of 0.1º from 2001 to the present. This product improves the IMERG Early Run data through machine learning techniques and meteorological reanalysis data (MERRA-2), outperforming the IMERG Final Run product and other global precipitation products (e.g. CHIRPS, PERSIANN-CDR, and MSWEP). IMERG BraMaL also presents the following advantages when compared to most global products: lower latency for end-users, no dependence on field data, and no relationship between errors and local characteristics, greatly improving precipitation estimates in all regions of Brazil (Freitas et al., 2024). The annual average precipitation values used in this analysis were obtained for each area and for each representative land use and cover (vegetation, agriculture, urban, and non-vegetated areas) to verify the evolution of precipitation spatiotemporal trends in the two biomes during the last two decades. Pearson's correlation coefficient (r) was used to evaluate this relationship between ET and precipitation (Eq. 20).

$$r = \frac{\sum (x_i - \underline{x})(y_i - \underline{y})}{\sqrt{\sum (x_i - \underline{x})^2 \sum (y_i - \underline{y})^2}} \quad (20)$$

where x i is the value of variable x, y i is the value of variable y, x is the mean of variable x, and y is the mean of variable y. Values of r range from -1 to 1, with -1 indicating the strongest negative correlations and 1 indicating the strongest positive correlations.

In addition, the spatial variability of ET in the two biomes was analysed considering different climatic patterns, i.e. distinguishing drier, average, and wetter years throughout the

study period (2003–2020). In Caatinga, the year 2012 was selected as a dry year based on the studies of Marengo et al. (2018), the year 2017 was chosen as an average year based on the precipitation analyses of the biome obtained from IMERG BraMaL, while the year 2004 was selected as a wet year based on the studies of Alves et al. (2006). For Pantanal, the year 2020 was selected as a dry year (Costa et al., 2023), 2015 as an average year based on the IMERG BraMaL data, and 2011 as a wet year (Pereira et al., 2021). Once the years were defined, the annual ET maps for each entire biome were considered.

The restriction on the number of biomes and the temporal resolution of the analyses, which was monthly instead of daily, resulted from processing limitations imposed by the Google Earth Engine (GEE) platform. This cloud-based geospatial analysis platform limited the size and processing time of files per user, resulting in prolonged processing of results (e.g. 1 day to download the monthly shapefile of the Caatinga, 3 to 4 days for biomes with larger territorial extents, such as the Amazon). Thus, to enable the analyses, regions and temporal scales were selected, preserving the finer spatial scale (250 m) of ESTIMET. New strategies for processing daily data are being developed.

5.2.3 Analysis of ET patterns in response to rapid land use and land cover changes

To demonstrate the potentialities of ESTIMET for obtaining finer spatiotemporal resolution (daily with 500 m) data, the impacts of daily ET on rapid biophysical and/or anthropogenic changes were analysed. For this analysis, the variability of ET in locations where rapid and significant land use and land cover changes occurred due to wildfire and deforestation processes was selected in two specific locations within each biome (Fig. 25a and 25d).

The regions affected by forest fires were selected using the 1 km Burned Area system from the INPE's Burned Area Program. This system provides annual and monthly information on the burned areas (km²) for the Brazilian biomes, delimited using the AQ1Km product, which is constructed from data from MODIS Collection 6, collected simultaneously by the AQUA and TERRA satellites, with a 1-km spatial resolution (INPE, 2025). Thus, based on the data provided by the system, and considering the analysis period (2003-2022), the years and months with the highest occurrence of forest fires in each biome were defined. In Caatinga, the year 2015 (47,543 km², representing 5.6% of the biome's area) and the month of September (9,797 km²) were selected, while in Pantanal, the year 2020 (39,768 km², representing 26.4% of the biome's area) and the month of September (14,264 km²) were

chosen. Given the large number of forest fire outbreaks identified for the two biomes, protected areas were used as a selection criterion because they contain large portions of the biome's native vegetation. Thus, for the Caatinga biome, the region of Chapada Diamantina National Park (2,41 km² hotspot) was selected (Fig. 25b), which in 2015 was devastated by several fires that occurred from September to December (Santos et al., 2020). For Pantanal, the region of the Encontro das Águas State Natural Park (a 1.82 km² hotspot) was selected (Fig. 25e), one of the conservation units most severely affected by the 2020 forest fires (Magalhães Neto et al., 2022).

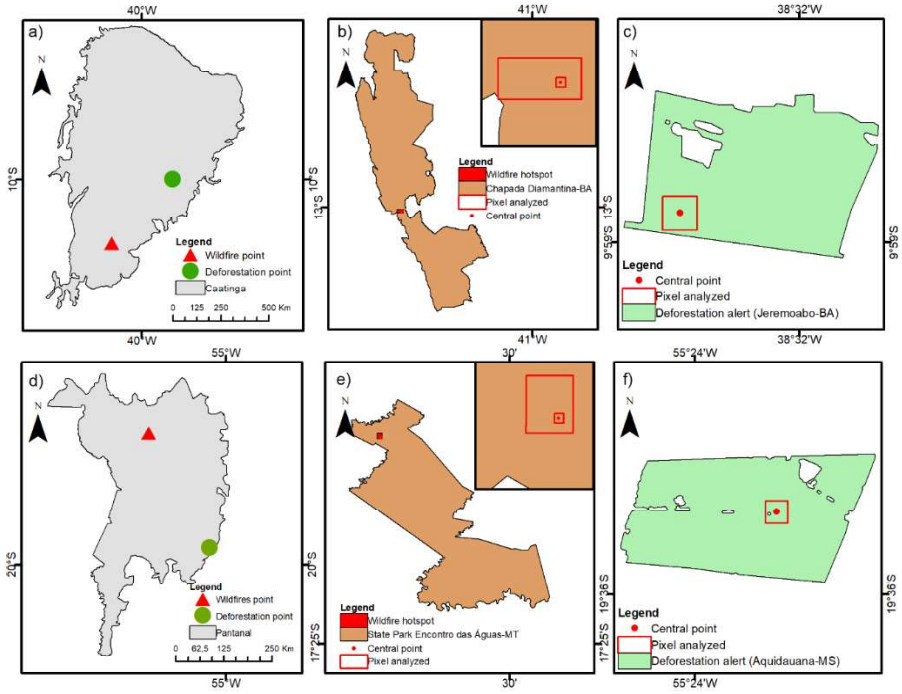

Figure 25 – Location in the biome: (a) Caatinga, (b) Chapada Diamantina–BA where a fire occurred, (c) Jeremoabo–BA where a deforestation alert was issued, and in the biome (d) Pantanal, (e) Encontro das Águas State Park–MT where a fire occurred, (f) Aquidauana–MS where a deforestation alert was issued.

The MapBiomas Alerta system (MapBiomas, 2025) was utilised to identify deforested areas within the biomes. This system validates and refines deforestation alerts with high-resolution imagery, gathering information from various systems for all Brazilian biomes. The platform also provides detailed reports of each native vegetation loss event. For the selection of deforestation events, the area needs to be protected and larger than the ESTIMET pixel (62,500 m², 0.0625 km²). In Caatinga, a legal reserve area in the municipality of Jeremoabo-BA was selected (Alert Code 138612, an area of 1.4673 km²) (Fig. 25c), while in Pantanal, the region defined a Permanent Preservation Area in the

municipality of Aquidauana-MS (Alert Code 468462, an area of 3.23 km²) was chosen (Fig. 25f).

Once the regions were defined, the high temporal variability of ET (daily) was analysed in cases of forest fires, in the month of the alert indicated by INPE, and in the same month of the previous year, to ensure that the area had vegetation without degradation. For deforestation scenarios, the analysis covered the months indicated in the MapBiomas alert reports.

5.3 Results and discussion

5.3.1 Long-term (2002-2023) and continuous monthly ET trends

The Mann–Kendall test performed on the monthly time-series, considering the entire biome extents, indicates decreasing trends ($s < 0$) in 7 months for both biomes (Table 7). However, a significant increasing trend was identified for Pantanal in February ($p = 0.03$ and $s = 1.48$ mm/month), which represents the end of the rainy and flood season in most of the biome, i.e. the period with higher water availability, with expanded floodplains, soil saturation, maximum leaf area of vegetation, and intense solar radiation (Sanches et al., 2011; Leivas et al., 2015; Fleischmann et al., 2023). Under these conditions, vegetation maintains high transpiration rates, while the higher net radiation and surface temperatures increase the atmospheric demand (VPD), favouring higher ET fluxes during this period (Leivas et al., 2015; Marengo et al., 2016; Fleischmann et al., 2023). This increase tends to reduce from March to June.

When analysing the trends for the monthly time series according to land use and land cover, Caatinga showed a relative balance. For this biome, each land use generally exhibited 6 months of increasing and 6 months of decreasing ET trends, a behaviour that reflects the defined high and low ET cycles throughout the year (Table 8). In contrast, a predominance of decreasing trends was observed in non-vegetated and urban areas of Pantanal, with 11 months showing decreasing trends, including 3 months (January, November, and December) that exhibited significant decreasing trends. This behaviour may reflect anthropogenic changes in land cover (urban expansion, conversion of pastures, or agricultural lands) in the region, which reduce the flooded areas and soil moisture with an increase in vegetation loss, thereby reducing transpiration and modifying the energy balance. Thus, any decline in flooding or baseflow reduces ET even during months of the rainy season in Pantanal, which

historically exhibit high evaporative demand (Leivas et al., 2015; Marques and Rodriguez, 2022). Decreasing ET trends were also identified by Patriota et al. (2024) when analysing 21 metropolitan regions across different Brazilian biomes. Regarding agricultural areas in Pantanal, most months (8 months) exhibited negative trends, while vegetated areas showed increasing ET trends in 7 months, although none of these trends were significant. Considering the entire extent of the biomes and all analysed land use and land covers, ET values showed an annual decline, particularly in non-vegetated areas of the Pantanal ($p = 0.04$ and $s = -7.37$ mm/year). likely related to recent fire and deforestation impacts (Fleischmann et al., 2023).

Table 7 - Monthly and annual ET trends for each land use and land cover in the Pantanal biome, assessed using the Mann–Kendall test and Sen's slope. A "+" indicates an increasing trend (shaded in red), "–" a decreasing trend (shaded in green), and "0" denotes no trend. The values in the second row represent the trend (t), p-value (p), and Sen's slope (s), respectively.

Monthly/ Annual	Agricultural and Pasture			Vegetation			Non vegetated			Urban			Entire biome		
	t	p	s	t	p	s	t	p	s	t	p	s	t	p	s
Jan	0	0.28	-0.57	0	0.45	-0.40	-	0	-1.05	-	0.04	-0.65	0	0.41	-0.43
Feb	0	0.31	0.43	0	0.01	1.75	0	0.14	-0.46	0	0.14	-0.42	+	0.03	1.48
Mar	0	0.77	-0.07	0	0.18	1.06	0	0.12	-0.55	0	0.09	-0.52	0	0.16	0.89
Apr	0	0.92	-0.22	0	0.62	0.26	0	0.58	-0.36	0	0.62	-0.31	0	0.72	0.29
May	0	0.82	0.22	0	0.45	0.68	0	0.92	-0.06	0	0.72	0.18	0	0.49	0.61
Jun	0	0.97	0.01	0	0.43	0.28	0	0.25	-0.20	0	0.62	-0.09	0	0.58	0.20
Jul	0	0.34	-0.25	0	0.45	-0.53	0	0.07	-0.30	0	0.07	-0.21	0	0.45	-0.48
Aug	0	0.92	0.02	0	0.82	-0,06	0	0.29	-0.13	0	0.34	-0.11	0	0.77	-0.07
Sep	0	0.77	-0.12	0	1	0	0	0.29	-0.25	0	0.22	-0.22	0	0.97	-0.02
Oct	0	0.16	-0.81	0	0.31	-1.24	0	0.07	-0.62	0	0.06	-0.53	0	0.25	-1.11
Nov	0	0.07	-2.53	0	0.17	-2.54	-	0	-1.63	-	0.01	-1.21	0	0.25	-1.15
Dec	0	0.38	-0.99	0	0.39	-0.78	-	0.01	-1.35	-	0.01	-0.91	0	0.34	-0.75
Annual	0	0.41	-3.47	0	0.97	-0.59	-	0.04	-7.37	0	0.07	-4.28	0	0.97	-1.43

Table 8 - Monthly and annual ET trends for each land use and land cover in the Caatinga biome, assessed using the Mann–Kendall test and Sen's slope. A "+" indicates an increasing trend (shaded in red), "–" a decreasing trend (shaded in green), and "0" denotes no trend. The values in the second row represent the trend (t), p-value (p), and Sen's slope (s), respectively.

Monthly/ Annual	Agricultural and Pasture			Vegetation			Non vegetated			Urban			Entire biome		
	t	p	s	t	p	s	t	p	s	t	p	s	t	p	s
Jan	0	0.82	-0.34	0	0.90	0.22	0	0.82	0.16	0	0.77	0.12	0	1	0.03
Feb	0	0.63	-0.25	0	0.82	-0.55	0	0.92	-0.10	0	0.87	-0.19	0	0.67	-0.61
Mar	0	0.31	-0.91	0	0.62	-1.22	0	0.77	-0.15	0	0.69	-0.20	0	0.67	-1.19
Apr	0	0.82	-0.38	0	0.58	-0.48	0	0.97	-0.01	0	0.87	-0.16	0	0.62	-0.43
May	0	1	0	0	0.82	-0.23	0	0.87	-0.05	0	0.72	-0.10	0	0.82	-0.30
Jun	0	0.54	-0.38	0	0.82	-0.16	0	0.87	-0.06	0	0.77	-0.04	0	0.77	-0.34
Jul	0	0.97	0.01	0	1	0.01	0	0.62	0.09	0	0.58	0.17	0	0.77	-0.17
Aug	0	0.72	0.11	0	0.77	-0.10	0	0.97	0.01	0	0.42	0.12	0	0.97	0.01
Sep	0	0.97	-0.02	0	0.82	-0.03	0	0.46	-0.04	0	0.77	-0.05	0	0.82	-0.02
Oct	0	0.62	0.11	0	0.26	0.20	0	0.72	0.07	0	1	0	0	0.31	0.19
Nov	0	0.38	0.52	0	0.16	1.18	0	0.34	0.34	0	0.63	0.08	0	0.31	0.19
Dec	0	0.25	1.24	0	0.28	1.43	0	0.38	0.52	0	0.31	0.34	0	0.34	1.28
Annual	0	0.82	-1.44	0	0.97	-1.40	0	0.92	-0.15	0	0.97	-0.21	0	0.87	-0.68

5.3.2 Variability of ET according to precipitation and land use/land cover patterns

The analysis of ET between 2003 and 2022 reveals that the monthly variations (Fig. 26 and Fig. 27) in both biomes exhibited similar behaviour, with cyclical oscillations of higher values during the rainy season and lower values during the dry season. In Caatinga, the rainy season lasts 3 to 5 months, mainly from January to May, while in Pantanal, the rainy season generally occurs from October to March (i.e. over 6 months). The interannual analysis (Fig. 28e and Fig. 29e) shows a greater discrepancy between the ET values observed for the biomes, where Caatinga exhibits higher variability with abrupt oscillations, while the Pantanal shows a more stable behaviour, with variation close to a linear pattern.

These cyclical patterns reflect the climate of the biomes, a factor indicated by the significant correlation between ET and precipitation in the biomes (Caatinga, with r = 0.73 and Pantanal, with r = 0.78). In Caatinga, where predominates the semi-arid climate marked by low annual precipitation, the lowest ET values were observed during the dry season (for Full biome extent the ET= 13.42 mm/month in Nov/2015 and ET= 483.41 mm/year in 2012) making water availability a limiting factor for ET in this biome (Menezes et al., 2012; Alvares et al., 2013; Pinheiro et al., 2013; Andrade et al., 2024). An example of this was the sharp reduction in ET observed during the period 2012-2015 that can be attributed to the severe drought that decreased water availability and limited ET (Silva et al., 2024).

In contrast, Pantanal exhibits well-defined dry and rainy seasons, with flooding cycles that contribute to increased evaporation (Ribas and Schoereder, 2007). Other factors influencing ET variability in biomes include latitudinal position, which affects radiation availability and air temperature, with higher-latitude regions exhibiting well-defined intra-annual periods (Andrade et al., 2024; Patriota et al., 2024).

When analysing the ET patterns in the main land uses and land covers of the biomes, greater variations and higher ET values can be observed in vegetated regions (Fig. 26, Fig. 27, Fig. 28 and Fig. 29). In Caatinga, the average values of ET for the whole period were 81.91 mm/month for vegetated areas, 56.64 mm/month for agricultural areas, 44.88 mm/month for urban areas, and 36.55 mm/month for non-vegetated areas 36.55 mm/month. Additionally, the ET values in vegetated regions, which comprise the majority of the Caatinga biome, show rapid responses to precipitation variability, reflecting the behaviour of vegetation predominantly composed of shrubs and small trees. The Caatinga vegetation is mostly composed of plant species that present structural and physiological adaptations to

the climate type (i.e. spines, leaf shedding during the dry season, water storage in roots and stems, stomatal closure during the hottest hours) (Palácio et al., 2016; Queiroz et al., 2017; Miranda et al., 2020; Bezerra et al., 2023). This allows for differentiation of the behaviour in the ET rates as vegetation changes between dry and rainy periods in response to rainfall events. Besides precipitation, a combination of high atmospheric temperatures, wind speeds, and radiation, along with low atmospheric water content, drives ET dynamics in the Brazilian Northeast (Andrade et al., 2024).

In Pantanal, the average ET values for vegetated regions (i.e. 87.21 mm/month) were over 30% higher than in agricultural areas (i.e. 75.12 mm/month, 86.15% of the ET in vegetated regions) and 48% higher than in urban (i.e. 32.55 mm/month, 37.32% of the ET in vegetated regions) and non-vegetated regions (i.e. 51.74 mm/month, 48.26% of the ET in vegetated regions). However, the variations of ET in vegetation areas presented fewer fluctuations, reflecting the vegetative behaviour of the region. The natural vegetation of the region is mostly composed of seasonal floodplains that drive its ecological complexity in vegetation patterns and contribute to a unique landscape with a diverse composition of savanna vegetation, aquatic plants, and floodplain forests (Evans et al., 2014; Pereira et al., 2021; Caballero et al., 2025), suggesting that water availability is not a limiting factor for vegetative development and ET in the region. Fleischmann et al. (2023) observed that tropical wetlands (e.g. Pantanal) and floodable savannas generally exhibit ET rates similar to those of forests during floods, but the similarity decreases during the dry season. They also concluded that river flood propagation and net radiation (Rn) drive ET dynamics in these highly inundated areas. Furthermore, Caballero et al. (2025) concluded that there is multidecadal variability in climate and extent of wetland areas, observing that potential evapotranspiration shows a negative correlation with wetland extent, suggesting that as the potential for water loss through evaporation and transpiration increases, the extent of the wetland decreases.

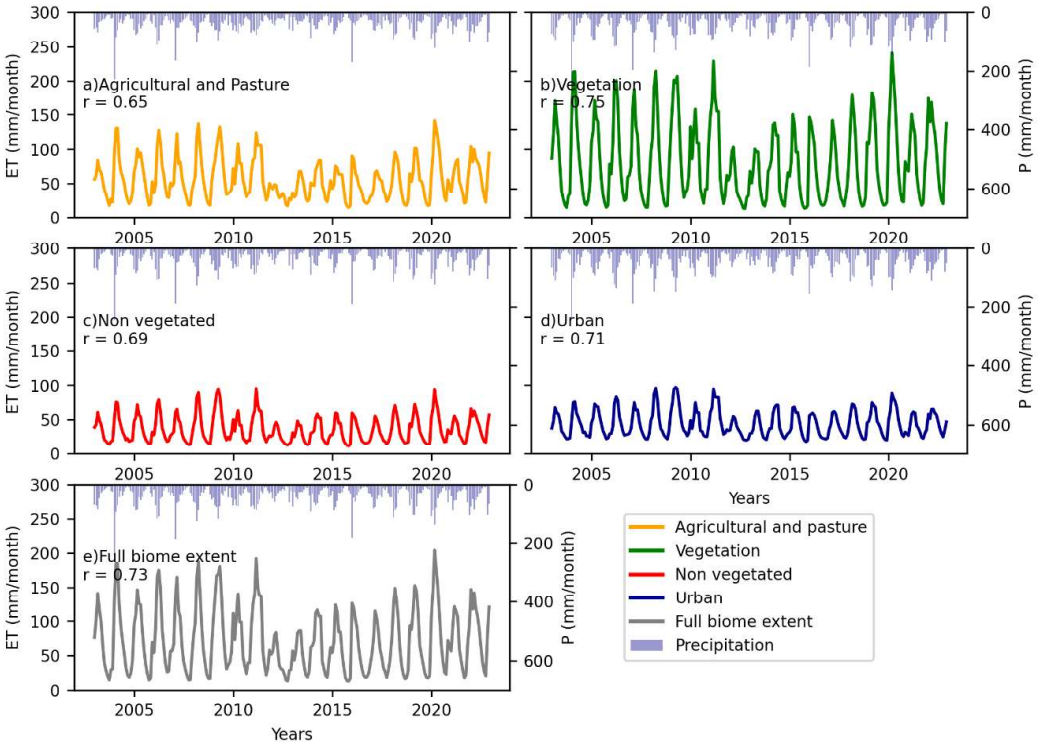

Figure 26 - Monthly mean variability of ET and precipitation over 20 years (2003–2020) for each land use: (a) agriculture and pasture, (b) vegetation, (c) non-vegetated, (d) urban, and (e) all land uses within the Caatinga biome. r denotes the correlation between ET and precipitation.

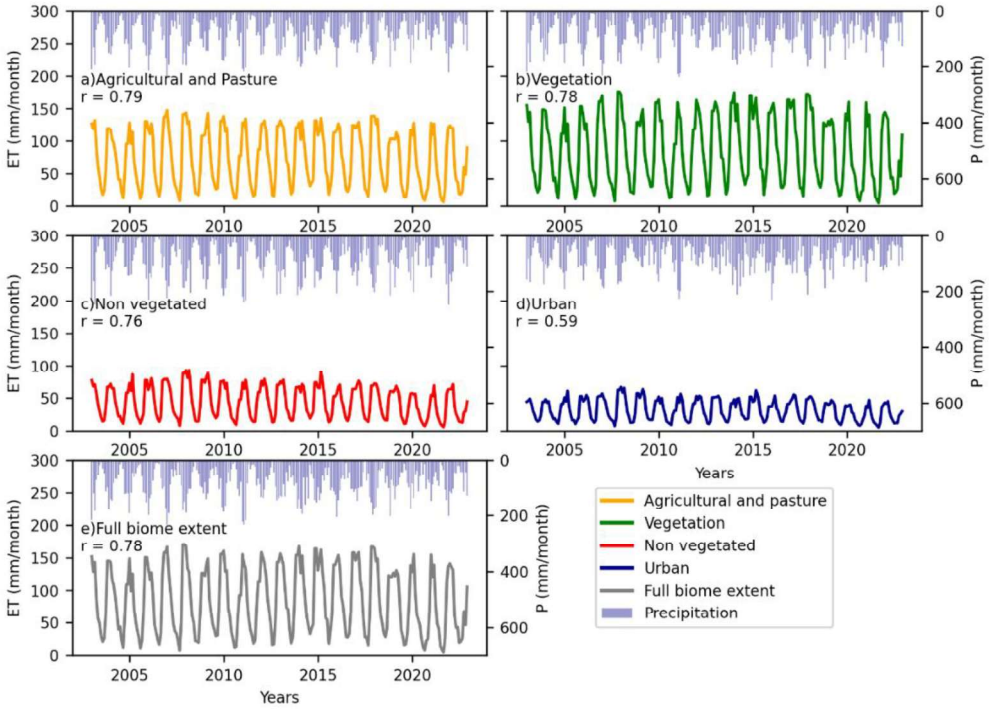

Figure 27 - Monthly mean variability of ET and precipitation over 20 years (2003–2020) for each land use: (a) agriculture and pasture, (b) vegetation, (c) non-vegetated, (d) urban, and (e) all land uses within the Pantanal biome. r denotes the correlation between ET and precipitation.

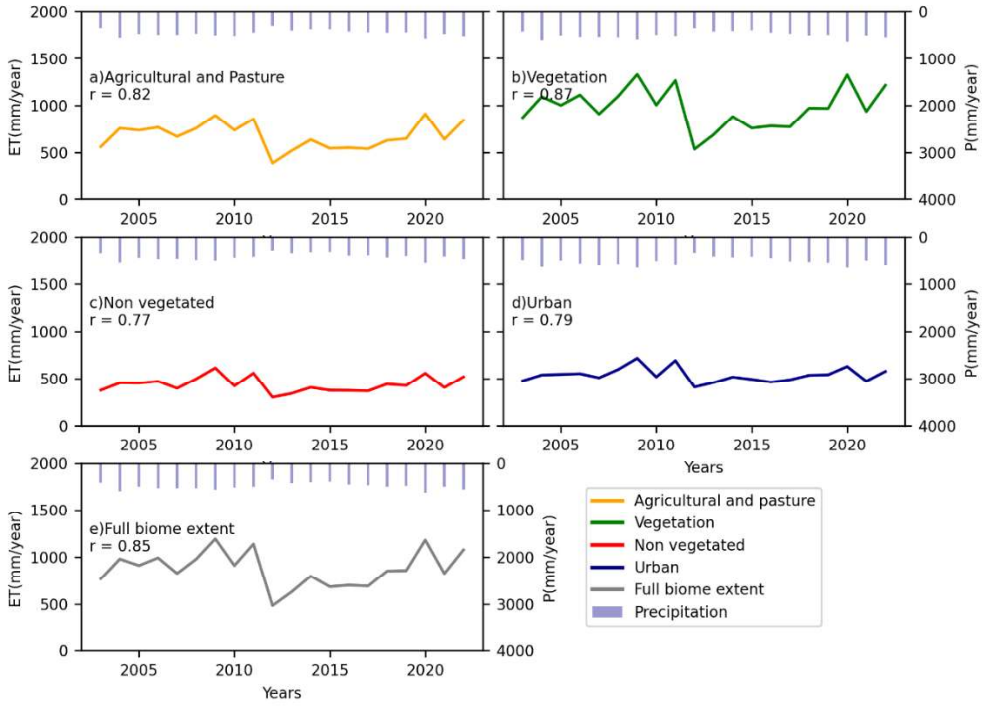

Figure 28 - Annual mean variability of ET and precipitation over 20 years (2003–2020) for each land use: (a) agriculture and pasture, (b) vegetation, (c) non-vegetated, (d) urban, and (e) all land uses within the Caatinga biome. r denotes the correlation between ET and precipitation.

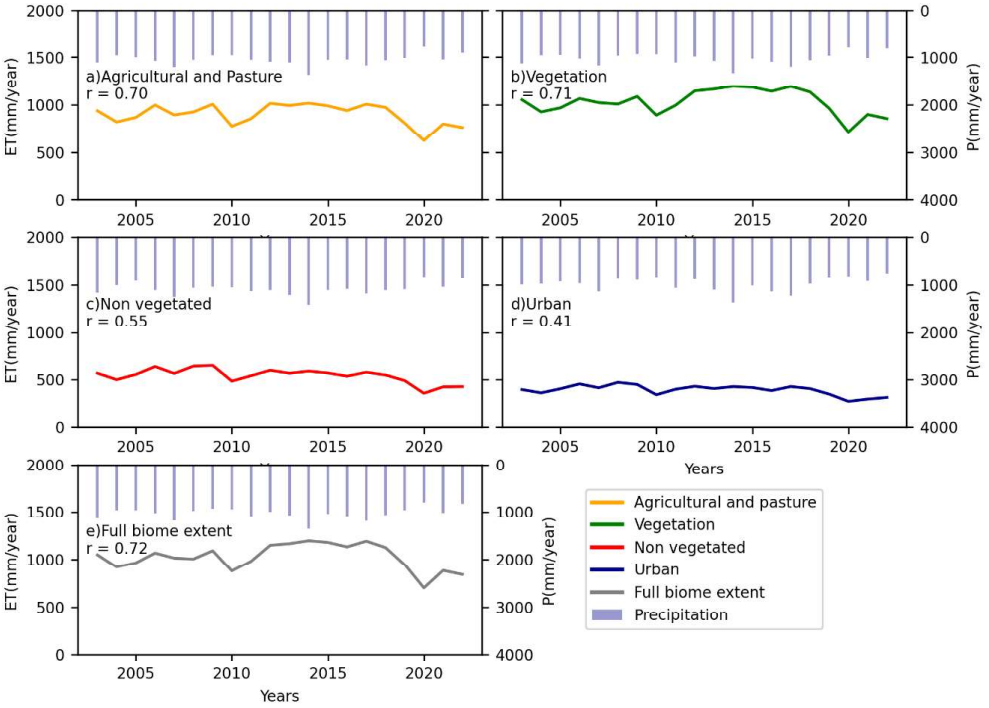

Figure 29 - Annual mean variability of ET and precipitation over 20 years (2003–2020) for each land use: (a) agriculture and pasture, (b) vegetation, (c) non-vegetated, (d) urban, and (e) all land uses within the Pantanal biome. r denotes the correlation between ET and precipitation.

The spatial variability patterns of ET in the dry, normal, and wet periods, correlated to rainfall variability, can be observed in Figs. 30 31. For Caatinga, the lower ET values (0–500 mm/year) were observed in the central region, while the higher values (ET > 1000 mm/year) were noticed in the northern (coastal) portion in a year without rainfall anomalies (Fig. 30cd). In the dry year (Fig. 30ab), the lower values of ET (i.e. <500 mm/year) in the central region were extended to almost the entire area of the biome. For the wet year, these annual values of ET lower than 500 mm were concentrated in a small portion of the central region (Fig. 30ef), a behaviour that clearly follows the rainfall dynamics.

In Pantanal, the ET variability partially follows the rainfall dynamics. In the analysed year without anomalies, the lowest ET values (0–500 mm/year) were concentrated in a small portion in the central area, with higher values in the north (ET > 1000 mm/year) (Fig. 31cd). In the dry year, the lowest ET values are distributed across almost the entire region (Fig. 31ab), while in the wet year, despite higher rainfall concentrations throughout the region, the lowest ET values occur in most of the southern portion (Fig. 31ef), contradicting the rainfall pattern of that year, which shows higher concentrations in the southern portion compared to the year without anomalies.

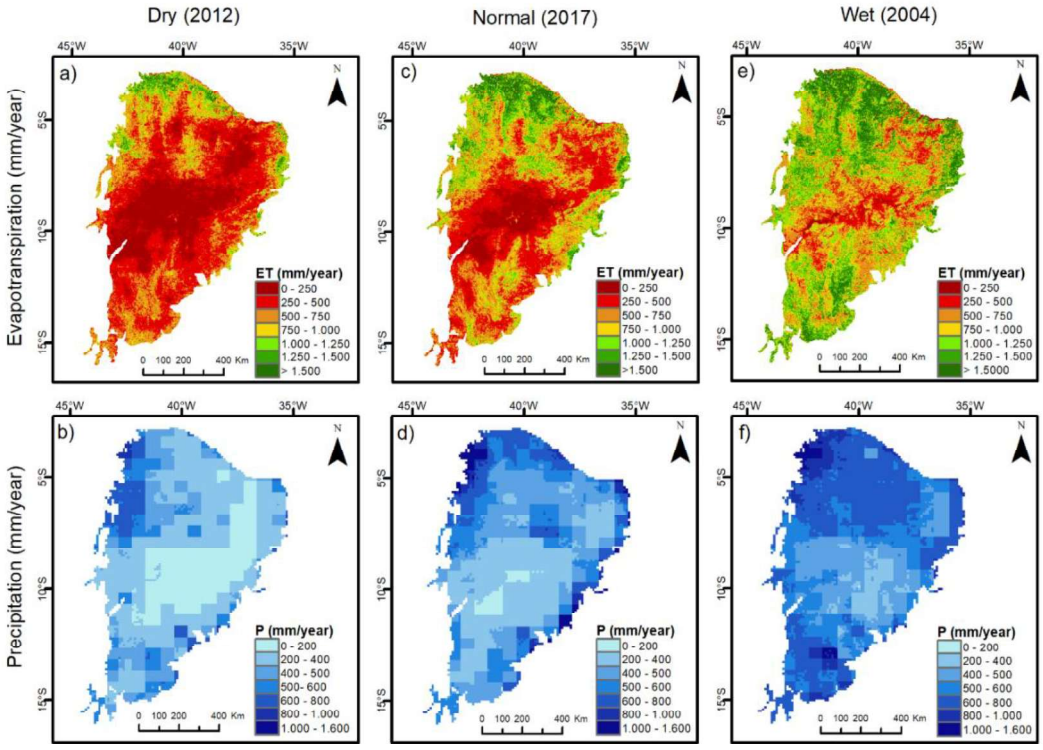

Figure 30 - Spatial variability of annual ET and precipitation in the Caatinga: 2012, a dry year (a) and (b); 2017, a year with normal rainfall (c) and (d); and 2004, a wet year (e) and (f).

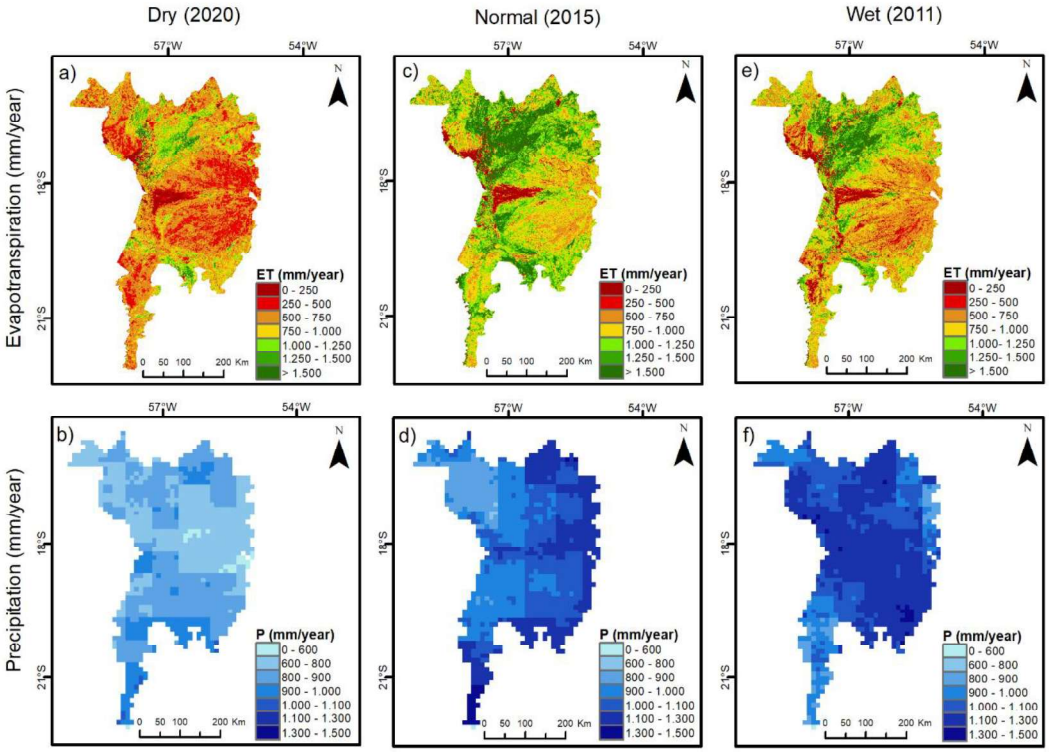

Figure 31 - Spatial variability of annual ET and precipitation in the Pantanal: 2012, a dry year (a) and (b); 2017, a year with normal rainfall (c) and (d); and 2004, a wet year (e) and (f).

5.3.3 Spatial variability of ET in response to deforestation and forest fires

The variability of the ET values before and after the land use and land cover change events shows the impact of burns in the decrease of the water movement into the atmosphere, with a decrease in the Caatinga natural vegetation from 2.7 mm/day to 1.27 mm/day (Fig. 32a–f), which represents a reduction of over 50% on the analysed day and over 20% in the monthly average (Sep/2014 mean ET = 1.90 mm/day and Sep/2015 mean ET = 1.46 mm/day).

A more pronounced decrease in the ET values was observed in Pantanal, with reductions of over 90% in the monthly average, as indicated by the comparison of the September 2019 mean ET (1.36 mm/day) and the September 2020 mean ET (0.11 mm/day). A similar pattern of ET decrease was identified in areas where native vegetation was deforested and converted to agricultural use (Fig. 32g–k and Fig. 33g–k), with monthly mean values in Caatinga decreasing by more than 50% (Apr/2021 mean ET = 4.76 mm/day and Jul/2021 mean ET = 2.12 mm/day) and in Pantanal by more than 80% (May/2021 mean ET = 1.33 mm/day and Sep/2021 mean ET = 0.18 mm/day). For these cases, in addition to

deforestation events, ET may also have been influenced by monthly precipitation, but the months were defined according to the alerts indicated by MapBiomas.

Land use changes caused by agricultural expansion, urban expansion, and fire events have been investigated in other studies in Brazil, identifying substantial reductions in ET rates (Laipelt et al., 2021; Carrillo-Quinete et al., 2022; Andrade et al., 2024). In Caatinga, water scarcity significantly limits ET in this biome, contributing to the intensification of drought events and vegetation loss. Thus, the combined effects of climatic variability and environmental degradation from deforestation, agricultural expansion, and fire occurrence lead to a significant reduction in ET (Oliveira et al., 2012; Andrade et al., 2024). In the Pantanal, a critical scenario exists, with a 30% loss of its wetlands primarily due to the expansion of pasture and agriculture. Moreover, the Pantanal has faced increasing challenges from recurrent droughts and intensified wildfires, degradations that affect hydrological regulation, aquifer recharge, and thermal control via evapotranspiration, thereby increasing the ecological vulnerability of the biome (Fleischmann, 2023; Caballero et al., 2025). Furthermore, the impacts of global climate change exacerbate the effects of land use changes (Andrade et al., 2024).

This evidence suggests that ET plays a crucial role in regulating the hydrological cycle. This reduction of ET, resulting from the replacement of native vegetation with impermeable surfaces or areas of low vegetation cover, compromises the climatic and hydric resilience of the affected regions (Patriota et al., 2024). Furthermore, these scenarios demonstrate that ESTIMET is a valuable tool for quantifying the hydrological impacts of deforestation and agricultural land expansion, as well as for monitoring the impacts of fires on ET in the Brazilian biomes.

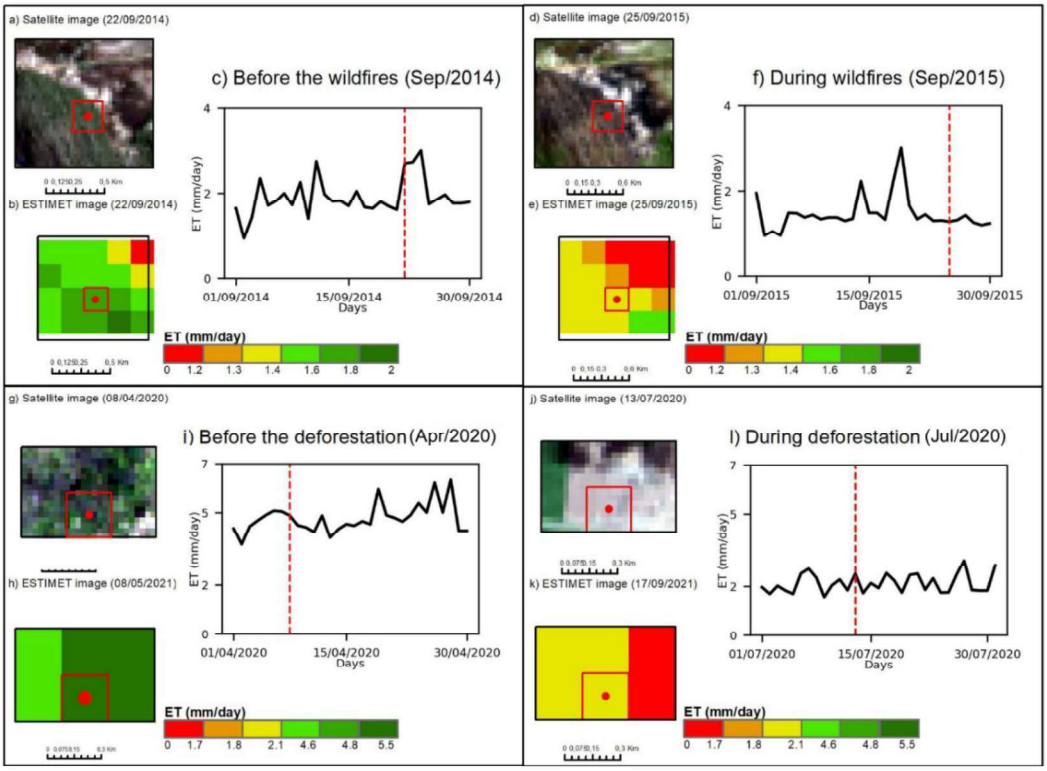

Figure 32 - Daily variability of ET in the Caatinga during the month preceding (a–c) and during (d–f) wildfire events, and before (g–i) and after (j–k) deforestation events, respectively.

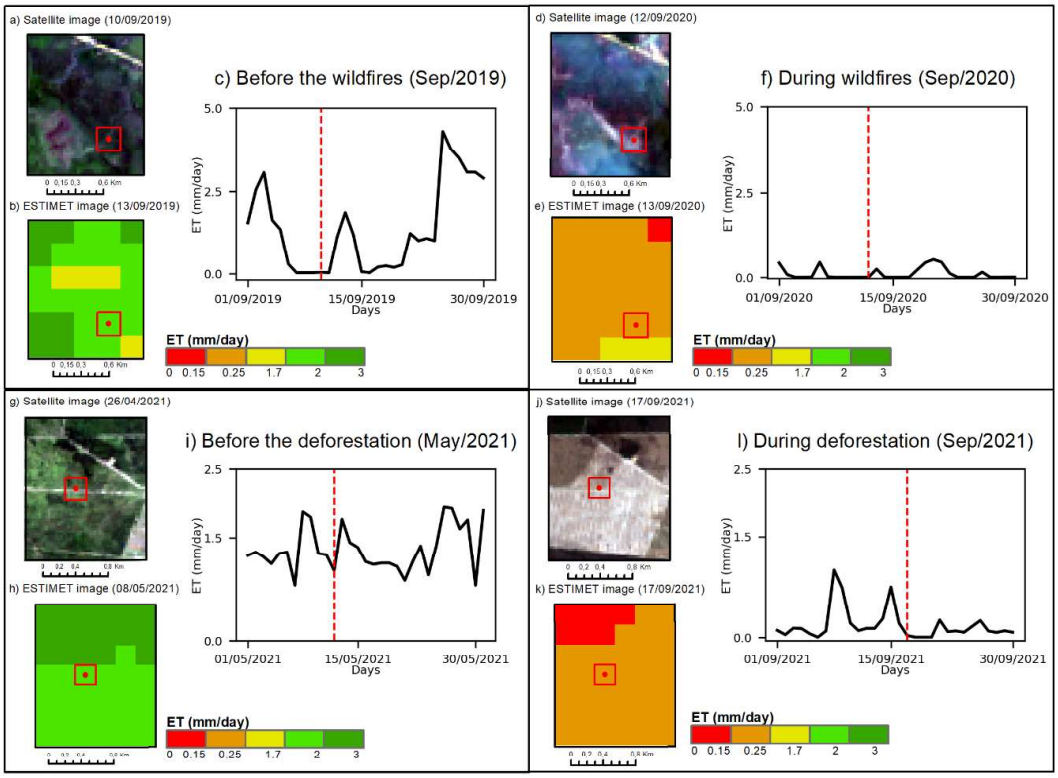

Figure 33 - Daily variability of ET in the Pantanal during the month preceding (a–c) and during (d–f) wildfire events, and before (g–i) and after (j–k) deforestation events, respectively. The red dashed line indicates the day corresponding to the images shown on the left.

6 CONCLUSIONS AND RECOMMENDATIONS

ESTIMET provides a unique remote sensing-based ET assessment tool that operates at a refined spatiotemporal scale and with low latency under any sky conditions. Such an enhanced spatiotemporal resolution of this model may be suitable to upscale the daily flux tower measurements, opening opportunities for a better understanding of this component of the hydrological cycle, especially in data-scarce areas frequently overcast by substantial cloud cover but playing a fundamental role in the broader analyses, in the context of water-energy balance, agricultural practices (e.g. irrigation), and long-term climate change impact monitoring.

The assessment of this model, developed for Brazil, demonstrated that the underlying hypotheses to refine the MODIS evaluation are relevant and do not significantly degrade ET evaluation, even allowing better assessment when compared to EC daily ET, especially for the Caatinga, Cerrado, and Pantanal Biomes. Two potential issues should be considered when using eddy covariance observations of ET as ground-truth data. Firstly, eddy covariance data are affected by uncertainties due to the energy balance closure problem. Secondly, discrepancies in scale and classification errors can cause a mismatch in vegetation between the pixels and the site, complicating the comparisons. Nevertheless, the daily ET simulated from ESTIMET usually present good representativeness of what is measured by the EC towers and seems to be efficient for continuous assessment with a short latency (1 month at maximum), not only at the daily scale, by catching biophysical reactivity to meteorological or ecological processes at a detailed scale, but also for applications at coarser scales (e.g. 8-days, similar to MOD16A2GF and PML_V2). The regional scale assessment also demonstrated that ESTIMET was able to better capture the annual ET calculated by the water balance approach in the three major Brazilian biomes (Amazon, Atlantic Forest, and Cerrado) when compared to the analysed global products MOD16A2GF, PML_V2, and GLEAM 4.1a. Overall, this ESTIMET outperformance results from the higher resolution and/or improved input datasets, as the model's modifications were made to incorporate this adapted information. Although developed for Brazil, the model can be applied to other tropical regions since a land cover map with 30-m spatial resolution or higher is available and some empirical parameters (e.g. surface albedo) are recalibrated.

This model is sensitive to certain underlying hypotheses regarding land characteristics (e.g. albedo and EVI2), which can be altered from both spatial and temporal perspectives in anthropised landscapes, such as agricultural land and semi-urban zones. This

can be an issue, especially for local applications of ESTIMET. Nevertheless, this model is expected to be further adaptable to such local conditions. An illustration of this adaptability is provided within the framework of this study. The lack of available data for some biomes (Pampa and Atlantic Forest) has been fixed by assuming biophysical similarities (regarding albedo) with other tropical biomes, before further adjustment, if relevant.

From a practical application, this study also demonstrated the possibilities of ESTIMET to characterise the spatial-temporal variability of ET over the past 20 years, considering intra- and interannual scales. This study assessed the correlation between ET and another meteorological parameter (precipitation) and the responses to land use and land cover changes. This highlighted the fact that contrasting Brazilian biomes (e.g. Pantanal and Caatinga) present ET variation cycles correlated with precipitation variability, with an overall decreasing trend in ET across different land uses in both biomes. This decrease in ET was also identified at a more detailed temporal scale (daily) in areas where land use changes occurred due to burn and deforestation events. Finally, further studies could improve ESTIMET estimations through bias corrections of the daily data, based on machine learning techniques and meteorological reanalysis data (i.e. not relying on observed data). In addition, new analyses can be carried out through correlations of ET with other climatic parameters (e.g. land surface temperature, wind speed, soil moisture) and in other Brazilian biomes.

REFERENCES

Adeyeri, O.E., Ishola, K.A., 2021. Variability and trends of actual evapotranspiration over West Africa: the role of environmental drivers. Agric. For. Meteorol. 308–309, 108574. https://doi.org/10.1016/j.agrformet.2021.108574

Aguilar, A., Flores, H., Crespo, G., Marín, M., Campos, I., Calera, A., 2018. Performance Assessment of MOD16 in Evapotranspiration Evaluation in Northwestern Mexico. Water. 10, 901. https://doi.org/10.3390/w10070901

Ahamed, A., Knight, R., Alam, S., Pauloo, R., Melton, F., 2022. Assessing the utility of remote sensing data to accurately estimate changes in groundwater storage. Science of The Total Environment. 807, 150635. https://doi.org/10.1016/j.scitotenv.2021.150635

Albertz, 2007. Einführung in die Fernerkundung. Grundlagen der Interpretation von Luft- & Satellitenbildern. Darmstadt, 254 pp.

Alho, C., Sabino, J., 2011. A conservation agenda for the Pantanal's biodiversity. Braz. J. Biol. 71(1 Suppl 1), 327–335. https://doi.org/10.1590/S1519-69842011000200012

Allen, R., Irmak, A., Trezza, R., Hendrickx, J.M.H., Bastiaanssen, W., Kjaersgaard, J., 2011. Satellite-based ET estimation in agriculture using SEBAL and METRIC. Hydrological Processes. 25, 4011–4027. https://doi.org/10.1002/hyp.8408

Allen, R.G., Dhungel, R., Dhungana, B., Huntington, J., Kilic, A., Morton, C., 2021. Conditioning point and gridded weather data under aridity conditions for calculation of reference evapotranspiration. Agric. Water Manag. 245. https://doi.org/10.1016/j.agwat.2020.106531

Allen, R.G., Tasumi, M., Trezza, R., 2007. Satellite-Based Energy Balance for Mapping Evapotranspiration with Internalized Calibration (METRIC)—Model. J. Irrig. Drain Eng. 133, 380–394. https://doi.org/10.1061/(ASCE)0733-9437(2007)133:4(380)

Almagro, A., Oliveira, P.T.S., Meira Neto, A.A., Roy, T., Troch, P., 2021. CABra: a novel large-sample dataset for Brazilian catchments. Hydrol. Earth Syst. Sci. 25, 3105–3135. https://doi.org/10.5194/hess-25-3105-2021

Alvares, C.A., Stape, J.L., Sentelhas, P.C., De Moraes Gonçalves, J.L., Sparovek, G., 2013. Köppen's climate classification map for Brazil. Metz. 22, 711–728. https://doi.org/10.1127/0941-2948/2013/0507

Alves, J.M.B., et al., 2006. Mecanismos atmosféricos associados a ocorrência de precipitação intensa sobre o nordeste do Brasil durante Janeiro/2004. Rev. Bras. Meteorol. 21(1), 56–76.

AmeriFlux, 2022. AmeriFlux Year of Methane Featured Site – US-ONA. Available from: https://ameriflux.lbl.gov/ameriflux-year-of-methane-featured-site-us-ona/. Acessado em: 11 ago. 2025.

Anderson, M. C.; Kustas, W. P.; Norman, J. M., 2007. Upscaling flux observations from local to continental scales using thermal remote sensing. Agronomy Journal.240–254. https://doi.org/10.2134/agronj2005.0096S

Andrade, B. C., Laipelt, L., Fleischmann, A., Huntington, J., Morton, C., Melton, F., Erickson, T., Roberti, D.R., De Arruda Souza, V., Biudes, M., Gomes Machado, N., Antonio Costa Dos Santos, C., Cosio, E.G., Ruhoff, A., 2024. geeSEBAL-MODIS: Continental-scale evapotranspiration based on the surface energy balance for South America. ISPRS Journal of Photogrammetry and Remote Sensing 207, 141–163. https://doi.org/10.1016/j.isprsjprs.2023.12.001

Andrade, B.C.C., De Andrade Pinto, E.J., Ruhoff, A., Senay, G.B., 2021. Remote sensing-based actual evapotranspiration assessment in a data-scarce area of Brazil: A case study of the Urucuia Aquifer System. International Journal of Applied Earth Observation and Geoinformation 98, 102298. https://doi.org/10.1016/j.jag.2021.102298

Andrade, J.M., Neto, A.R., Bezerra, U.A., Moraes, A.C.C., Montenegro, S.M.G.L., 2022. A comprehensive assessment of precipitation products: temporal and spatial analyses over terrestrial biomes in Northeastern Brazil. Remote Sens. Appl.: Soc. Environ. 28, 100842 https://doi.org/10.1016/j.rsase.2022.100842.

Andrade, J.M., Ribeiro Neto, A., Nóbrega, R.L.B., Rico-Ramirez, M.A., Montenegro, S.M.G.L., 2024 b. Efficiency of global precipitation datasets in tropical and subtropical catchments revealed by large sampling hydrological modelling. J. Hydrol. 633, 131016. https://doi.org/10.1016/j.jhydrol.2024.131016

Andrade, N. L. R., Sandwiches, L., Zeilhofer, P., João, G., Gutieres, C. B., & Carlo, R. D., 2023. Different spatial and temporal arrangements for validating the latent heat flux obtained using the MOD16 product in a forest in the Western Amazon. Int. J. Hydro, 7, 18-25.

Antonino, 2019. AmeriFlux BASE BR-CST Caatinga Serra Talhada, Ver. 1-5, AmeriFlux AMP, (Dataset). https://doi.org/10.17190/AMF/1562386

Antunes, S.C.R., Ribeiro, C.B.M., Lima, R.N.S., Getirana, A., 2024. Effects of changes in use and soil cover on real evapotranspiration from the creation of a remote sensing product in the Xingu basin. Rev. Bras. Cienc. Ambient. 59, 1–13. https://doi.org/10.5327/Z2176-94781658

Araújo, A. C., Nobre, A. D., Kruijt, B., Elbers, J. A., Dallarosa, R., Stefani, P., von Randow, C., Manzi, A. O., Culf, A. D., Gash, J. H. C., Valentini, R., Kabat, P., 2002. Comparative Measurements Of Carbon Dioxide Fluxes From Two Nearby Towers In A Central Amazonian Rainforest: The Manaus Lba Site. Journal Of Geophysical Research. 107.https://doi.org/10.1029/2001JD000676

Araújo, C. S. P. D., Silva, I. A. C. E., Ippolito, M., & Almeida, C. D. G. C. D., 2022. Evaluation of air temperature estimated by ERA5-Land reanalysis using surface data in Pernambuco, Brazil. Environmental Monitoring and Assessment, 194(5), 381. https://doi.org/10.1007/s10661-022-10047-2

Araújo, H. F. P., Canassa, N. F., Machado, C. C. C.,Tabarelli, M. (2023). Human disturbance is the major driver of vegetation changes in the Caatinga dry forest region. Scientific Reports, 13. https://doi.org/10.1038/s41598-023-45571-9

Astuti, I.S., Wiwoho, B.S., Purwanto, P., Wagistina, S., Deffinika, I., Sucahyo, H.R., Herlambang, G.A., Alfarizi, I.A.G., 2022. An Application of Improved MODIS-Based Potential Evapotranspiration Estimates in a Humid Tropic Brantas Watershed—Implications for Agricultural Water Management. IJGI, 11, 182. https://doi.org/10.3390/ijgi11030182

Baik, J., Liaqat, U.W., Choi, M., 2018. Assessment of satellite- and reanalysis-based evapotranspiration products with two blending approaches over the complex landscapes and climates of Australia. Agricultural and Forest Meteorology. 263, 388–398. https://doi.org/10.1016/j.agrformet.2018.09.007

Bala, A., Rawat, K.S., Misra, A.K., Srivastava, A., 2016. Assessment and validation of evapotranspiration using SEBAL algorithm and Lysimeter data of IARI agricultural farm, India. Geocarto International. 31, 739–764. https://doi.org/10.1080/10106049.2015.1076062

Bastiaanssen, W.G.M., Pelgrum, H., Wang, J., Ma, Y., Moreno, J.F., Roerink, G.J., Van Der Wal, T., 1998a. A remote sensing surface energy balance algorithm for land (SEBAL). 1. Formulation. Journal of Hydrology. 212–213, 198-212. https://doi.org/10.1016/S0022-1694(98)00253-4

Bastiaanssen, W.G.M., Pelgrum, H., Wang, J., Ma, Y., Moreno, J.F., Roerink, G.J., Van Der Wal, T., 1998b. A remote sensing surface energy balance algorithm for land (SEBAL).: Part 2: Validation. Journal of Hydrology 212–213, 213–229. https://doi.org/10.1016/S0022-1694(98)00254-6

Berenguer, E., Ferreira, J., Gardner, T.A., Aragão, L.E.O.C., De Camargo, P.B., Cerri, C.E., Durigan, M., De Oliveira Junior, R.C., Vieira, I.C.G., Barlow, J., 2014. A large-scale field assessment of carbon stocks in human-modified tropical forests. Glob. Change Biol. 20(12), 3713–3726. https://doi.org/10.1111/gcb.12627

Bergier, I., 2013. Effects of highland land-use over lowlands of the Brazilian Pantanal. Sci. Total Environ. 463–464, 1060–1066. https://doi.org/10.1016/j.scitotenv.2013.06.036

Bernoux, M., Carvalho, M.C.S., Volkoff, B., Cerri, C.C., 2002. Brazil's soil carbon stocks. Soil Sci. Soc. Am. J. 66(3), 888–896. https://doi.org/10.2136/sssaj2002.8880

Bezerra, U.A., Cunha, J., Valente, F., Nóbrega, R.L.B., Andrade, J.M., Moura, M.S.B., Verhoef, A., Perez-Marin, A.M., Galvão, C.O., 2023. STEEP: A remotely-sensed energy balance model for evapotranspiration estimation in seasonally dry tropical forests. Agricultural and Forest Meteorology. 333, 109408. https://doi.org/10.1016/j.agrformet.2023.109408

Bhattarai, N., Mallick, K., Stuart, J., Vishwakarma, B.D., Niraula, R., Sen, S., Jain, M., 2019. An automated multi-model evapotranspiration mapping framework using remotely sensed and reanalysis data. Remote Sensing of Environment. 229, 69–92. https://doi.org/10.1016/j.rse.2019.04.026

Biggs, T.W., Marshall, M., Messina, A., 2016. Mapping daily and seasonal evapotranspiration from irrigated crops using global climate grids and satellite imagery: Automation and methods comparison. Water Resources Research. 52, 7311–7326. https://doi.org/10.1002/2016WR019107

Binetti, M.S., Campanale, C., Uricchio, V.F., Massarelli, C., 2023. In-depth monitoring of anthropic activities in the Puglia Region: what is the acceptable compromise between economic activities and environmental protection? Sustainability 15, 8875. https://doi.org/10.3390/su15118875

Biudes, M.S., Geli, H.M.E., Vourlitis, G.L., Machado, N.G., Pavão, V.M., Dos Santos, L.O.F., Querino, C.A.S., 2022. Evapotranspiration Seasonality over Tropical Ecosystems in Mato Grosso, Brazil. Remote Sensing. 14, 2482. https://doi.org/10.3390/rs14102482

Bolton, D.K., Friedl, M.A., 2013. Forecasting crop yield using remotely sensed vegetation indices and crop phenology metrics. Agricultural and Forest Meteorology .173, 74–84. https://doi.org/10.1016/j.agrformet.2013.01.007

Borma, L. S., Rocha, H. R. d., Cabral, O. M., Randow, C. v., Collicchio, E., Kurzatkowski, D., et al., 2009. Atmosphere and hydrological controls of the evapotranspiration over a floodplain forest in the Bananal Island region, Amazonia. Journal of Geophysical Research. 114. https://doi.org/10.1029/2007JG000641

Brust, C., Kimball, J.S., Maneta, M.P., Jencso, K., He, M., Reichle, R.H., 2021. Using SMAP Level-4 soil moisture to constrain MOD16 evapotranspiration over the contiguous USA. Remote Sensing of Environment. 255, 112277. https://doi.org/10.1016/j.rse.2020.112277

Butchart, S.H.M., Walpole, M., Collen, B., van Strien, A., Scharlemann, J.P.W., Almond, R.E.A., Baillie, J.E.M., Bomhard, B., Brown, C., et al., 2010. Global biodiversity: indicators of recent declines. Science 328(5982), 1164–1168. https://doi.org/10.1126/science.1187512

Caballero, C.B., Biggs, T.W., Vergopolan, N., Camelo, L.G.G., Andrade, B.C., Laipelt, L., Ruhoff, A.L., 2025. Decadal hydroclimatic changes in the Pantanal, the world's largest tropical wetland. Sci. Rep. 15, 17675. https://doi.org/10.1038/s41598-025-01980-6

Cabral Júnior, J.B., Silva, H.J.F., Reis, J.S., 2022. Características da cobertura do solo em anos de contrastes climáticos (chuvoso e seco) no Oeste da Amazônia, Rio Branco–Acre. Rev. Bras. Geogr. Fis. 15(6), 2704–2714. https://doi.org/10.26848/rbgf.v15.6.p2704-2714

Cabral, O. M. R., da Rocha, H. R., Gash, J. H., Freitas, H. C., & Ligo, M. A. V., 2015. Water and energy fluxes from a woodland savanna(cerrado) in southeast Brazil. Journal of Hydrology: Regional Studies. 4, 22–40. https://doi.org/10.1016/j.ejrh.2015.04.010

Cabral, O. M. R., Gash, J. H. C., Rocha, H. R., Marsden, C., Ligo, M. A. V., Freitas, H. C., et al., 2011. Fluxes of CO2 above a plantation of Eucalyptus in southeast Brazil. Agricultural and Forest Meteorology. 151, 49–59. https://doi.org/10.1016/j.agrformet.2010.09.0034

Cabral, O. M. R., Rocha, H. R., Gash, J. H., Ligo, M. A. V., Tatsch, J. D., Freitas, H. C., & Brasilio, E., 2012. Water use in a sugarcane plantation. GCB Bioenergy. 4, 555-565. https://doi.org/10.1111/j.1757-1707.2011.01155.

Campos, S., Mendes, K. R., da Silva, L. L., Mutti, P. R., Medeiros, S. S., et al., 2019. Closure and partitioning of the energy balance in a preserved area of a Brazilian seasonally dry tropical forest. Agricultural and Forest Meteorology. 271, 398–412. https://doi.org/10.1016/j.agrformet.2019.03.018

Carrillo-Niquete, G.A., Andrade, J.L., Valdez-Lazalde, J.R., Reyes-García, C., Hernández-Stefanoni, J.L., 2022. Characterizing spatial and temporal deforestation and its effects on surface urban heat islands in a tropical city using Landsat time series. Landsc. Urban Plan. 217, 104280. https://doi.org/10.1016/j.landurbplan.2021.104280

Chang, Y., Qin, D., Ding, Y., Zhao, Q., Zhang, S., 2018. A modified MOD16 algorithm to estimate evapotranspiration over alpine meadow on the Tibetan Plateau, China. Journal of Hydrology. 561, 16–30. https://doi.org/10.1016/j.jhydrol.2018.03.054

Chen, J.M., Chen, X., Ju, W., Geng, X., 2005. Distributed hydrological model for mapping evapotranspiration using remote sensing inputs. Journal of Hydrology. 305, 15–39. https://doi.org/10.1016/j.jhydrol.2004.08.029

Chen, J.M., Liu, J., 2020. Evolution of evapotranspiration models using thermal and shortwave remote sensing data. Remote Sensing of Environment. 237, 111594. https://doi.org/10.1016/j.rse.2019.111594

Chen, Y., Xia, J., Liang, S., Feng, J., Fisher, J.B., Li, Xin, Li, Xianglan, Liu, S., Ma, Z., Miyata, A., Mu, Q., Sun, L., Tang, J., Wang, K., Wen, J., Xue, Y., Yu, G., Zha, T., Zhang, L., Zhang, Q., Zhao, T., Zhao, L., Yuan, W., 2014. Comparison of satellite-based evapotranspiration models over terrestrial ecosystems in China. Remote Sensing of Environment. 140, 279–293. https://doi.org/10.1016/j.rse.2013.08.045

Chu, H., Luo, X., Ouyang, Z., Chan, W. S., Dengel, S., Biraud, S. C., Torn, M. S. et al., 2021. Representativeness of Eddy-Covariance Flux Footprints for Areas Surrounding AmeriFlux Sites Agricultural and Forest Meteorology. 108350, 301–302. https://doi.org/10.1016/j.agrformet.2021.108350.

Claudino, C.M.A., Bertrand, G.F., Nóbrega, R.L.B., Almeida, C.N., Gusmão, A.C.V., Montenegro, S.M.G.L., Silva, B.B., Patriota, E.G., Lemos, F.C., Coutinho, J.V., Sousa, J.W.G., Andrade, J.M., Melo, D.C.D., Rodrigues, D.F.B., Oliveira, L.M., Xuan, Y., Moura, M.S.B., Montenegro, A.A.A., Brocca, L., Corbari, C., Jin, Y., Suvočarev, K., Bezerra, B., Lima, J.R.S., Souza, E., Anache, J.A.A., Coelho, V.H.R., 2025. ESTIMET: Enhanced and spatial-temporal improvement of MODIS EvapoTranspiration algorithm for all sky conditions in tropical biomes. Remote Sens. Environ. 325, 114771. https://doi.org/10.1016/j.rse.2025.114771

Cleugh, H.A., Leuning, R., Mu, Q., Running, S.W., 2007. Regional evaporation estimates from flux tower and MODIS satellite data. Remote Sensing of Environment. 106, 285–304. https://doi.org/10.1016/j.rse.2006.07.007

Collar, N.M., Ebel, B.A., Saxe, S., Rust, A.J., Hogue, T.S., 2023. Implications of fire-induced evapotranspiration shifts for recharge–runoff generation and vegetation conversion in the western United States. J. Hydrol. 621, 129646. https://doi.org/10.1016/j.jhydrol.2023.129646

Costa, D. P., Lentini, C. A. D., Cunha Lima, A. T., *et al.* (2024). All deforestation matters: Deforestation alert system for the Caatinga biome in South America's tropical dry forest. Sustainability, 16(20), 9006. https://doi.org/10.3390/su16209006

Costa, M.C., Marengo, J.A., Alves, L.M., Paula, A., 2023. Multiscale Analysis of Drought, Heatwaves, and Compound Events in the Brazilian Pantanal in 2019–2021. Theor. Appl. Climatol. 155, 661–677. https://doi.org/10.1007/s00704-023-04655-2

Costa-Filho, E., Chávez, J.L., Zhang, H., Andales, A.A., 2021. An optimized surface aerodynamic temperature approach to estimate maize sensible heat flux and evapotranspiration. Agricultural and Forest Meteorology. 311, 108683. https://doi.org/10.1016/j.agrformet.2021.108683

Davidson, E.A., de Araújo, A.C., Artaxo, P., Balch, J.K., Brown, I.F., Bustamante, M.M.C., Coe, M.T., DeFries, R.S., Keller, M., Longo, M., Munger, J.W., Schroeder, W., Soares-Filho, B.S., Souza, C.M., Wofsy, S.C., 2012. The Amazon basin in transition. Nature 481(7381), 321–328. https://doi.org/10.1038/nature10717

de Andrade, B.C.C., et al., 2021. Remote sensing-based actual evapotranspiration assessment in a data-scarce area of Brazil: A case study of the Urucuia Aquifer System. Int. J. Appl. Earth Obs. Geoinf. 98. https://doi.org/10.1016/j.jag.2021.102396

DeBano, L.F., Neary, D.G., Ffolliott, P.F., 1998. Fire effects on ecosystems. John Wiley & Sons, New York. 352 pp. ISBN 9780471163565.

Degano, M.F., Rivas, R.E., Carmona, F., Niclòs, R., Sánchez, J.M., 2021. Evaluation of the MOD16A2 evapotranspiration product in an agricultural area of Argentina, the Pampas region. Egypt. J. Remote Sens. Spc. Sci. 24(2), 319-328. https://doi.org/10.1016/j.ejrs.2020.08.004

Di, S.-C., Li, Z.-L., Tang, R., Wu, H., Tang, B.-H., Lu, J., 2015. Integrating two layers of soil moisture parameters into the MOD16 algorithm to improve evapotranspiration estimations. International Journal of Remote Sensing. 36, 4953–4971.

Dias, S.H.B., Filgueiras, R., Fernandes Filho, E.I., Arcanjo, G.S., Silva, G.H.D., Mantovani, E.C., Cunha, F.F.D., 2021. Reference evapotranspiration of Brazil modeled with machine learning techniques and remote sensing. PLoS ONE. 16, e0245834. https://doi.org/10.1371/journal.pone.0245834

El Masri, B., Rahman, A.F., Dragoni, D., 2019. Evaluating a new algorithm for satellite-based evapotranspiration for North American ecosystems: Model development and validation. Agricultural and Forest Meteorology. 268, 234–248. https://doi.org/10.1016/j.agrformet.2019.01.025

Evans, T.L., Costa, M., Tomas, W.M., Camilo, A.R., 2014. Large-scale habitat mapping of the Brazilian Pantanal wetland: A synthetic aperture radar approach. Remote Sens. Environ. 155, 89–108. https://doi.org/10.1016/j.rse.2013.08.051

Farella, M.M., Fisher, J.B., Jiao, W., Key, K.B., Barnes, M.L., 2021. Thermal remote sensing for plant ecology from leaf to globe. J. Ecol. https://doi.org/10.1111/1365-2745.13957

Feng, X., Porporato, A., Rodriguez-Iturbe, I., 2013. Changes in rainfall seasonality in the tropics. Nature Climate Change.3, 811-815. https://doi.org/10.1038/nclimate1907

Ferreira, T.R., Silva, B.B.D., Moura, M.S.B.D., Verhoef, A., Nóbrega, R.L.B., 2020. The use of remote sensing for reliable estimation of net radiation and its components: a case study for contrasting land covers in an agricultural hotspot of the Brazilian semiarid region. Agricultural and Forest Meteorology. 291, 108052. https://doi.org/10.1016/j.agrformet.2020.108052

Filgueiras, R., Almeida, T.S., Mantovani, E.C., Dias, S.H.B., Fernandes-Filho, E.I., Da Cunha, F.F., Venancio, L.P., 2020. Soil water content and actual evapotranspiration predictions using regression algorithms and remote sensing data. Agricultural Water Management. 241, 106346. https://doi.org/10.1016/j.agwat.2020.106346

Fisher, J. B., et al., 2017. The future of evapotranspiration: Global requirements for ecosystem functioning, carbon and climate feedbacks, agricultural management, and water resources. Water Resources Research. 53, 2618–2626. https://doi.org/10.1002/2016WR020175

Fisher, J.B., Tu, K.P., Baldocchi, D.D., 2008. Global estimates of the land–atmosphere water flux based on monthly AVHRR and ISLSCP-II data, validated at 16 FLUXNET sites. Remote Sensing of Environment. 112, 901–919. https://doi.org/10.1016/j.rse.2007.06.025

Fleischmann, A.S., Laipelt, L., Papa, F. et al., 2023. Patterns and drivers of evapotranspiration in South American wetlands. Nature Communications.14, 6656. https://doi.org/10.1038/s41467-023-42467-0

Franca Rocha, W.J.S., Vasconcelos, R.N., Costa, D.P., Duverger, S.G., Lobão, J.S.B., Souza, D.T.M., Herrmann, S.M., Santos, N.A., Franca Rocha, R.O., Ferreira-Ferreira, J., et al., 2024. Towards uncovering three decades of LULC in the Brazilian drylands: Caatinga biome dynamics (1985–2019). Land 13, 1250. https://doi.org/10.3390/land13081250

Freitas, E.S. da, Coelho, V.H.R., Bertrand, G.F., Lemos, F.C., Almeida, C.N., 2024. IMERG BraMaL: An improved gridded monthly rainfall product for Brazil based on satellite-based IMERG estimates and machine learning techniques. Int. J. Climatol. 44(11), 3976–3997. https://doi.org/10.1002/joc.8357

Gadelha, A.N., Coelho, V.H.R., Xavier, A.C., Barbosa, L.R., Melo, D.C.D., Xuan, Y., Huffman, G.J., Petersen, W.A., Almeida, C.D.N., 2019. Grid box-level evaluation of IMERG over Brazil at various space and time scales. Atmospheric Research 218, 231–244. https://doi.org/10.1016/j.atmosres.2018.12.001

Galvanin, G. and Caldas, A. (2025). Evaluating Public Policies in Fire-affected Conservation Priority Areas of the Brazilian Pantanal. Environmental Management. https://doi.org/10.1007/s00267-025-02253-8

Godoy, M.R.V., Markonis, Y., 2023. pRecipe: A global precipitation climatology toolbox and database. Environ. Model. Softw. 165, 105711. https://doi.org/10.1016/j.envsoft.2023.105711

Golubkov, G.V., Manzhelii, M.I., Berlin, A.A., Lushnikov, A.A., Eppelbaum, L.V., 2018. Russian Journal of Physical Chemistry B 12(4), 725–748. https://doi.org/10.1134/S1990793118040055

Grosso, C., Manoli, G., Martello, M., Chemin, Y., Pons, D., Teatini, P., Piccoli, I., Morari, F., 2018. Mapping Maize Evapotranspiration at Field Scale Using SEBAL: A Comparison with the FAO Method and Soil-Plant Model Simulations. Remote Sensing. 10, 1452. https://doi.org/10.3390/rs10091452

Guerra, A., Roque, F. de O., Garcia, L. C., Ochoa-Quintero, J. M., de Oliveira, P. T. S., Guariento, R. D., & Rosa, I. M. D. (2020). Drivers and projections of vegetation loss in the Pantanal and surrounding ecosystems. *Land Use Policy, 91*, 104388. https://doi.org/10.1016/j.landusepol.2019.104388

Guerschman, J. P, McVicar, T. R. Vleeshower,J., Van Niel, T. G.,Peña-Arancibia, J. L., Chen, Y., 2022. Estimating actual evapotranspiration at field-to-continent scales by calibrating the CMRSET algorithm with MODIS, VIIRS, Landsat and Sentinel-2 data. Journal of Hydrology. 605. https://doi.org/10.1016/j.jhydrol.2021.127318

Guo, M., Huang, Y., Li, J., Luo, Z., 2023. The Modified Soil Moisture Constraint Scheme Significantly Enhances the Evapotranspiration Simulation Accuracy of the MOD16 Model. Sustainability. 15, 12460. https://doi.org/10.3390/su151612460

Hamilton, S.K., 2002. Hydrological controls of ecological structure and function in the Pantanal wetland (Brazil). In: Salz, H., Kundzewicz, Z.W., editors. The ecohydrology of South American rivers and wetlands. IAHS Special Publication, Wallingford, p. 133–158.

He, M., Kimball, J.S., Yi, Y., Running, S.W., Guan, K., Moreno, A., Wu, X., Maneta, M., 2019. Satellite data-driven modeling of field scale evapotranspiration in croplands using the MOD16 algorithm framework. Remote Sensing of Environment. 230, 111201. https://doi.org/10.1016/j.rse.2019.05.020

Hernandes, T. A. D., de Oliveira Bordonal, R., Duft, D. G., et al. (2022). Implications of regional agricultural land use dynamics and deforestation associated with sugarcane expansion for soil carbon stocks in Brazil. *Regional Environmental Change, 22*(49). https://doi.org/10.1007/s10113-022-01907-1

Hobeichi, S., Abramowitz, G., Evans, J., Ukkola, A., 2018. Derived Optimal Linear Combination Evapotranspiration (DOLCE): a global gridded synthesis ET estimate. Hydrol. Earth Syst. Sci. 22, 1317–1336. https://doi.org/10.5194/hess-22-1317- 2018

Hobeichi, S., Abramowitz, G., Evans, J.P., 2021. Robust historical evapotranspiration trends across climate regimes. Hydrol. Earth Syst. Sci. 25, 3855–3874. https://doi.org/10.5194/hess-25-3855-2021

Horning, N., 2019. Remote sensing. In: Encyclopedia of Ecology. Elsevier, pp. 404–413. https://doi.org/10.1016/B978-0-12-409548-9.10607-4

Hu, G., Jia, L., Menenti, M., 2015. Comparison of MOD16 and LSA-SAF MSG evapotranspiration products over Europe for 2011. Remote Sensing of Environment. 156, 510–526. https://doi.org/10.1016/j.rse.2014.10.017

Huete, A., Didan, K., Miura, T., Rodriguez, E.P., Gao, X., Ferreira, L.G., 2002. Overview of the radiometric and biophysical performance of the MODIS vegetation indices. Remote Sensing of Environment. 83, 195–213. https://doi.org/10.1016/S0034-4257(02)00096-2

Huete, A.R., 1988. A soil-adjusted vegetation index (SAVI). Remote Sensing of Environment. 25, 295–309. https://doi.org/10.1016/0034-4257(88)90106-X

Hutyra, L. R., Munger, J. W., Saleska, S. R., Gottlieb, E., Daube, B. C., Dunn, A. L., et al., 2007. Seasonal controls on the exchange of carbon and water in an Amazonian rain forest. Journal of Geophysical Research. 112. https://doi.org/10.1029/2006JG000365

Immerzeel, W.W., Droogers, P., 2008. Calibration of a distributed hydrological model based on satellite evapotranspiration. Journal of Hydrology. 349, 411–424. https://doi.org/10.1016/j.jhydrol.2007.11.017

INPE (Instituto Nacional de Pesquisas Espaciais), 2025. Área Queimada 1 km (AQ1 km) – Programa Queimadas, TerraBrasilis. Disponível em: https://terrabrasilis.dpi.inpe.br/queimadas/aq1km/. Acessado em: 9 ago. 2025.

Jang, K., Kang, S., Lim, Y., Jeong, S., Kim, J., Kimball, J.S., Hong, S.Y., 2013. Monitoring daily evapotranspiration in Northeast Asia using MODIS and a regional Land Data Assimilation System. JGR Atmospheres. 118. https://doi.org/10.1002/2013JD020639

Jiang, Z., Huete, A., Didan, K., Miura, T., 2008. Development of a two-band enhanced vegetation index without a blue band. Remote Sensing of Environment. 112, 3833–3845. https://doi.org/10.1016/j.rse.2008.06.006

Jiménez, C., Martens, B., Miralles, D.M., Fisher, J.B., Beck, H.E., Fernandez-Prieto, D., 2018. Exploring the merging of the global land evaporation WACMOS-ET products based on local tower measurements. Hydrol. Earth Syst. Sci. 22, 4513–4533. https://doi.org/10.5194/hess-22-4513-2018

Jin, Y., Randerson, J. T., Goulden, M. L, 2011. Continental-scale net radiation and evapotranspiration estimated using MODIS satellite observations. Remote Sensing of Environment, 115, pp. 2302-2319. https://doi.org/10.1016/j.rse.2011.04.031

Jung, M., Henkel, K., Herold, M., Churkina, G., 2006. Exploiting synergies of global land cover products for carbon cycle modeling. Remote Sensing of Environment. 101, 534–553. https://doi.org/10.1016/j.rse.2006.01.020

Kacic, P., Kuenzer, C., 2022. Forest biodiversity monitoring based on remotely sensed spectral diversity—A review. Remote Sens. 14, 5363. https://doi.org/10.3390/rs14215363

Kalma, J.D., McVicar, T.R., McCabe, M.F., 2008. Estimating Land Surface Evaporation: A Review of Methods Using Remotely Sensed Surface Temperature Data. Surv Geophys. 29, 421–469. https://doi.org/10.1007/s10712-008-9037-z

Kara, T., G., Elbir, T., 2024. Evaluation of ERA5 and MERRA-2 Reanalysis Datasets over the Aegean Region, Türkiye. Deu Muhendislik Fakultesi Fen ve Muhendislik, 26(76), 9-21. https://doi.org/10.21205/deufmd.2024267602

Ke, Y., Im, J., Park, S., Gong, H., 2016. Downscaling of MODIS One Kilometer Evapotranspiration Using Landsat-8 Data and Machine Learning Approaches. Remote Sensing. 8, 215. https://doi.org/10.3390/rs8030215

Ke, Y., Im, J., Park, S., Gong, H., 2017. Spatiotemporal downscaling approaches for monitoring 8-day 30 m actual evapotranspiration. ISPRS Journal of Photogrammetry and Remote Sensing. 126, 79–93. https://doi.org/10.1016/j.isprsjprs.2017.02.006

Kendall, M., Stuart, A., 1983. The advanced theory of statistics: Design and analysis and time-series. Griffin.

Khan, M.S., Jeong, J., Choi, M., 2021. An improved remote sensing based approach for predicting actual Evapotranspiration by integrating LiDAR. Advances in Space Research. 68, 1732–1753. https://doi.org/10.1016/j.asr.2021.04.017

Khan, M.S., Liaqat, U.W., Baik, J., Choi, M., 2018. Stand-alone uncertainty characterization of GLEAM, GLDAS and MOD16 evapotranspiration products using an extended triple collocation approach. Agricultural and Forest Meteorology. 252, 256–268. https://doi.org/10.1016/j.agrformet.2018.01.022

Kumar, U., Rashmi, Srivastava, A., Kumari, N., Chatterjee, C., Raghuwanshi, N.S., 2023. Evaluation of Standardized MODIS-Terra Satellite-Derived Evapotranspiration Using Genetic Algorithm for Better Field Applicability in a Tropical River Basin. J Indian Soc Remote Sens. 51, 1001–1012. https://doi.org/10.1007/s12524-023-01675-3

Kustas, W.P., Norman, J.M., 1999. Evaluation of soil and vegetation heat flux predictions using a simple two-source model with radiometric temperatures for partial canopy cover. Agricultural and Forest Meteorology. 94, 13–29. https://doi.org/10.1016/S0168-1923(99)00005-2

Laipelt, L., Henrique Bloedow Kayser, R., Santos Fleischmann, A., Ruhoff, A., Bastiaanssen, W., Erickson, T.A., Melton, F., 2021. Long-term monitoring of evapotranspiration using the SEBAL algorithm and Google Earth Engine cloud computing. ISPRS Journal of Photogrammetry and Remote Sensing. 178, 81–96. https://doi.org/10.1016/j.isprsjprs.2021.05.018

Landsberg, J. J.; Gower, S. T.,1997. Applications of physiological ecology to forest management. Academic Press.

Lang, J., Jin, X., Zhang, X., 2024. Trends analysis of evapotranspiration and responses to soil moisture and wind speed over the Taklimakan Desert, China. Arid Land Res. Manag. https://doi.org/10.1080/15324982.2024.2393337

Leivas, J.F., Teixeira, A.H.C., Andrade, R.G., Victoria, D.C., Torresan, F.E., 2015. Spatiotemporal variability of evapotranspiration in Pantanal, Brazil, using satellite images.

Lemos, F. C.; Coelho, V. H. R.; Freitas, E. S.; Tomasella, J.; Bertrand, G. F.; Meira, M. A.; Filho, Geraldo, M. R.; Fullhart, A.; Almeida, C. N., 2023. Spatiotemporal distribution of precipitation and its characteristics under tropical atmospheric systems of: Insights from a large sub-hourly database. Hydrological Processes. 37, 1-11. https://doi.org/10.1002/hyp.15017

Li, Q., Tian, J., Tian, Q., 2023. Deep learning application for crop classification via multi-temporal remote sensing images. Agriculture 13, 906. https://doi.org/10.3390/agriculture13040906

Li, Z.-L., Tang, R., Wan, Z., Bi, Y., Zhou, C., Tang, B., Yan, G., Zhang, X., 2009. A Review of Current Methodologies for Regional Evapotranspiration Estimation from Remotely Sensed Data. Sensors. 9, 3801–3853. https://doi.org/10.3390/s90503801

Liu, D., Lu, Y., Wang, L., Zhang, M., Qin, W., Feng, L., Wang, Z., 2025. Performance evaluation of different cloud products for estimating surface solar radiation. Atmospheric Environment, 121023. https://doi.org/10.1016/j.atmosenv.2024.121023

Liu, K., Song, C., Wang, J., Ke, L., Zhu, Y., Zhu, J., Ma, R., Luo, Z., 2020. Remote Sensing-Based Modeling of the Bathymetry and Water Storage for Channel-Type Reservoirs Worldwide. Water Resources Research. 56, e2020WR027147. https://doi.org/10.1029/2020WR027147

Liu, R., Zhang, X., Wang, W., Wang, Y., Liu, H., Ma, M., & Tang, G., 2024. Global-scale ERA5 product precipitation and temperature evaluation. Ecological Indicators, 166, 112481. https://doi.org/10.1016/j.ecolind.2024.112481

Liu, S., Han, Y., Su, H., 2022. Regional Evapotranspiration Estimation by the Improved MOD16-sm Model and Its Application in Central China. Water. 14, 1491. https://doi.org/10.3390/w14091491

Liu, Y., Guo, W., Huang, H., Ge, J., Qiu, B., 2021. Estimating global aerodynamic parameters in 1982–2017 using remote-sensing data and a turbulent transfer model. Remote Sensing of Environment. 260, 112428. https://doi.org/10.1016/j.rse.2021.112428

Lu, H., Huang, W., Zeng, Y., Wang, P., Pi, X., Liu, W., 2022. An unmixing-based spatial downscaling fusion approach for the MODIS evapotranspiration product. Geocarto International. 37, 12488–12508. https://doi.org/10.1080/10106049.2022.2068674

Luo, T., Jutla, A., Islam, S., 2015. Evapotranspiration estimation over agricultural plains using MODIS data for all sky conditions. International Journal of Remote Sensing. 36, 1235–1252. https://doi.org/10.1080/01431161.2015.1009648

Machado, C. B., Lima, J. R. d. S., Antonino, A. C. D., Souza, E. S. d., Souza, R. M. S., Alves, E. M., et al. 2016. Daily and seasonal patterns of CO2 fluxes and evapotranspiration in maize-grass intercropping. Revista Brasileira de Engenharia Agrícola e Ambiental. 20, 777–782. https://doi.org/10.1590/1807-1929/agriambi.v20n9p777-782

Machado, C.C., Silva, B.B.D., De Albuquerque, M.B., Galvíncio, J.D., 2014. Estimativa do balanço de energia utilizando imagens TM - Landsat 5 e o algoritmo SEBAL no litoral sul de Pernambuco. Rev. bras. meteorol. 29, 55–67. https://doi.org/10.1590/S0102-77862014000100006

Maeda, E.E., Ma, X., Wagner, F.H., Kim, H., Oki, T., Eamus, D., Huete, A., 2017. Evapotranspiration seasonality across the Amazon Basin. Earth Syst. Dynam. 8, 439–454. https://doi.org/10.5194/esd-8-439-2017

Magalhães Neto, N. de, Evangelista, H., 2022. Human Activity Behind the Unprecedented 2020 Wildfire in Brazilian Wetlands (Pantanal). Front. Environ. Sci. 10, 888578. https://doi.org/10.3389/fenvs.2022.888578

Mann, H.B., 1945. Non-Parametric Test against Trend. Econometrica 13, 245–259. http://dx.doi.org/10.2307/1907187

MapBiomas, 2021. Desmatamento, queimadas e retração da superfície da água aumentam o risco de desertificação da Caatinga. Available from: https://brasil.mapbiomas.org/2021/10/06/desmatamento-queimadas-e-retracao-da-superficie-da-agua-aumentam-o-risco-de-desertificacao-da-caatinga/

MapBiomas, 2025. Alerta – Sistema de Validação e Refinamento de Alertas de Desmatamento com Imagens de Alta Resolução. Disponível em: https://plataforma.alerta.mapbiomas.org/. Acessado em: 09 ago. 2025.

Marengo, J.A., Alves, L.M., Alvala, R.C.S., Cunha, A.P., Brito, S., Moraes, O.L.L., 2018. Climatic characteristics of the 2010–2016 drought in the semiarid northeast Brazil region. Ann. Braz. Acad. Sci. 90(2). https://doi.org/10.1590/0001-3765201720170206

Marques, M.C.S., Rodriguez, D.A., 2022. Impacts of the landscape changes in the low streamflows of Pantanal headwaters—Brazil. Hydrol. Process. https://doi.org/10.1002/hyp.14617

Matsunaga, W.K., Sales, E.S.G., Júnior, G.C.A. et al., 2024. Application of ERA5-Land reanalysis data in zoning of climate risk for corn in the state of Bahia—Brazil. Theor Appl Climatol, 155, 945–963. https://doi.org/10.1007/s00704-023-04670-3

Melo, D.C.D., Anache, J.A.A., Borges, V.P., Miralles, D.G., Martens, B., Fisher, J.B., Nóbrega, R.L.B., Moreno, A., Cabral, O.M.R., Rodrigues, T.R., Bezerra, B., Silva, C.M.S., Neto, A.A.M., Moura, M.S.B., Marques, T.V., Campos, S., Nogueira, J.S., Rosolem, R., Souza, R.M.S., Antonino, A.C.D., Holl, D., Galleguillos, M., Perez-Quezada, J.F., Verhoef, A., Kutzbach, L., Lima, J.R.S., Souza, E.S., Gassman, M.I., Perez, C.F., Tonti, N., Posse, G., Rains, D., Oliveira, P.T.S., Wendland, E., 2021. Are Remote Sensing Evapotranspiration Models Reliable Across South American Ecoregions? Water Resources Research. 57, e2020WR028752. https://doi.org/10.1029/2020WR028752.

Menezes, R.S.C.I., Sampaio, E.V.S.B.I., Giongo, V., Pérez-Marin, A.M., 2012. Biogeochemical cycling in terrestrial ecosystems of the Caatinga Biome. Braz. J. Biol. 72(3 suppl). https://doi.org/10.1590/S1519-69842012000400004

Miller, S.D., Goulden, M.L., Menton, M.C., Rocha, H.R., Freitas, H.C., Figueira, A.M. S., Sousa, C.A.D. ,2004. Biometric and micrometeorological measurements of tropical forest carbon balance. Ecol. Appl., 14 , pp. S114-S126.

Miralles, D.G., Holmes, T. R. H., De Jeu, R. A. M., Gash, J. H., Meesters, A. G. C. A., Dolman, A. J.,2011. Global land-surface evaporation estimated from satellite-based observations. Hydrology and Earth System Sciences.15, 453–469.https://doi.org/10.5194/hess-15-453-2011.

Miranda, R.D.Q., Galvíncio, J.D., Morais, Y.C.B., De Moura, M.S.B., Jones, C.A., Srinivasan, R., 2018. Dry forest deforestation dynamics in Brazil's Pontal Basin. Rev. Caatinga 31(2), 385–395. https://doi.org/10.1590/1983-21252018v31n215rc

Miranda, R.Q., Nóbrega, R.L.B., Moura, M.S.B., Raghavan, S., Galvíncio, J.D., 2020. Realistic and simplified models of plant and leaf area indices for a seasonally dry tropical forest. Int. J. Appl. Earth Obs. Geoinf. 85, 101992. https://doi.org/10.1016/j.jag.2019.101992

Mohan, P.M.M., Rajitha, K., Varma, M.R.R., 2020. Integration of soil moisture as an auxiliary parameter for the anchor pixel selection process in SEBAL using Landsat 8 and Sentinel - 1A images. International Journal of Remote Sensing. 41, 1214–1231. https://doi.org/10.1080/01431161.2019.1658239

Moreira, A.A., Adamatti, D.S., Ruhoff, A.L., 2018. Avaliação dos produtos de evapotranspiração baseados em sensoriamento remoto MOD16 e GLEAM em sítios de fluxos turbulentos do Programa LBA. CeN. 40, 112. https://doi.org/10.5902/2179460X30714

Moreira, A.A., Ruhoff, A.L., Roberti, D.R., Souza, V.A., Ribeiro da Rocha, H., Paiva, R.C.D., 2019. Assessment of terrestrial water balance using remote sensing data in South America. J. Hydrol. 575, 131–147. https://doi.org/10.1016/j.jhydrol.2019.05.045

Morillas, L., Leuning, R., Villagarcía, L., García, M., Serrano-Ortiz, P., Domingo, F., 2013. Improving evapotranspiration estimates in Mediterranean drylands: The role of soil evaporation: Evapotranspiration Estimation in Mediterranean Dry Lands. Water Resour. Res. 49, 6572–6586. https://doi.org/10.1002/wrcr.20468

Moro, M.F., Nic Lughadha, E.M., de Araújo, F.S., Martins, F.R., 2016. A phytogeographical metaanalysis of the semiarid Caatinga domain in Brazil. Bot. Rev. 82(2), 91–148. https://doi.org/10.1007/s12229-016-9164-z

Mu, Q., Heinsch, F.A., Zhao, M., Running, S.W., 2007. Development of a global evapotranspiration algorithm based on MODIS and global meteorology data. Remote Sensing of Environment. 111, 519–536. https://doi.org/10.1016/j.rse.2007.04.015.

Mu, Q., Zhao, M., Running, S.W., 2011. Improvements to a MODIS global terrestrial evapotranspiration algorithm. Remote Sensing of Environment. 115, 1781–1800. https://doi.org/10.1016/j.rse.2011.02.019

Muñoz, S. J., 2019. ERA5-Land monthly averaged data from 1950 to present. https://doi.org/10.24381/CDS.68D2BB30

NOAA, 2025. Class-A evaporation pan. U.S. National Weather Service. Available from: https://web.archive.org/web/20050507152124/http://www.crh.noaa.gov/gid/Local_Information/coop/evapStations/#sec1. Acessado em: 11 ago. 2025.

Norman, J.M., Kustas, W.P., Humes, K.S., 1995. Source approach for estimating soil and vegetation energy fluxes in observations of directional radiometric surface temperature. Agricultural and Forest Meteorology. 77, 263–293. https://doi.org/10.1016/0168-1923(95)02265-Y

Oliveira, G., Araújo, M.B., Rangel, T.F., et al., 2012. Conserving the Brazilian semiarid (Caatinga) biome under climate change. Biodivers. Conserv. 21, 2913–2926. https://doi.org/10.1007/s10531-012-0346-7

Oliveira, M.L., Dos Santos, C.A.C., De Oliveira, G., Silva, M.T., Silva, B.B., Cunha, J.E.D.B.L., Ruhoff, A., Santos, C.A.G., 2022. Remote sensing-based assessment of land degradation and drought impacts over terrestrial ecosystems in Northeastern Brazil. Science of The Total Environment. 835, 155490. https://doi.org/10.1016/j.scitotenv.2022.155490

Oliveira, P. T. S., Wendland, E., Nearing, M. A., Scott, R. L., Rosolem, R., Rocha, H. R, 2015. The water balance components of undisturbed tropical woodlands in the Brazilian cerrado. Hydrol. Earth Syst. Sci., 19, 2899–2910. https://doi.org/10.5194/hess-19-2899-2015

Ollivier, C., Olioso, A., Carrière, S.D., Boulet, G., Chalikakis, K., Chanzy, A., Charlier, J.-B., Combemale, D., Davi, H., Emblanch, C., Marloie, O., Martin-StPaul, N., Mazzilli, N., Simioni, G., Weiss, M., 2021. An evapotranspiration model driven by remote sensing data for assessing groundwater resource in karst watershed. Science of The Total Environment. 781, 146706. https://doi.org/10.1016/j.scitotenv.2021.146706

Oren, R., Sperry, J.S., Katul, G.G., Pataki, D.E., Ewers, B.E., Phillips, N., Schäfer, K.V.R., 1999. Survey and synthesis of intra- and interspecific variation in stomatal sensitivity to vapour pressure deficit. Plant Cell & Environment. 22, 1515–1526. https://doi.org/10.1046/j.1365-3040.1999.00513

OTT HydroMet, 2016. New Microwave Scintillometer, RPG-MWSC-160. Available from: https://blog.otthydromet.com/en/new-microwave-scintillometer-rpg-mwsc-160/. Acessado em: 11 ago. 2025.

Paca, V. H. d. M., Espinoza-Dávalos, G. E., Hessels, T. M., Moreira, D. M., Comair,G. F., & Bastiaanssen, W. G. M., 2019. The spatial variability of actual evapotranspiration across the Amazon River Basin based on remote sensing products validated with ux towers. Ecological Processes, 8 (1), 6. https://doi.org/10.1186/s13717-019-0158-8

Palácio, H.A.Q. de, Ribeiro Filho, J.C., Santos, J.C.N., Andrade, E.M., Brasil, J.B., 2016. Precipitação efetiva e perdas de solo em diferentes sistemas de cobertura vegetal no Bioma Caatinga. Rev. Caatinga 29(4). https://doi.org/10.1590/1983-21252016v29n421rc

Paloschi, R.A., Ramos, D.M., Ventura, D.J., Souza, R., Souza, E., Morellato, L.P.C., Nóbrega, R.L.B., Coutinho, I.A.C., Verhoef, A., Körting, T.S., Borma, L.D.S., 2020. Environmental drivers of water use for Caatinga woody plant species: combining remote sensing phenology and sap flow measurements. Remote Sens. 13(1), 75. https://doi.org/10.3390/rs13010075

Patriota, E.G., Bertrand, G.F., Almeida, C.N., Claudino, C.M.A., Coelho, V.H.R., 2024. Heat the road again! Twenty years of surface urban heat island intensity (SUHII) evolution and forcings in 21 tropical metropolitan regions in Brazil from remote sensing analyses. Sustain. Cities Soc. 113, 105629. https://doi.org/10.1016/j.scs.2024.105629

Pereira, G., Ramos, R.C., Rocha, L.C., Brunsell, N.A., Merino, E.R., Mataveli, G.A.V., Cardozo, F.S., 2021. Rainfall patterns and geomorphological controls driving inundation frequency in tropical wetlands: How does the Pantanal flood? Prog. Phys. Geogr. 45(5), 669–686. https://doi.org/10.1177/0309133320987719

Petropoulos, G., Carlson, T.N., Wooster, M.J., Islam, S., 2009. A review of Ts/VI remote sensing based methods for the retrieval of land surface energy fluxes and soil surface moisture. Progress in Physical Geography: Earth and Environment. 33, 224–250. https://doi.org/10.1177/0309133309338997

Pinheiro, E.A.R., Costa, C.A.G., de Araújo, J.C., 2013. Effective root depth of the Caatinga biome. J. Arid Environ. 89, 1–4. https://doi.org/10.1016/j.jaridenv.2012.10.003

Prudente, V.H.R., Martins, V.S., Vieira, D.C., Silva, N.R.F., Adami, M., Sanches, I.D.A., 2020. Limitations of cloud cover for optical remote sensing of agricultural areas across South America. Remote Sens. Appl. Soc. Environ. 20, 100414. https://doi.org/10.1016/j.rsase.2020.100414

Queiroz, L.P., Cardoso, D., Fernandes, M.F., Moro, M.F., 2017. Diversity and evolution of flowering plants of the Caatinga domain. In: Silva, J.M.C., Leal, I.R., Tabarelli, M. (Eds.), Caatinga: the largest tropical dry forest region in South America. Springer, Cham, pp. 23–63. https://doi.org/10.1007/978-3-319-68339-3_2

R Core Team, 2017. R: A language and environment for statistical computing. R Foundation for Statistical Computing, Vienna, Austria.

Racetin, I., Krtalić, A., 2021. Systematic review of anomaly detection in hyperspectral remote sensing applications. Appl. Sci. 11, 4878. https://doi.org/10.3390/app11114878

Ramoelo, A., Majozi, N., Mathieu, R., Jovanovic, N., Nickless, A., Dzikiti, S., 2014. Validation of Global Evapotranspiration Product (MOD16) using Flux Tower Data in the African Savanna, South Africa. Remote Sensing. 6, 7406–7423. https://doi.org/10.3390/rs6087406

Read, J.M., Chambers, C., Torrado, M., 2020. Remote sensing. In: Department of Geography, Maxwell School of Syracuse University, Syracuse, NY, United States. Elsevier. (Revised from: Read, J.M., Torrado, M., 2009. Encyclopedia of Geography, vol. 9, pp. 335–346).

Ribas, C.R., Schoereder, J.H., 2007. Ant communities, environmental characteristics and their implications for conservation in the Brazilian Pantanal. Biodivers. Conserv. 16(5), 1511–1520.

Rocha, A.V., Shaver, G.R., 2009. Advantages of a two band EVI calculated from solar and photosynthetically active radiation fluxes. Agricultural and Forest Meteorology. 149, 1560–1563. https://doi.org/10.1016/j.agrformet.2009.03.016

Rocha, W. J. S. F., Vasconcelos, R. N., Costa, D. P., et al. (2024). Towards uncovering three decades of LULC in the Brazilian drylands: Caatinga biome dynamics (1985–2019). Land, 13(8), 1250. https://doi.org/10.3390/land13081250

Rodell, M., Houser, P.R., Jambor, U., Gottschalck, J., Mitchell, K., Meng, C.-J., Arsenault, K., Cosgrove, B., Radakovich, J., Bosilovich, M., Entin, J.K., Walker, J.P., Lohmann, D., Toll, D., 2004. The Global Land Data Assimilation System. Bull. Amer. Meteor. Soc. 85, 381–394. https://doi.org/10.1175/BAMS-85-3-381

Rodrigues, T. R., Vourlitis, G. L., Lobo, F. d. A., Oliveira, R. G. d., & Nogueira, J. d. S., 2014. Seasonal variation in energy balance and canopy conductance for a tropical savanna ecosystem of south central Mato Grosso, Brazil. Journal of Geophysical Research: Biogeosciences. 119, 1–13. https://doi.org/10.1002/2013JG002472

Roesch, L.F., Vieira, F., Pereira, V., Schünemann, A.L., Teixeira, I., Senna, A.J., Stefenon, V.M., 2009. The Brazilian Pampa: A Fragile Biome. Diversity. 1, 182–198. https://doi.org/10.3390/d1020182

Ruhoff, A., de Andrade, B. C., Laipelt, L., Fleischmann, A. S., Siqueira, V. A., Moreira, A. A., Barbedo, R., Cyganski, G. L., Fernandez, G. M. R., Brêda, J. P. L. F., Paiva, R. C. D. d., Meller, A., Teixeira, A. d. A., Araújo, A. A., Fuckner, M. A.,Biggs, T. (2022). Global Evapotranspiration Datasets Assessment Using Water Balance in South America. Remote Sensing, 14(11), 2526. https://doi.org/10.3390/rs14112526

Ruhoff, A.L., Paz, A.R., Aragao, L.E.O.C., Mu, Q., Malhi, Y., Collischonn, W., Rocha, H.R., Running, S.W., 2013. Assessment of the MODIS global evapotranspiration algorithm using eddy covariance measurements and hydrological modelling in the Rio Grande basin. Hydrological Sciences Journal. 58, 1658–1676. https://doi.org/10.1080/02626667.2013.837578

Ruhoff, A.L., Paz, A.R., Collischonn, W., Aragao, L.E.O.C., Rocha, H.R., Malhi, Y.S., 2012. A MODIS-Based Energy Balance to Estimate Evapotranspiration for Clear-Sky Days in Brazilian Tropical Savannas. Remote Sensing. 4, 703–725. https://doi.org/10.3390/rs4030703

Running, S.W., Mu, Q., Zhao, M., Moreno, A., 2017. NASA Earth Observing System MODIS Land Algorithm User's Guide: MODIS Global Terrestrial Evapotranspiration (ET) Product (NASA MOD16A2/A3). https://doi.org/10.5067/MODIS/MOD16A2.006

Running, S.W., Mu, Q., Zhao, M., Moreno, A., 2021. NASA Earth Observing System MODIS Land Algorithm (For Collection 6.1) User's Guide MODIS Global Terrestrial Evapotranspiration (ET) Product (MOD16A2/A3 and Year-end Gap-filled MOD16A2GF/A3GF). https://doi.org/10.5067/MODIS/MOD16A2GF.061

Sabino, M., Silva, A.C., Almeida, F.T., Souza, A.P., 2024. Reference evapotranspiration in climate change scenarios in Mato Grosso, Brazil. Hydrology 11, 91. https://doi.org/10.3390/hydrology11070091

Saddique, N., Mahmood, T., Bernhofer, C., 2020. Quantifying the impacts of land use/land cover change on the water balance in the afforested River Basin, Pakistan. Environ. Earth Sci. 79(19), 448. https://doi.org/10.1007/s12665-020-09206-w

Salazar-Martínez, D., Holmes, T. R.H., Yépez, E. A., Hain, C. R., Alvarado-Barrientos, S., Ángeles-Pérez, G., Arredondo-Moreno, T., Delgado-Balbuena, J., Figueroa-Espinoza, B., Garatuza-Payán, J., Castillo, E. G., Rodríguez, J. C., Rojas-Robles, N. E., Uuh-Sonda, J. M., Vivoni, E. R., 2022. Evaluation of remote sensing-based evapotranspiration products at low-latitude eddy covariance sites. Journal of Hydrology, 610, https://doi.org/10.1016/j.jhydrol.2022.127786.

Sampaio, E.V.S.B., 1995. Overview of the Brazilian Caatinga. In: Bullock, S.H., Mooney, H.A., Medina, E., editors. Seasonally dry tropical forests. Cambridge Univ. Press, Cambridge, p. 35–63.

Sanches, L., Vourlitis, G.L., Alves, M.C., Pinto-Júnior, O.B., Nogueira, J.S., 2011. Seasonal patterns of evapotranspiration for a Vochysia divergens forest in the Brazilian Pantanal. Wetlands Ecol. Manage. https://doi.org/10.1007/s13157-011-0233-0

Santos, C.A.C., Mariano, D.A., das Chagas, A., do Nascimento, F.C., Dantas, F.R., de Oliveira, G., Silva, M.T., Neale, C.M.U., 2020. Spatio-temporal patterns of energy exchange and evapotranspiration during an intense drought for drylands in Brazil. Int. J. Appl. Earth Obs. Geoinf. 85, 101982. https://doi.org/10.1016/j.jag.2019.101982

Schumann, G.J.-P., Moller, D.K., 2015. Microwave remote sensing of flood inundation. Phys. Chem. Earth 83–84, 84–95. https://doi.org/10.1016/j.pce.2015.05.002

Seidl, A.F., Silva, J.D.S.V., Moraes, A.S., 2001. Cattle ranching and deforestation in the Brazilian Pantanal. Ecol. Econ. 36(3), 413–425. https://doi.org/10.1016/S0921-8009(00)00238-X

Sen, P.K., 1968. Estimates of the regression coefficient based on Kendall's tau. J. Am. Stat. Assoc. 63(324), 1379–1389.

Shuttleworth, W.J., Wallace, J.S., 1985. Evaporation from sparse crops-an energy combination theory. Quart J Royal Meteoro Soc. 111, 839–855. https://doi.org/10.1002/qj.49711146910

Silva, B.B., Wilcox, B.P., Silva, V.D.P.R., Montenegro, S.M.G.L., De Oliveira, L.M.M., 2015. Changes to the energy budget and evapotranspiration following conversion of tropical

savannas to agricultural lands in São Paulo State, Brazil. Ecohydrology. 8, 1272–1283. https://doi.org/10.1002/eco.1580

Silva, G. J. F., Silva, R. M., Brasil Neto, R. M., Silva, J. F. C. B. C., Dantas, A. P. X., & Santos, C. A. G. (2024). Multi-datasets to monitor and assess meteorological and hydrological droughts in a typical basin of the Brazilian semiarid region. Environmental Monitoring and Assessment, 196, 367. doi: 10.1007/s10661-024-12461-0

Silva, I.W., Marques, T.V., Urbano, S.A., Mendes, K.R., Oliveira, A.C.C., Nascimento, F.D.S., Morais, L.F., Pereira, W.S., Mutti, P.R., Emernciano Neto, J.V., Lima, J.R.S., Oliveira, P.E.S., Costa, G.B., Santos e Silva, C.M., Bezerra, B.G., 2024. Meteorological and biophysical controls of evapotranspiration in tropical grazed pasture under rainfed conditions. Agric. Water Manag. 299, 108884. https://doi.org/10.1016/j.agwat.2024.108884

Silva, J.M.C., Leal, I.R., Tabarelli, M., 2017. Caatinga: the largest tropical dry forest region in South America. Cham: Springer.

Silva, P. F. d., Lima, J. R. d. S., Antonino, A. C. D., Souza, R., Souza, E. S. d., Silva, J. R. I., Alves, E. M., 2017. Seasonal patterns of carbon dioxide, water and energy fluxes over the Caatinga and grassland in the semi-arid region of Brazil. Journal of Arid Environments. 147, 71–82. https://doi.org/10.1016/j.jaridenv.2017.09.003

Som-ard, J., Atzberger, C., Izquierdo-Verdiguier, E., Vuolo, F., Immitzer, M., 2021. Remote sensing applications in sugarcane cultivation: a review. Remote Sens. 13, 4040. https://doi.org/10.3390/rs13204040

Sousa-Neto, E.R., Gomes, L., Nascimento, N., Pacheco, F., Ometto, J.P., 2018. Land use and land cover transition in Brazil and their effects on greenhouse gas emissions. In: Soil management and climate change. Elsevier, Amsterdam, p. 309–321. https://doi.org/10.1016/B978-0-12-812128-3.00020-3

Souza Jr., C.M., Shimbo, J.Z., Rosa, M.R., Parente, L.L., Alencar, A.A., Rudorff, B.F.T., Hasenack, H., Matsumoto, M., Ferreira, L.G., Souza-Filho, P.W.M., de Oliveira, S.W., Rocha, W.F., Fonseca, A.V., Marques, C.B., Diniz, C.G., Costa, D., Monteiro, D., Rosa, E.R., et al., 2020. Reconstructing three decades of land use and land cover changes in Brazilian biomes with Landsat archive and Earth Engine. Remote Sens. 12(17), 2735. https://doi.org/10.3390/rs12172735

Souza, V.D.A., Roberti, D.R., Alves, R.D.C.M., Diaz, M.B., Tatsch, J.D., 2016. Validação do produto de evapotranspiração MOD16 para uma cultura de arroz irrigado em Cachoeira do Sul - RS. CeN. 38, 270. https://doi.org/10.5902/2179460X20230

Souza, W.O., Reis, L.G.M., Ruiz-Armenteros, A.M., Veleda, D., Ribeiro Neto, A., Fragoso Jr., C.R., Cabral, J.J.S.P., Montenegro, S.M.G.L., 2022. Analysis of environmental and atmospheric influences in the use of SAR and optical imagery from Sentinel-1, Landsat-8, and Sentinel-2 in the operational monitoring of reservoir water level. Remote Sens. 14, 2218. https://doi.org/10.3390/rs14092218

Souza,R., Feng, X., Antonino, A., Montenegro, S., Souza, E., Porporato, A., 2016. Vegetation response to rainfall seasonality and interannual variability in tropical dry forests Hydrological Processes, 30, pp. 3583–3595. https://doi.org/10.1002/hyp.10953

Srivastava, A., Sahoo, B., Raghuwanshi, N.S., Singh, R., 2017. Evaluation of Variable-Infiltration Capacity Model and MODIS-Terra Satellite-Derived Grid-Scale Evapotranspiration Estimates in a River Basin with Tropical Monsoon-Type Climatology. J. Irrig. Drain Eng. 143, 04017028. https://doi.org/10.1061/(ASCE)IR.1943-4774.0001199

Sun, L., Liang, S., Yuan, W., Chen, Z., 2013. Improving a Penman–Monteith evapotranspiration model by incorporating soil moisture control on soil evaporation in semiarid areas. International Journal of Digital Earth. 6, 134–156. https://doi.org/10.1080/17538947.2013.783635

Sur, C., Kang, S., Kim, J., Choi, M., 2015. Remote sensing-based evapotranspiration algorithm: a case study of all sky conditions on a regional scale. GIScience & Remote Sensing. 52, 627–642. https://doi.org/10.1080/15481603.2015.1056288

Tang, R., Li, Z.-L., Sun, X., 2013. Temporal upscaling of instantaneous evapotranspiration: An intercomparison of four methods using eddy covariance measurements and MODIS data. Remote Sensing of Environment. 138, 102–118. https://doi.org/10.1016/j.rse.2013.07.001

Tang, R., Shao, K., Li, Z.-L., Wu, H., Tang, B.-H., Zhou, G., Zhang, L., 2015. Multiscale Validation of the 8-day MOD16 Evapotranspiration Product Using Flux Data Collected in China. IEEE J. Sel. Top. Appl. Earth Observations Remote Sensing. 8, 1478–1486. https://doi.org/10.1109/JSTARS.2015.2420105

Tapley, B.D., Bettadpur, S., Ries, J.C., Thompson, P.F., Watkins, M.M., 2004. GRACE measurements of mass variability in the Earth system. Science 305, 503–505. https://doi.org/10.1126/science.1099192

Teixeira, A. H. C., Scherer-Warren, M., Hernandez, F., Andrade, R., Leivas, J., 2013. Large-Scale Water Productivity Assessments with MODIS Images in a Changing Semi-Arid Environment: A Brazilian Case Study. Remote Sensing. 5, 5783–5804. https://doi.org/10.3390/rs5115783

Teixeira, A.H.D.C., Bastiaanssen, W.G.M., Ahmad, M.D., Bos, M.G., 2009. Reviewing SEBAL input parameters for assessing evapotranspiration and water productivity for the Low-Middle São Francisco River basin, Brazil. Agricultural and Forest Meteorology. 149, 462–476. https://doi.org/10.1016/j.agrformet.2008.09.016

Timmermans, W.J., Kustas, W.P., Anderson, M.C., French, A.N., 2007. An intercomparison of the Surface Energy Balance Algorithm for Land (SEBAL) and the Two-Source Energy Balance (TSEB) modeling schemes. Remote Sensing of Environment. 108, 369–384. https://doi.org/10.1016/j.rse.2006.11.028

UFSM, 2004. Rede de pesquisa em bacias representativas e experimentais no bioma Mata Atlântica na região sul do Brasil (MATASUL) – Monitoramento. Available from: http://jararaca.ufsm.br/websites/matasul-furb/7b1e8e82b886b38317fcd4358ccadde3.htm. Acessado em: 11 ago. 2025.

Valeriano, M.M., Salvi, L.L., Aragão, J.R.L., 2012. Relações entre a distribuição da precipitação e o relevo da bacia do Alto Paraguai. In: Anais 4º Simpósio de Geotecnologias no Pantanal. Bonito-MS.

Van Niel, T.G., McVicar, T.R., Roderick, M.L., Van Dijk, A.I.J.M., Beringer, J., Hutley, L.B., Van Gorsel, E., 2012. Upscaling latent heat flux for thermal remote sensing studies: Comparison of alternative approaches and correction of bias. Journal of Hydrology. 468–469, 35–46. https://doi.org/10.1016/j.jhydrol.2012.08.005

Van Niel, T.G., McVicar, T.R., Roderick, M.L., Van Dijk, A.I.J.M., Renzullo, L.J., Van Gorsel, E., 2011. Correcting for systematic error in satellite-derived latent heat flux due to assumptions in temporal scaling: Assessment from flux tower observations. Journal of Hydrology. 409, 140–148. https://doi.org/10.1016/j.jhydrol.2011.08.011

Verburg, P.H., Crossman, N., Ellis, E.C., Heinimann, A., Hostert, P., Mertz, O., Nagendra, H., Sikor, T., Erb, K.-H., Golubiewski, N., Grau, R., Grove, M., Konaté, S., Meyfroidt, P., Parker, D.C., Roy Chowdhury, R., Shibata, H., Thomson, A., Zhen, L., 2015. Land system science and sustainable development of the earth system: a global land project perspective. Anthropocene 12, 29–41. https://doi.org/10.1016/j.ancene.2015.09.004

Vicente-Serrano, S. M., Beguería, S., & López-Moreno, J. I., 2010. A multiscalar drought index sensitive to global warming: The standardized precipitation evapotranspiration index. Journal of Climate, 23(7), 1696–1718. https://doi.org/10.1175/2009jcli2909.1

Vinukollu, R.K., Wood, E.F., Ferguson, C.R., Fisher, J.B., 2011. Global estimates of evapotranspiration for climate studies using multi-sensor remote sensing data: Evaluation of three process-based approaches. Remote Sensing of Environment. 115, 801–823. https://doi.org/10.1016/j.rse.2010.11.006

Vourlitis, G. L., Nogueira, J. d. S., Lobo, F. d. A., Sendall, K. M., Paulo, S. R. d., Dias, C. A. A., et al., 2008. Energy balance and canopy conductance of a tropical semi-deciduous forest of the southern Amazon Basin. Water Resources Research. 44. https://doi.org/10.1029/2006WR005526

Vourlitis, G., Dalmagro, H., Nogueira, J. S., Johnson, M., Arruda, P., 2019. AmeriFlux BASE BR-Npw Northern Pantanal Wetland, Ver. 1-5, AmeriFlux AMP, (Dataset). https://doi.org/10.17190/AMF/1579716

Wang, K., Dickinson, R.E., 2012. A review of global terrestrial evapotranspiration: Observation, modeling, climatology, and climatic variability. Reviews of Geophysics 50, 2011RG000373. https://doi.org/10.1029/2011RG000373

Wang, X.; Zhou, J.; Ma, J.; Luo, P.; Fu, X.; Feng, X.; Zhang, X.; Jia, Z.; Wang, X.; Huang, X, 2024. Evaluation and Comparison of Reanalysis Data for Runoff Simulation in the Data-Scarce Watersheds of Alpine Regions. Remote Sens. 16, 751. https://doi.org/10.3390/rs16050751

Wang, Y., Wang, X., Gao, Y., He, H., Su, Y., 2021. Radiation scattering effects in the processing of optical quantitative remote sensing data. Remote Sens. Lett. 12(9), 921–931. https://doi.org/10.1080/2150704X.2021.1947538

Wong, A. J., Jin, Y., Medellín-Azuara, J., Paw U, K. T., Kent, E. R.,Clay, J. M., et al., 2021. Multiscaleassessment of agricultural consumptivewater use in California's CentralValley. Water Resources Research,57. https://doi.org/10.1029/2020WR028876

Wu, B., Zhu, W., Yan, N., Feng, X., Xing, Q., Zhuang, Q., 2016. An Improved Method for Deriving Daily Evapotranspiration Estimates From Satellite Estimates on Cloud-Free Days. IEEE J. Sel. Top. Appl. Earth Observations Remote Sensing. 9, 1323–1330. https://doi.org/10.1109/JSTARS.2015.2514121

Xu, C., Wang, W., Hu, Y., & Liu, Y., 2024. Evaluation of ERA5, ERA5-Land, GLDAS-2.1, and GLEAM potential evapotranspiration data over mainland China. Journal of Hydrology: Regional Studies, 51, 101651. https://doi.org/10.1016/j.ejrh.2023.101651

Xu, L., Baldocchi, D.D., 2003. Seasonal trends in photosynthetic parameters and stomatal conductance of blue oak (Quercus douglasii) under prolonged summer drought and high temperature. Tree Physiology. 23, 865–877. https://doi.org/10.1093/treephys/23.13.865

Xue, W., Ko, J., 2022. Radiation estimation and crop growth trajectory reconstruction by novel algorithms improve MOD16 evapotranspiration predictability for global multi-site paddy rice ecosystems. Journal of Hydrology. 612, 128204. https://doi.org/10.1016/j.jhydrol.2022.128204

Yang, Y., 2025. Estimating actual evapotranspiration across China by improving the PML algorithm with a shortwave infrared-based surface water stress constraint. Remote Sensing of Environment, 318, 114544.

Yeom, J.-M., Lee, C.-S., Park, S.-J., Ryu, J.-H., Kim, J.-J., Kim, H.-C., Han, K.-S., 2015. Evapotranspiration in Korea estimated by application of a neural network to satellite images. Remote Sensing Letters. 6, 429–438. https://doi.org/10.1080/2150704X.2015.1041169

Yilmaz, M. T., Anderson, M. C., Zaitchik, B., Hain, C. R., Corvo, W. T., Ozdogan,M., Jong, A. C., Evans, J., 2014. Comparação de abordagens prognósticas e diagnósticas de modelagem de fluxo superficial na bacia do Rio Nilo. Water Resources Research. 50, 386-408.https://doi.org/10.1002/2013WR014194

Zegait, R., Bouznad, I.E., Remini, B., Bengusmia, D., Ajia, F., Guastaldi, E., Lopane, N., Petrone, D., 2024. Comprehensive model for sustainable water resource management in Southern Algeria: integrating remote sensing and WEAP model. Model. Earth Syst. Environ. 10, 1027–1042. https://doi.org/10.1007/s40808-023-01826-y

Zhang, K., Kimball, J.S., Running, S.W., 2016. A review of remote sensing based actual evapotranspiration estimation. WIREs Water. 3, 834–853. https://doi.org/10.1002/wat2.1168

Zhang, W., Koch, J., Wei, F., Zeng, Z., Fang, Z., & Fensholt, R., 2023. Soil Moisture and Atmospheric Aridity Impact Spatio-Temporal Changes in Evapotranspiration at a Global Scale. Journal of Geophysical Research: Atmospheres, 128(8), e2022JD038046.

Zhang, Y., Kong, D., Gan, R., Chiew, F.H.S., McVicar, T.R., Zhang, Q., Yang, Y., 2019. Coupled estimation of 500 m and 8-day resolution global evapotranspiration and gross primary production in 2002–2017. Remote Sensing of Environment. 222, 165–182. https://doi.org/10.1016/j.rse.2018.12.031

Zhu, W., Tian, S., Wei, J., Jia, S., Song, Z., 2022. Multi-scale evaluation of global evapotranspiration products derived from remote sensing images: Accuracy and uncertainty. Journal of Hydrology. 611, 127982. https://doi.org/10.1016/j.jhydrol.2022.127982

Zou, J., Lu, N., Jiang, H., Qin, J., Yao, L., Xin, Y., & Su, F., 2022. Performance of air temperature from ERA5-Land reanalysis in coastal urban agglomeration of Southeast China. Science of The Total Environment, 828, 154459. https://doi.org/10.1016/j.scitotenv.2022.154459

Zuo, C., Chen, J., Zhang, Y., Jiang, Y., Liu, M., Liu, H., Zhao, W., Yang, X., 2023. Evaluation of four meteorological reanalysis datasets for satellite-based PM2.5 retrieval over China. Atmospheric Environment, 305, 119795. https://doi.org/10.1016/j.atmosenv.2023.119795